NASA CR-72413

COATINGS FOR REGENERATIVE ENGINES

by

W. J. Lewis

FINAL REPORT NO. 1

Prepared for

NATIONAL AERONAUTICS AND SPACE ADMINISTRATION

Contract NAS 3-7955

12 July 1968

NASA CR-72413

Final Report No. 1

COATINGS FOR REGENERATIVE ENGINES

By
W. J. Lewis

Prepared for

National Aeronautics and Space Administration

12 July 1968

Contract NAS 3-7955

Technical Management
NASA-Lewis Research Center
Cleveland, Ohio
Chemical and Nuclear Rocket Proc. Section
Rudy Duscha

Aerojet-General Corporation
Sacramento, California

28238T

PREFACE

This report was prepared by W. J. Lewis for NASA-LeRC under Contract NAS 3-7955 for Mr. R. A. Duscha, the NASA-LeRC Project Manager. The author wishes to acknowledge the contributions of J. A. Cunningham and A. Kobayashi for the heat transfer analysis, G. Fuller for the plasma tests evaluation, J. Milne and R. Hayes for the flox/propane evaluations.

The report was reviewed and approved by C. A. Auble, Manager, Component Evaluation Group, and A. V. Levy, Manager of the Materials Technology Section.

TABLE OF CONTENTS

TABLE LIST

FIGURE LIST

FIGURE LIST (cont.)

I. SUMMARY

Thermal barriers are under development to reduce the heat flux to the coolant for a 5000-lb-thrust flox/propane regeneratively cooled chamber. An analysis conducted to establish thermal and chemical environment for the thermal barriers revealed that thermal resistance of 1400 $in.^2$-sec-°F/Btu would be required with coating surface temperatures of 3000°F. The theoretical exhaust-gas environment at the throat of the chamber on a volume basis was calculated at 55.7% HF, 24.7% CO, 1.2% H_2, 8.3% H, 0.1% C_2F_2, and 10% F for an engine operating at 100-psia chamber pressure and at a flox/propane mixture ratio of 4.5. Theoretical flame temperature was 7000°F. Based on the thermal and chemical environment and material properties W, Mo, Al_2O_3, and ZrO_2 were selected for the basic thermal barrier materials.

Screening tests were made on the coatings in the laboratory using a plasma torch to simulate the thermal environment but not the chemical environment of the flox/propane engine. The final tests consisted of exposing coated 5-tube specimens to the exhaust stream of a flox/propane rocket engine. During the tests, the specimens were cooled similar to tubes in a regeneratively cooled chamber. The specimen was positioned in the exhaust stream to obtain exhaust gas species, gas velocities, and temperatures at the specimen surface similar to those at the throat. In addition, the specimen was positioned to obtain a minimum of air entrainment at the surface of the specimen. However, severe regression was obtained on the graphite shield (used to protect specimen water inlets) indicating that air entrainment occurred. This would make the chemical environment more severe than originally analyzed.

The regression rate of the coatings exposed to the flox/propane environment varied with coating composition. The lowest regression rates occurred in coatings with flame liners containing 100% Mo, W, or ZrC/C. The regression rates for these flame liners were 0.4 mils/sec, which is relatively high for thermal barrier systems. This high regression rate is thought to be a result of the increased severity of the exhaust chemistry reacting with air entrainment.

I, Summary (cont.)

Regresssion rates increased with ZrO_2 or Al_2O_3 additions to the flame liner of the coating. However, the best coatings were obtained using a combination of (1) 3 to 5 mils of Nichrome for primer, (2) 10 mils of 20%Ni-80% Al_2O_3 for thermal resistance, (3) 14 mils of 30% Mo-70% Al_2O_3 for thermal resistance, and (4) 15 to 20 mils of W, Mo or ZrC/C for the flame barrier. The density of the plasma-sprayed tungsten coatings which were less than theoretical were estimated to range from 75 to 90%. In solid rocket motor firings, a regression rate of nozzle inserts decreased from 4 mils/sec for 75% dense Mo to 0 regression in 100% dense Mo. Based on this information, regression resistance of the flame liner should be significantly improved by increasing the density to 95% or greater.

II. INTRODUCTION

Cooling limitations are reached in regeneratively cooled rocket engines when propellants are used which have poor cooling capabilities. For these situations, various supplementary schemes become of interest, such as film cooling or transpiration cooling. Thrust chambers, using high-energy propellants such as fluorine, would require excessive film cooling to maintain reasonable gas-side temperatures with a substantial loss in performance. The use of an insulating thermal barrier coating on the inner thrust chamber wall would reduce the heat flux to the coolant without a loss in performance. Thermal barriers have been used successfully on conventional regeneratively cooled engines (the X-15 and Titan engines) for controlling the gas-side temperature and decreasing the heat flux to the coolant.

The thermal barrier allows the use of regenerative cooling concept with a space-storable propellant combination such as flox/propane in a pressure-fed system. The objective of this program was to develop thermal barrier coatings for the inner walls of regeneratively cooled thrust chambers operating with flox/propane propellants. The thermal barriers were designed to reduce the heat flux to the coolant and still be compatible with the exhaust gas environment of the engine.

An analysis was conducted to establish the thermal and chemical environment for the coating in a 5000-lb thrust engine. This information provided the basis for establishing the thermal resistance (thickness of the coating divided by the thermal conductivity of the coating) and the selection of the thermal barrier materials.

The selected thermal barrier materials were applied to stainless-steel disks and tube specimens and evaluated in the laboratory for thermal resistance properties and thermal shock resistance. Final evaluation was made by placing coated tube specimens in the exhaust of a flox/propane engine, which had been modified for use on this program.

The thermal and chemical analysis, the selection of materials, and the coating evaluation are summarized in this report.

III. BACKGROUND

A. THERMAL BARRIER

The earliest significant use of thermal barriers for liquid fueled (LO_2/LNH_3) rocket engines occurred in the XLR-99 thrust chamber of the X-15 research aircraft. Originally in the X-15 program (1962), zirconia was flame sprayed on the inside diameter of the XLR-99 thrust chamber over a Nichrome primer. The purpose of the thermal barrier was to reduce the heat flux to the coolant.

Excessive coating loss was observed on the XLR-99 chambers during short operations, which Smith and Wurst attributed to a combination of poor coating adherence and poor thermal shock resistance (Reference 1). Because of the poor performance, Plasmakote Corporation was awarded a contract (AF 33(616)-7323) to develop thermal barrier coatings for the XLR-99 thrust chamber. The development program by Plasmakote revealed that (1) molybdenum as a primer coat substantially improved adherence and thermal shock resistance of the coating, (2) minor variations in the percentage of metal in the intermediate layers of a graded ceramic had little effect upon thermal shock resistance, (3) two and three layered graded systems performed well, (4) topcoats of TiN and ZrH_2 were not satisfactory, and (5) thermal shock resistance of Nichrome-graded ZrO_2 was better than either the Mo or W graded coatings. As a result of this work, the X-15 chamber was prime coated with Mo and topcoated with Nichrome ZrO_2 mixtures.

Since 1964, thermal barriers have been investigated at Aerojet (References 2 and 3), to develop metal-rich cermets for thermal barrier liners for temperatures in the range of 3000 to 4000°F, well above the melting point of Nichrome. Work was concentrated on developing adherent, thermal shock resistance coatings which were compatible with the combustion products of the engine.

III, A, Thermal Barrier (cont.)

Adherence of the coating was improved, as evidenced by shear bond tests, by grit blasting the stainless-steel substrate surfaces to obtain surface finishes in the range of 250 to 300 microinches. In addition, the use of primers (2 to 3 mils thick) such as nichrome, nickel aluminide, or molybdenum significantly improved coating adherence. The improvement of bond adherence with primers and roughened surfaces has been demonstrated by other investigators (References 4 and 5).

Thermal shock resistance of the coatings was improved by using relatively high metal contents for reinforcing the ceramic. The high metal content would be expected to result in higher thermal conductivity mixtures and thicker coatings. This would overshadow any thermal shock improvement. However, the increase in thermal conductivity of the cermet mixture is not as much as would be expected because of the relatively low density of the plasma spray coatings. The measured thermal conductivity of plasma sprayed Mo and Al_2O_3 mixtures as compared with wrought Mo and Al_2O_3 mixtures is shown in Figure 1. The difference in thermal conductivity resulted in sprayed mixtures reinforced with metal for thermal shock resistance, while still maintaining reasonable thickness coatings. For example, the thickness of a sprayed mixture of 100% Mo would be about 0.050 in. to maintain a thermal resistance of 200 $in.^2$ sec °F/Btu (thickness/thermal conductivity) compared to 0.200 in. of wrought molybdenum for the same thermal resistances.

The thermal shock resistance of the thermal barriers was also improved by using an intermediate coat between the primer and topcoat. The intermediate consisted of ceramic and ductile metal such as nickel or nickel base alloys. In the latter system, the nickel and ceramic mixture is designed to operate at a maximum temperature of 2000°F. The topcoat is designed to operate from 2000°F to the designed surface temperature and to be compatible with the combustion products of the exhaust gas.

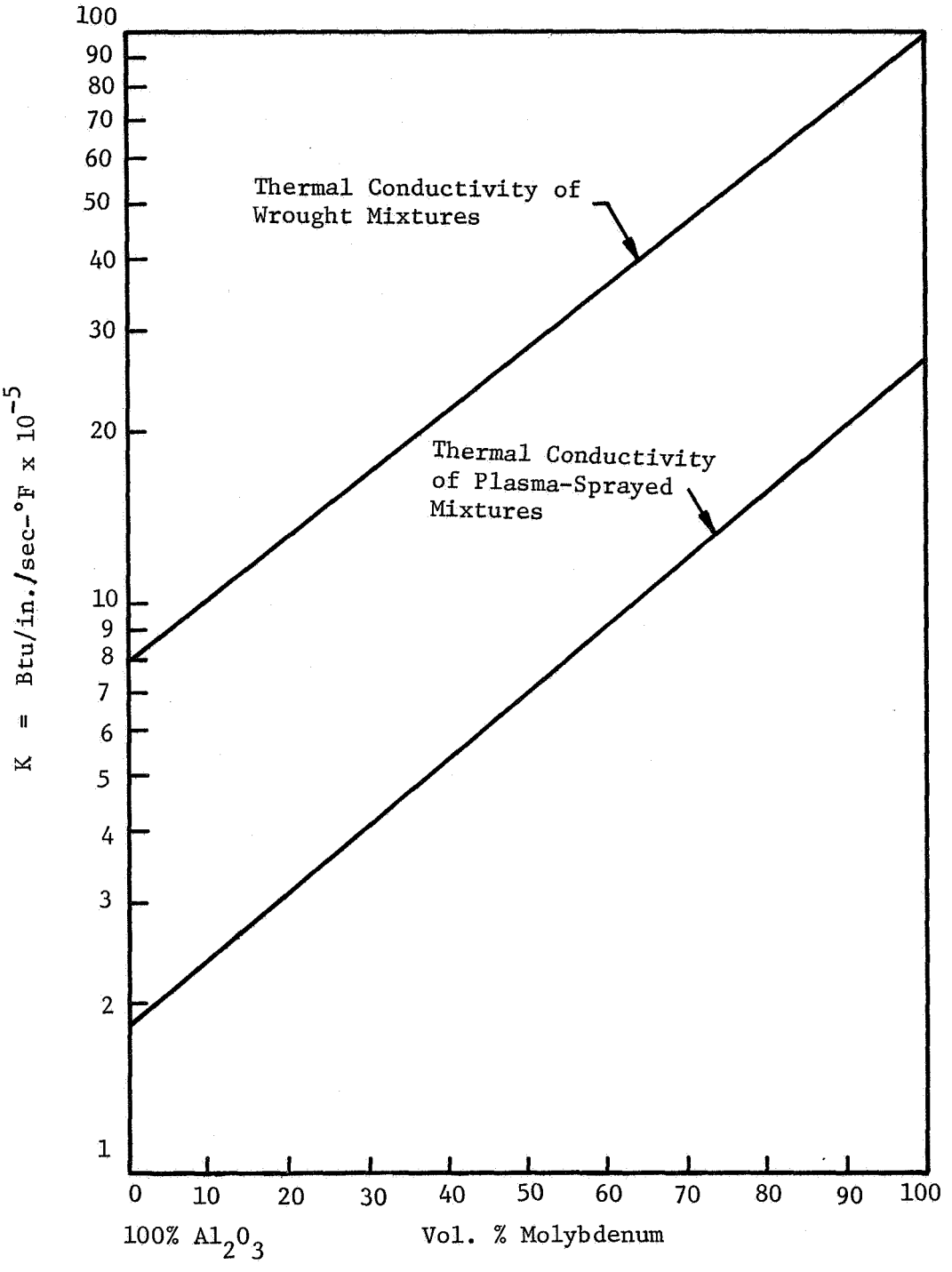

Figure 1. Thermal Conductivity of Wrought and Plasma-Sprayed Mixture as a Function of Mo Content in Al_2O_3.

III, A, Thermal Barrier (cont.)

The thermal barrier must be compatible with the combustion gases at the coating operating temperature. As a consequence, both ceramic-rich and metal-rich coatings have been evaluated for flame liner service. The ceramic rich coatings (Al_2O_3 and ZrO_2) provide excellent compatibility with oxidizing exhaust gases consisting primarily of water vapor and oxygen containing compounds. The metal-rich coatings (primarily W and Mo) generally provide less oxidation resistance but are more compatible than the oxides with exhaust gases containing fluorine compounds. The metal-rich coatings also provide more thermal shock resistances than the ceramic-rich coatings. Alloying of tungsten with rhenium or hafnium to improve oxidation resistancy was not successful (References 2 and 3). The use of additives of silicon or tungsten silicide has been more successful in Aerojet studies with significant increases in oxidation resistance.

In summary, considerable improvements have been made in thermal barrier coatings since 1962. Coating adherence is improved significantly by using primer coatings of nichrome, nickel-aluminide, or molybdenum, along with substrate surface finishes in the range of 250 to 300 microinches. Thermal shock resistance was found to be improved by using metal-reinforced coatings including under layers of nickel alloy and ceramic mixtures. In addition to the adherence and thermal shock resistance, oxidation resistance has been improved by designing the coating to be compatible with the thermal and chemical environment of the exhaust gases.

B. MATERIAL COMPATIBILITY WITH FLUORINE GAS SPECIES AT HIGH TEMPERATURES

The compatibility of refractory materials with fluorine gas species at high temperatures has been investigated by several investigators (References 6 through 12). These investigations conducted in the laboratory revealed that all of the high temperature materials react with free fluorine, with iridium

the most resistant at temperatures above 3500°F. Graphite, tungsten, and the carbides were found to be compatible with HF at high temperature, with the ceramic oxides exhibiting decreasing compatibility.

Thermodynamic calculations were reported by Peters (Reference 8) on numerous materials, including graphite, tungsten, tantalum carbide, hafnium nitride, titanium carbide, zirconium carbide, zirconium boride, magnesium oxide, and hafnium oxide. Gas species HF, LiF, AlF_2, BF_3, F_2, H_2O, Hcl, CO_2, and CO were used in the calculations at temperatures from 2300 to 8000°F. Peters' study showed that tungsten and graphite were generally the most resistant materials to the mentioned gas species, with graphite best for atmospheres containing fluorine compounds and tungsten best for atmospheres containing oxygen and hydrogen.

The initial laboratory investigations of compatibility of refractory materials with high-temperature fluorine propellant combustion species was reported by Ebner (Reference 9) in 1961. He evaluated graphite (C), silicon carbide (SiC), zircon ($ZrSiO_4$), alumina (Al_2O_3), zirconia (ZrO_2), and magnesia (MgO) at temperatures of 2800°F to 4000°F in a hydrogen-fluorine flame. Ebner reported that graphite and SiC had excellent chemical compatibility, while the compatibility of the others decreased in the order presented above. He also found that the rate of ablation was about three times faster in the fluorine-rich portion of the flame than in the well-mixed part of the flame.

In laboratory studies (Reference 10), tungsten and tantalum were exposed to HF (99.5% pure with max 0.04% H_2O) at temperatures of 3000°F to 5000°F, and found that the reactivity of W with HF was so low it could not be reliably measured. However, Ta was reactive, having a surface recession of 0.00036 in./sec. This data concurs with Batchelor, et al. (Reference 11), who also found tungsten to be compatible with HF and HCl while tantalum was attacked by these same gas species.

III, B, Material Compatibility with Fluorine Gas Species at High Temperatures (cont.)

Several carbides were also evaluated (Reference 10), in HF at 3000°F to 5000°F with NbC and TaC most reactive, TiC intermediate, and HfC and ZrC least reactive. All five carbides are considered resistant of HF at moderate temperatures, but corrosion rates increase a hundred-fold between 4000°F and 5000°F.

Hill and Rausch (Reference 12), exposed W, Ta, Ir, Re, Ir-33%Re, W-26%Re, and JTA graphite to fluorine-argon mixtures at temperatures of 3500°F to 5200°F. The results of these tests revealed that Ir and Ir-33%Re had the lowest corrosion rates, while Ta had the highest corrosion rate at all temperatures. At temperatures of 3500°F, the material loss for tungsten in a mixture of 6.5%F_2 (by vol) and argon was 2.6 mils/min compared to 0.4 mils/min for Ir.

The concensus of the data in available literature on compatibility of high temperature materials with F and HF is that all of the materials are attacked by free fluorine at temperatures in the range of 3000 to 5000°F, with iridium showing the best resistance. Data on the refractory material indicate that graphite, tungsten, and the carbides are compatible with HF while tantalum and the oxides $ZrSiO_4$, Al_2O_3, ZrO_2, and MgO are attacked.

IV. MATERIAL AND PROCESS SELECTION

The selection of materials for thermal barriers was based on the chemical and thermal environment and the material properties, including melting point, chemical compatibility, thermal conductivity, and thermal expansion. In addition, consideration was given to the compatibility of the metal with the ceramic in the thermal barrier mixtures.

The service environment from the thermal barrier in this program was based on a 5000-lb thrust, regeneratively cooled (propane) engine, operating at 100 psia chamber pressure, using flox (76 wt % F_2 and 24 wt % O_2), and propane (C_3H_8) at a mixture ratio of 4.5:1. These parameters were used to establish the chemical and thermal environments for the thermal barrier program.

A. CHEMICAL ENVIRONMENT

The chemical environment for thermal barriers was established in a computer by obtaining the equilibrium exhaust gas species for the flox/propane engine. Exhaust species were established at mixture ratios of 3, 3.5, 4, 4.5, and 5 and at chamber pressures of 100, 300, and 500 psi. The effect of mixture ratio on relative volumes of gas species is shown in Figure 2, and the effect of area ratio is shown in Figure 3.

The gas species at the throat at 100 psi chamber pressure and mixture ratio of 4.5 are 55.7% HF, 24.7% CO, 1.2% H_2, 8.3% H, 0.1% C_2F_2, and 10% F. These exhaust gas species were used as the basis for establishing and analytically calculating the chemical requirement for the thermal barrier coatings.

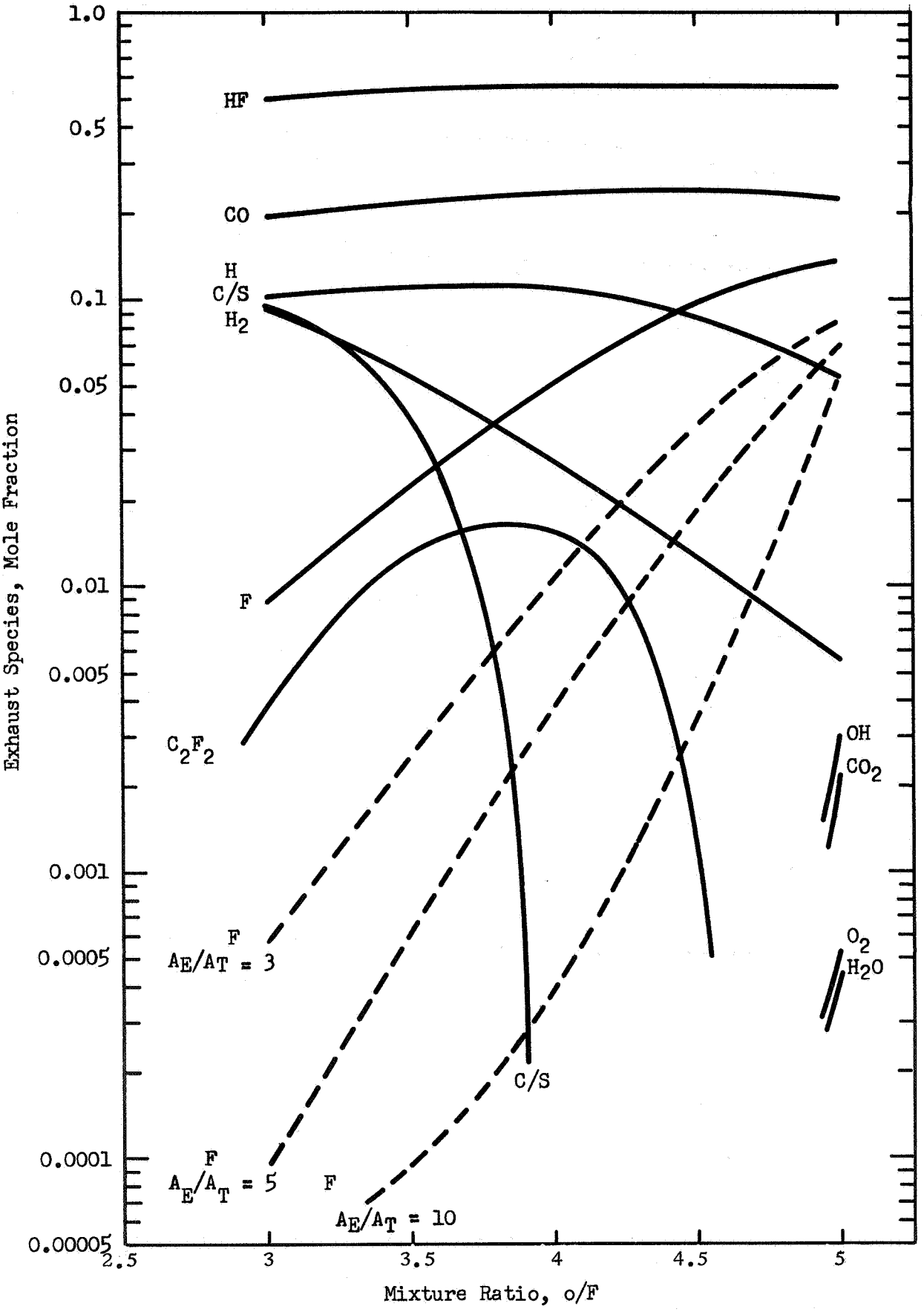

Figure 2. Exhaust Species vs Mixture Ratio for $(.76F_2 \ .24 \ O_2)/C_3H_8$ at Throat and Pc = 100 psia.

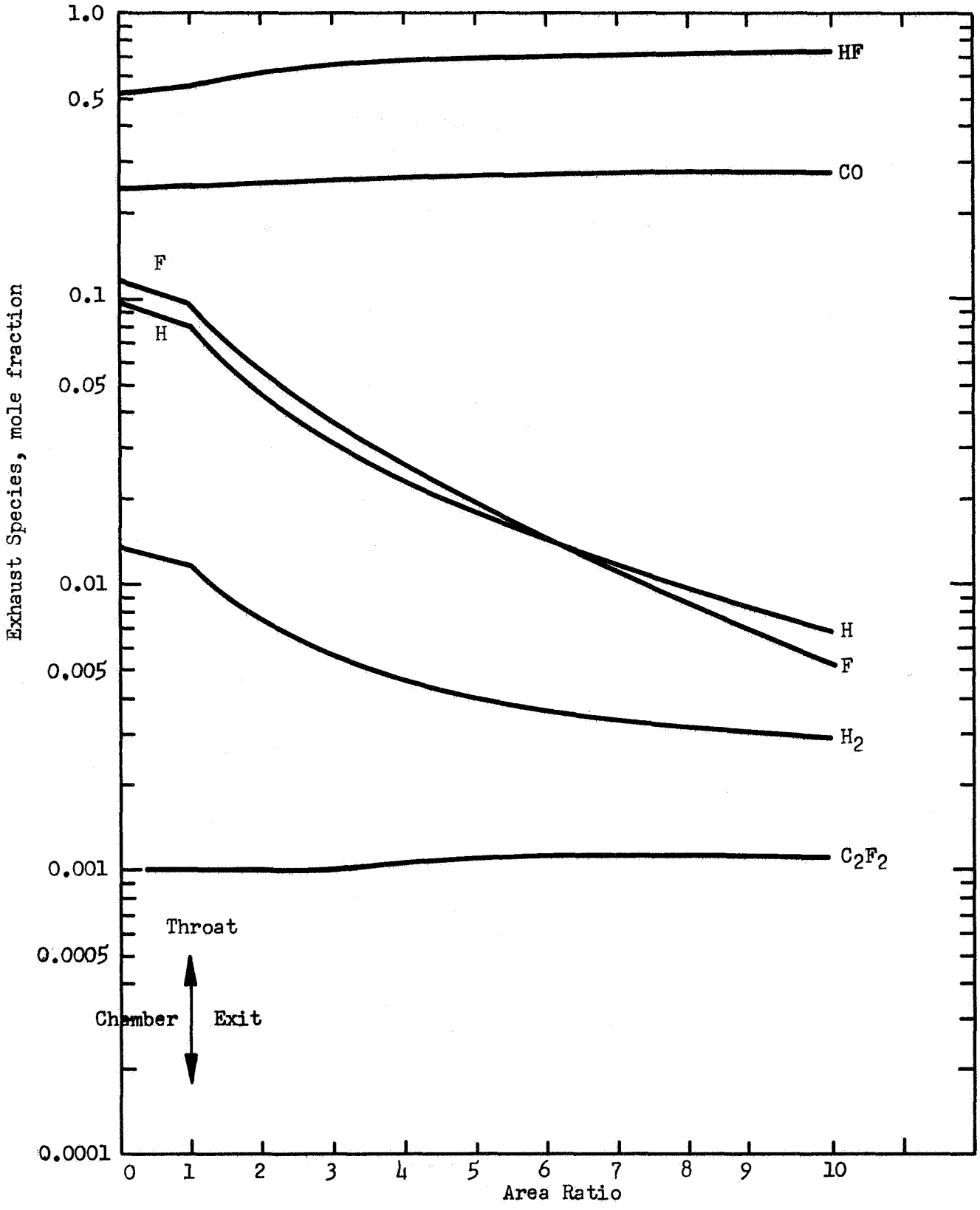

Figure 3. Exhaust Species vs Area Ratio for $(.76F_2$ $.24\ O_2)/C_3H_8$ at a Mixture Ratio of 4.5 and Pc = 100 psia.

B. THERMAL ANALYSIS

The thermal analysis was conducted to establish the range of coating thermal resistances required for the propane, regeneratively cooled 5000-lb-thrust chamber. The analysis included the effects of coolant (propane velocity), propane bulk temperatures, and tube size on coating resistance requirements. Additional considerations were coolant pressure drop, minimum tube size, coating surface temperature, and burnout heat flux of propane.

Operating conditions used for the analysis were 100 to 500 psia chamber pressure and a flox/propane mixture ratio of 4.5. Only the following data (Reference 13) on propane were available for velocities, subcooling, and burnout heat flux.

1.	Propane Burnout Flux:	0.24 to 0.90 Btu/in.^{2}-sec
2.	Bulk pressure:	150 psia
3.	Bulk Temperature:	434 to 535°F
4.	Velocity:	1.5 to 24.1 ft/sec
5.	Subcooling:	0 to 111°F

This data was used to correlate the burnout heat flux data with velocity and subcooling for convenience in the analysis. The following equation was used for the correlation:

$$\phi_{BO} = 0.35 + 0.001\ V^{1/2}\ \Delta T_{sub} \qquad \text{(Eq 1)}$$

where
- ϕ_{BO} = propane burnout heat flux, Btu/in.^{2}-sec
- V = coolant velocity, ft/sec
- ΔT_{sub} = subcooling temperature (saturation temperature, bulk temperature), °F

IV, B, Thermal Analysis (cont.)

The burnout correlation data is shown in Figure 4. Ninety-four percent of the data lie within ± 25% of the predicted flux. For the analysis, extrapolations were made beyond the correlated data range of coolant velocity subcooling.

The throat/gas-side film coefficient and the recovery temperature used in this investigation are shown in Figure 5. The film coefficient was calculated using a modified Bartz equation (Equation 3).

$$h_g = \frac{C_G}{D_c^{0.2}} \left[\frac{\mu^{0.2} C_P}{Pr^{0.6}} \right]_f \left(\frac{W_T}{A_c} \right)^{0.8} \left(\frac{T_s}{T_f} \right)^{0.8} \qquad \text{(Eq 3)}$$

where

h = film coefficient
C_G = correlation constant
C_p = specific heat
D_c = chamber diameter
μ = viscosity
Pr = Prandtl number
f = film condition
W_T = propellant flow rate
A_c = chamber area
T_s = static temperature
T_f = film temperature

A c* or combustion efficiency of 97% was assumed for the calculations.

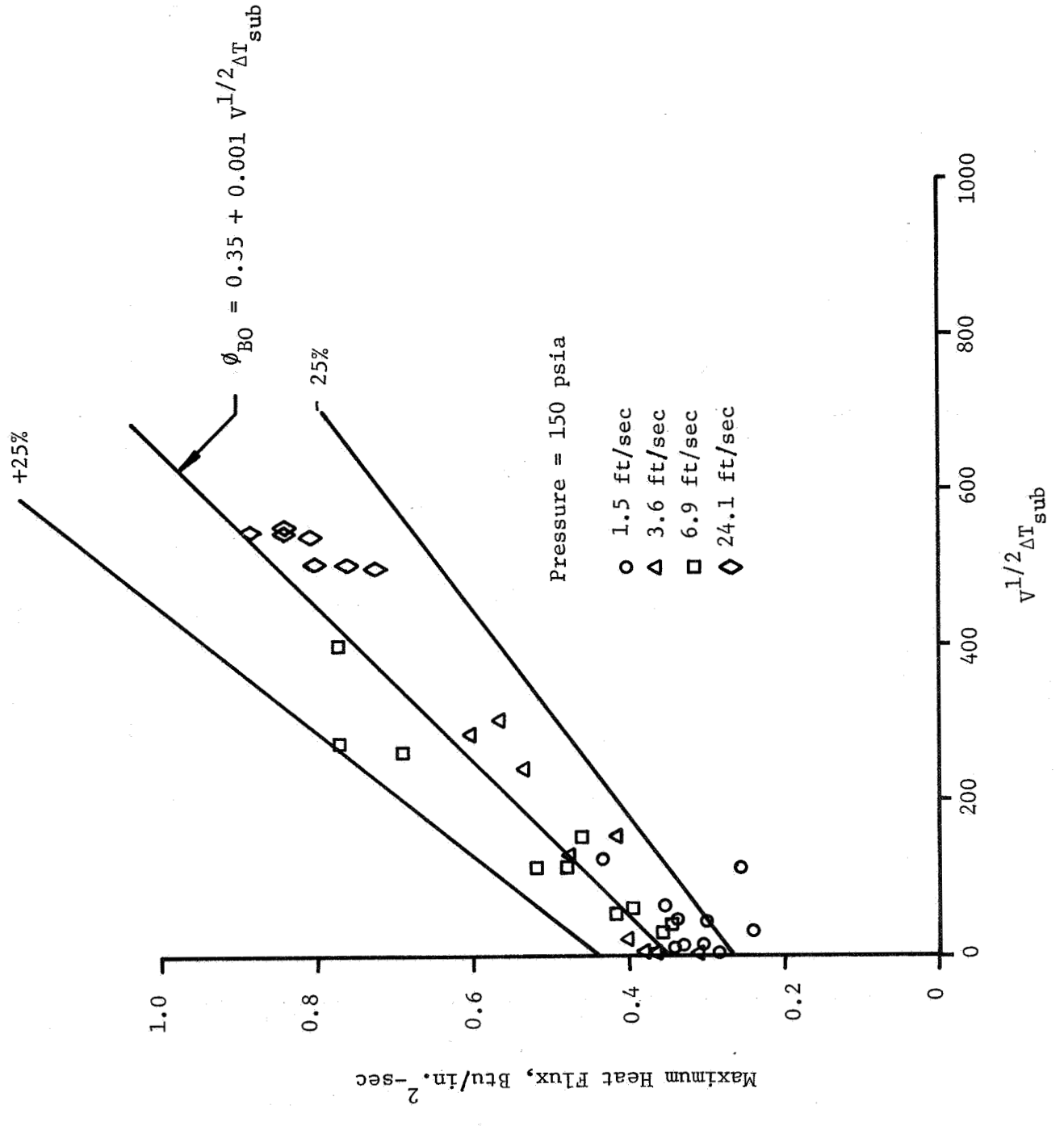

Figure 4. Maximum Heat Flux for Propane

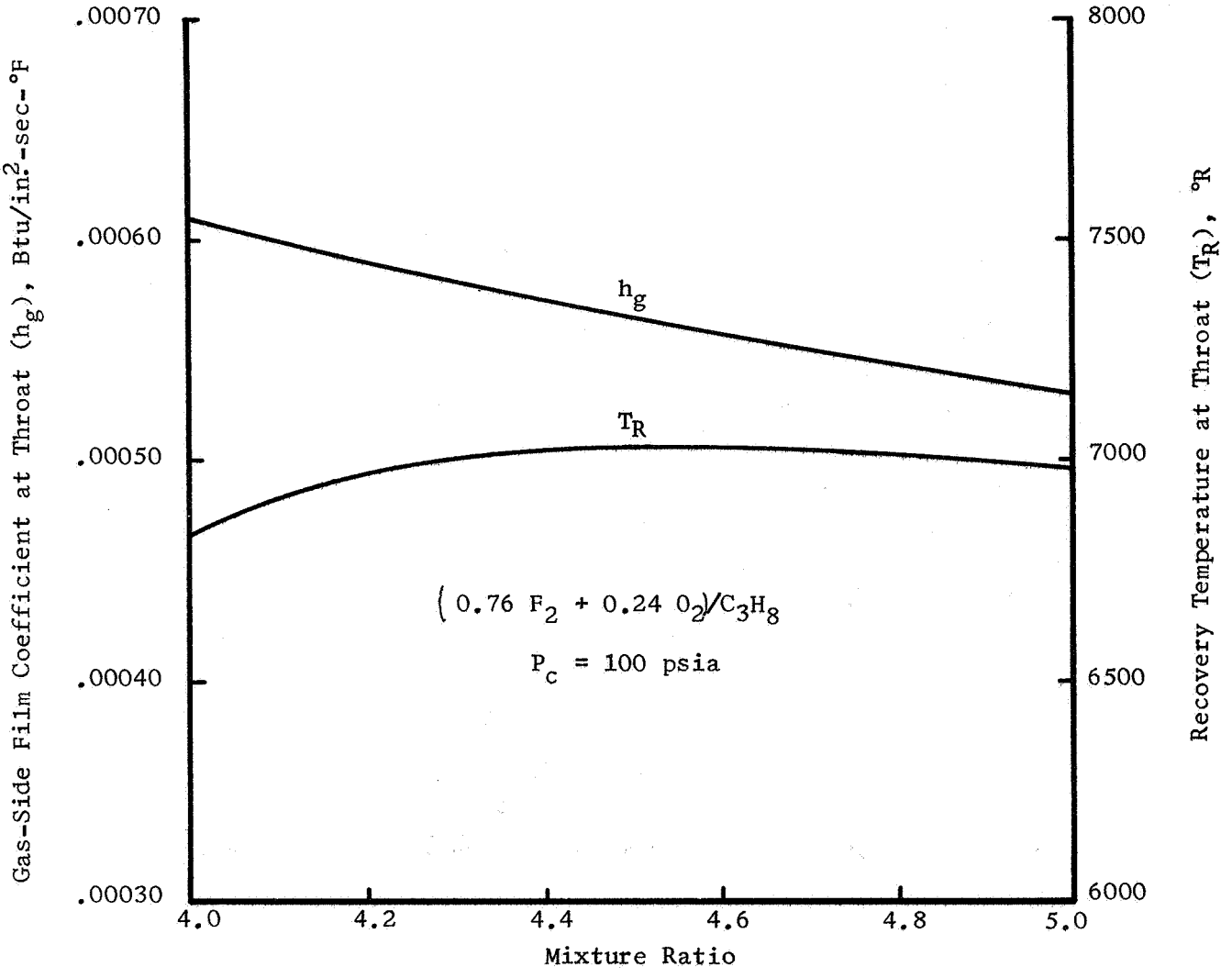

Figure 5. Film Coefficient and Recovery Temperature at Throat of Flox/Propane Chamber.

IV, B, Thermal Analysis (cont.)

The coolant-side convective heat-transfer correlation derived by Hines (Reference 15) (Equation 4) was used for both water and propane coolants.

$$h_L = \frac{0.005\ K_B}{D_h} \quad Re_B^{0.8} Pr_B^{0.4} \qquad \text{(Eq 4)}$$

where h_L = coolant film coefficient
K_B = thermal conductivity of coolant
D_h = hydraulic diameter
Re_B = Reynold's number of coolant
Pr_B = Prandtl number of coolant

The thermal analysis was made with the assumption that the entire converging-diverging nozzle was regeneratively cooled with propane. The uncoated tube-wall temperature was found to be 300°F. However, the heat flux will exceed the known burnout limits of the propane for practical coolant velocities.

The effect of coating resistance on the minimum required coolant velocity* and the gas-side wall temperature for a 100 psia chamber pressure are shown in Figure 6. A coating resistance of 3000 to 4000 $in.^2$-sec°F/Btu is required with velocities of 10 to 50 ft/sec, and coating temperatures of 4200 to 4700°F. The coolant pressure drop is 100 psi or less for this velocity range. Injector-region cooling requires a greater coating resistance (Figure 6) than the throat, even though the heat flux is lower in this region. This is due to the high bulk temperatures which decreases the subcooling and the propane burnout flux.

*The minimum required coolant velocity is the transition from nucleate boiling to film boiling.

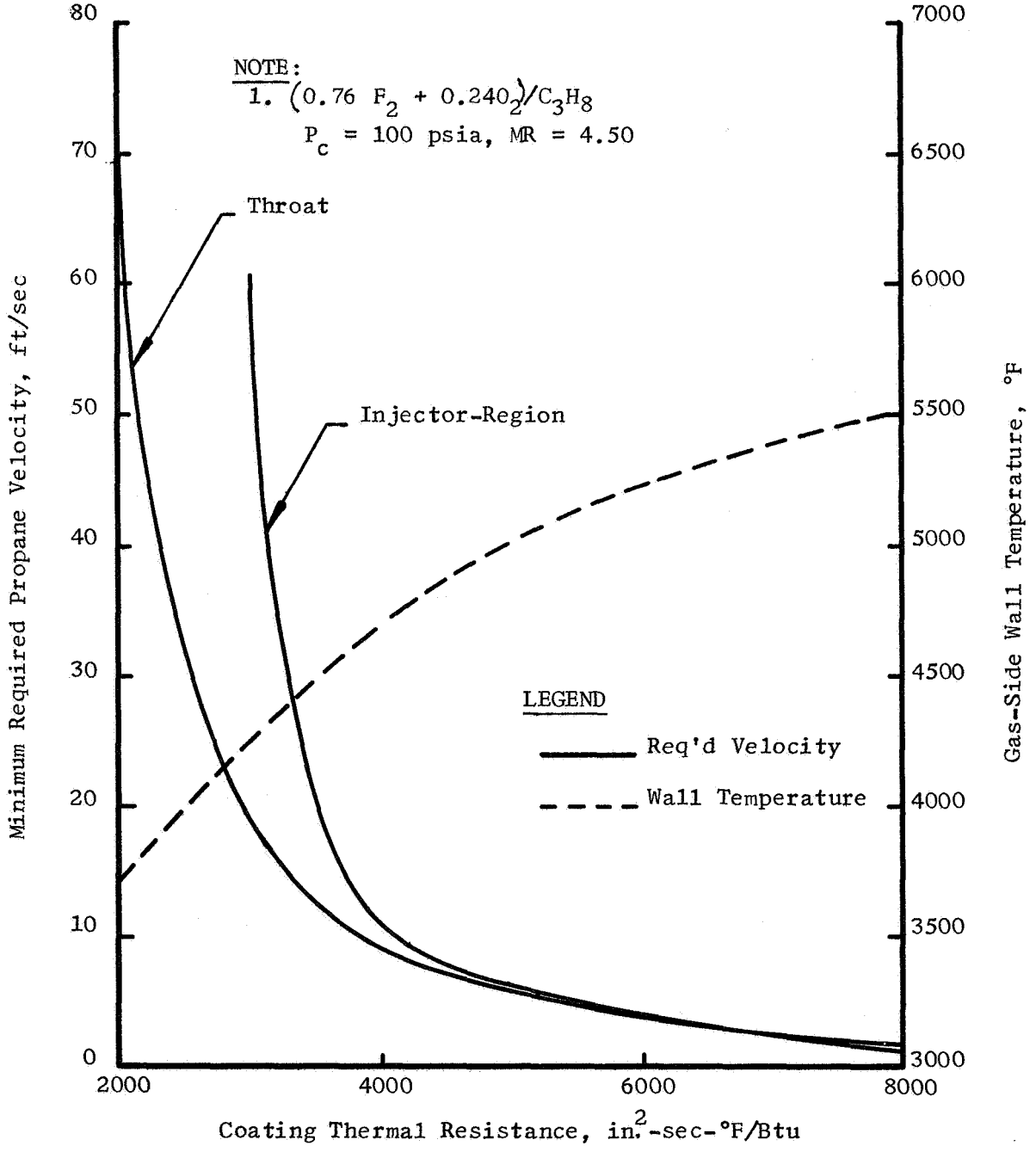

Figure 6. Effect of Thermal Resistance on Minimum Required Propane Coolant Velocity.

IV, B, Thermal Analysis (cont.)

Higher chamber pressure necessitated still larger coating resistances and higher coating temperatures to maintain the wall heat flux below the propane burnout flux. The required coating resistance and coating temperature range for 300 and 500 psia pressures are compared to the 100 psia requirements, as follows:

Chamber Pressure, psi	Required Coating Resistance, $in.^2$-sec°F/Btu	Maximum Coating Temperature, °F
100	3000 to 4000	4200 to 4700
300	3800 to 5800	6000 to 6300
500	4100 to 6300	6400 to 6700

To cool the entire chamber, excessive thermal resistance and excessively thick barriers would be required to keep bulk temperature at a reasonable level. Therefore, another analysis was made assuming only the throat region extending 2-in. upstream and 2-in. downstream was regeneratively cooled. With this approach, realistic coating thickness would be used along with an ablative, heat sink, or radiation-cooled converging on diverging areas.

Throat-region cooling permits the use of coatings with thermal resistance of about 1000 to 1500 $in.^2$-sec°F/Btu because the coolant velocity will be lower and the coolant velocity greater, resulting in a higher propane burnout flux. The required coolant velocity for chamber pressures of 100, 200, and 300 psia are shown in Figure 7 as a function of coating resistance, together with curves of constant coating temperature and pressure drop.

In Figure 7, an area was mapped out on the basis of coolant pressure drops of less than 90 psi, chamber pressures between 100 and 200 psia, and coating surface temperatures of 3000 to 4000°F. In this area, coating thermal resistance ranged from 1200 $in.^2$°F/Btu to 1800 $in.^2$°F/Btu, which established the thermal resistance requirements for the coating. To maintain surface

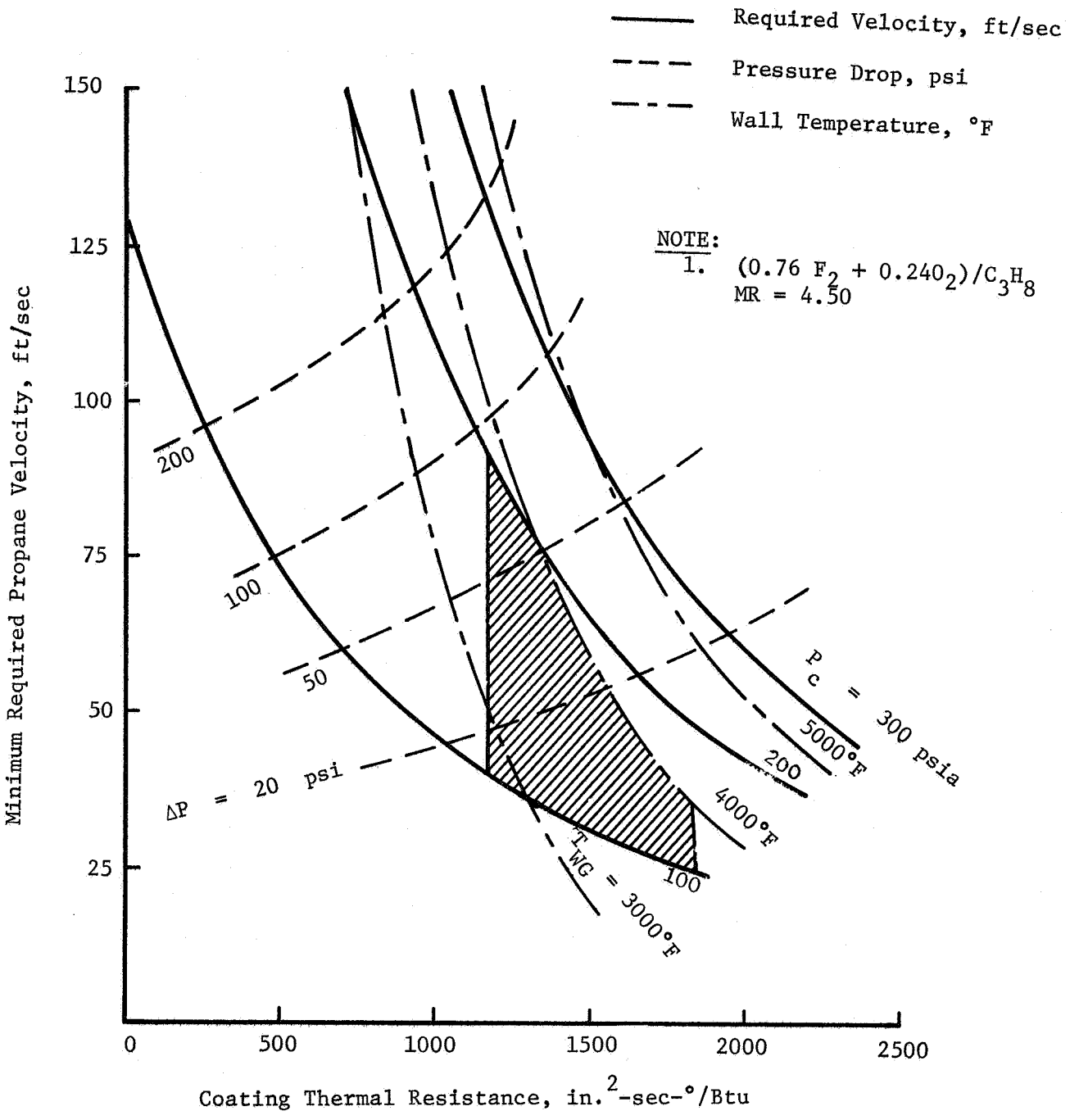

Figure 7. Coating Requirements for Propane Cooled Throat Region as Function of Coolant Velocity, Chamber Pressure, Pressure Drop, and Coating Surface Temperature.

temperatures at 3000°F and chamber pressures of 100 psia, a thermal resistance of 1400 $in.^2$-sec°F/Btu was selected for coatings.

Maximum heat flux at the throat and coating surface temperatures as a function of thermal resistance are shown in Figure 8. The heat flux for a thermal resistance of 1400 $in.^2$-sec°F/Btu and surface temperature of 3000°F is 2 Btu/$in.^2$-sec. This heating condition was selected for the plasma-arc heat source to simulate the throat conditions of a 100 psia flox/propane chamber.

C. MATERIAL SELECTION

The thermal barrier consists of a mixture of metal phase to provide high-temperature ductility and ceramic oxide to lower thermal conductivity. The concentration of the metal phase and ceramic oxide must be compromised to obtain a successful coating. With high concentrations of metal phase, thermal shock resistance increases. This may be offset by the increased coating thickness needed to provide thermal resistance.

The physical and thermal properties of the dense materials with melting points above 3000°F are shown in Table I. Thermodynamic calculations were made with the candidate materials and the exhaust gas species using available free-energy data (References 16, 17, and 18). The calculations were made with the assumption that complete equilibrium is reached and that the reaction occurred at 70 psia and at temperatures of 3000, 4000, and 5000°F. The results of these calculations are shown in Table II. Positive numbers indicate that the reactions will not occur.

The results of the thermodynamic analysis on the compatibility of the refractory metals with the exhaust gas species are summarized in Table III. At 3000°F, all of the metals except Hf are compatible with HF, but all of the

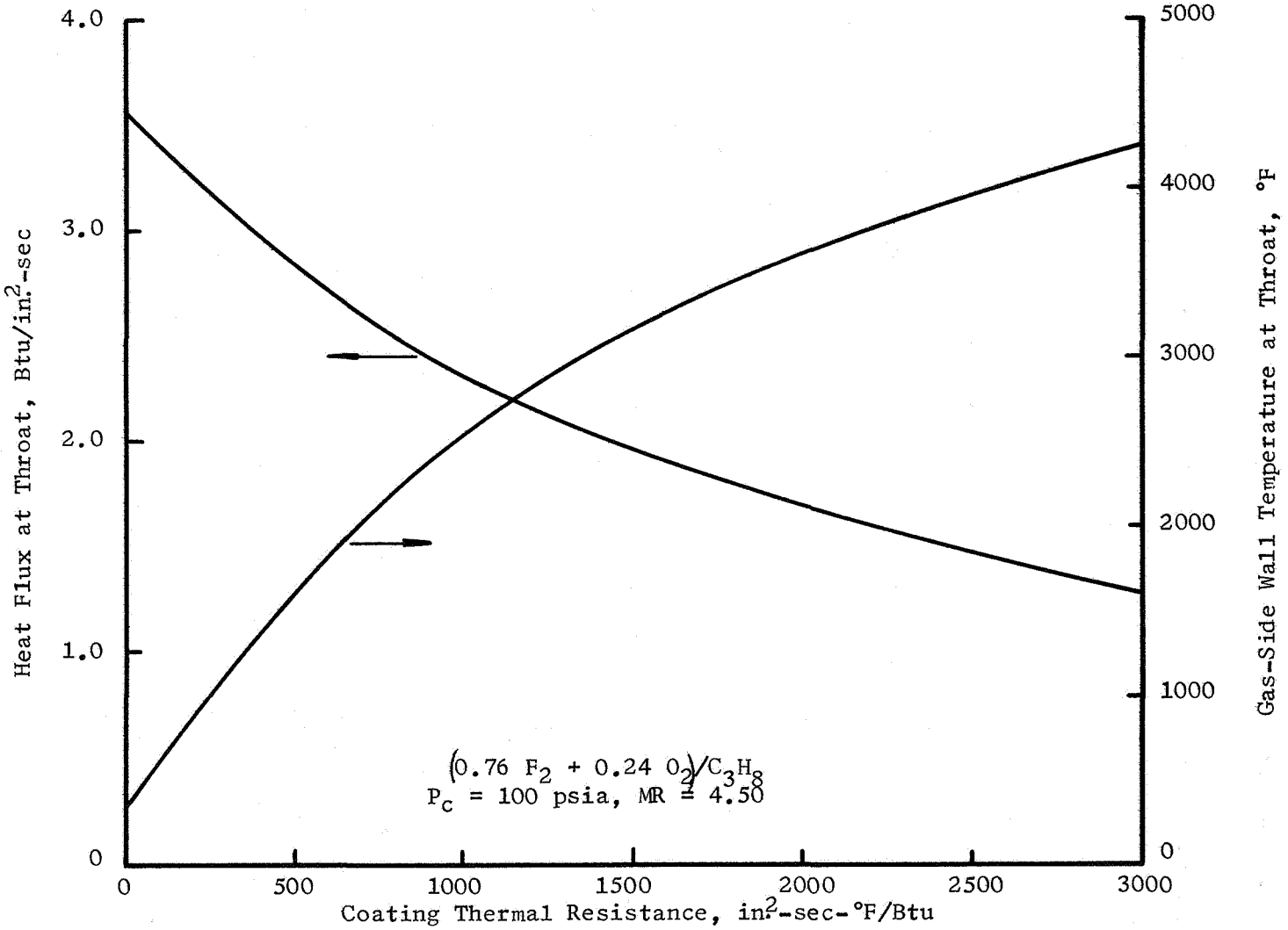

Figure 8. Thermal Resistance as a Function of Heat Flux and Wall Temperature at Throat with Propane Regenerative Cooling.

TABLE I

PROPERTIES OF PROSPECTIVE THERMAL BARRIER MATERIALS

Material	Melting Point, °F	Density, lb/ft^3	Thermal Conductivity, Btu/hr/ft-°F			Thermal Expansion % from Room Temperature to		
			500°F	3000°F	4000°F	500°F	3000°F	4000°F
Refractory Metals								
W	6170	1204	73	60	56	0.1	0.75	1.05
Mo	4760	638	72	46	40	0.15	1.1	1.6
Ir	4429	1405	84	--	--	0.16	1.5	--
Hf	4032	817	12.2	--	--	0.15	0.55(1800°F)	--
Ta	5425	1037	35	47	49	0.25	1.3	1.8
Re	5740		41(RT)	--	--	--	1.1	--
Graphites								
Graphite (Molded)	6600(Sub)	108	60	25	20	0.1	0.5	0.9
Pyrolytic a-Axis	6600(Sub)	137	130	45	45	0.01	0.35	0.45
b-Axis			1.2	0.6	0.5	0.2	4.5	5.5
Oxides								
Al_2O_3	3630	250	12	3.42	--	0.2	1.5	--
BeO	4540	188	125	10	15	0.3	1.8	2.5
HfO_2	5260	604	0.95	0.8	--	0.25	1.3	--
MgO	5070	223	12	2.5	4.0	0.25	2.4	3
SiO_2	3110	165	2.7	1.5	--	0.002	1.75(1800°F)	--
ThO_2	5910	624	5	1.0	--	0.25	1.6	--
ZrO_2 + 3% CaO	4700	360	0.9	1	1	0.25	1.7	--
Carbides								
TiC	5780	307	10	20	20	0.2	1.2	1.9
TaC	7010	899	19	20	20	0.2	0.8	1.2
WC	4710	985	--	30	32	0.1	0.8	1.3
ZrC	6380	427	28	22	25	0.25	1.2	1.9
HfC	7030	792	--	10	14	0.15	1.1	1.5
SiC	4500	200	50	6	--	0.2	1.0	1.5
Nitrides								
BN	4990	141	15	10	9	0.1	2+	--
TaN	5594	900	5	15	20	0.1	0.7	1
Borides								
TiB_2	5320	281	--	23	28	0.2	1.2	1.8
ZrB_2	5500	380	24	12	17	0.2	0.9	1.3

TABLE II

FREE ENERGY OF REACTIONS FOR MATERIALS EXPOSED TO
EXHAUST OF FLOX/PROPANE AT 70 PSIA AT THREE TEMPERATURES

FREE ENERGY OF REACTION, ΔF, kcal-mole^{-1} AT 70 PSIA

Wall Temperature	3000°F					4000°F					5000°F				
Gas Species Reacting	HF	CO	H	F	C_2F_2	HF	CO	H	F	C_2F_2	HF	CO	H	F	C_2F_2
METALS:															
$W + 6HF = WF_6 + 3H$	100					137					166				
$4W + 3CO = 3WC + WO_3$		66					152					WC,d			
$2W + 2CO = W_2C + CO_2$		20					41					86			
W + H = No Reaction															
$W + 6F = WF_6$				-266					-180					-108	
$7W + 3C_2F_2 = 6WC + WF_6$					-461					-214					WC,d
$Mo + 6HF = MoF_6 + 3H_2$	59					90					116				
$Mo + 2CO = MoC + CO_2$		-4					18					37			
Mo + H = No Reaction															
$Mo + 6F = MoF_6$				-285					-240					-221	
$Mo + C_2F_2 = MoC + MoF_6$					-102					-49					-8
$Ir + 6HF = IrF_6 + 3H_2$	349					371					388				
$Ir + 2CO = IrO_2$ (UNSTABLE) + 2C		109					186					219			
Ir + H = No Reaction															
$Ir + 6F = IrF_6$				-17					54					114	
$Ir + C_2F_2 = IrF_6 + 2C$					29					61					87
$Hf + 4HF = HfF_4 + 2H_2$	-108					-88					-73				
$3Hf + 2CO = HfO_2 + 2HfC$		-27					16					35			
Hf + H = Reacts															
$Hf + 4F = HfF_4$				-352					-299					-256	
$Hf + 2C_2F_2 = HfF_4 + 4HfC$					-396					-340					-297
$2Ta + 10HF = 2TaF_5 + 5H_2$	250					467					622				
$Ta + 2CO = TaC + CO_2$		-3					19					37			
Ta + H = Reacts															
$Ta + 5F = TaF_5$				-180					-30					102	
$12\ Ta + 5C_2F_2 = 10\ TaC + 2\ TaF_5$					-410					-158					-108
$Si + 4HF = SiF_4 + 2H_2$	-57					-35					-14				
$3\ Si + 2CO = 2SiC + SiO_2$		-46					+13					+55			
Si + H = Reacts															
$Si + 4F = SiF_4$				-301					-246					-197	
$5Si + 2C_2F_2 = 4SiC + SiF_4$					-245					-189					-150
OXIDES:															
$Al_2O_3 + 6HF = 2AlF_3 + 3\ H_2O$	29					34					43				
$Al_2O_3 + 6H = 2Al + 3H_2O$			-29					10					18		
$2Al_2O_3 + 12F = 4AlF_3 + 3O_2$				-452					-392					-427	
$2Al_2O_3 + 3C_2F_2 = 2AlF_3 + 6CO + 2Al$					-168					-273					-365
$ZrO_2 + 4HF = ZrF_4 + 2H_2O$	-71					-39					-8				
$2ZrO_2 + 2CO = 2ZrC + 3O_2$		202					228					253			
$ZrO_2 + 2H = Zr + H_2O$			-14					11					31		
$ZrO_2 + 4F = ZrF_4 + O_2$				-241					-190					-146	
$ZrO_2 + 2C_2F_2 = ZrF_4 + CO_2 + 3C$					-220					-188					-162
$HfO_2 + 4HF = HfF_4 + 2H_2O$	-105					-73					-47				
$2HfO_2 + 2CO = 2HfC + 3O_2$		125					169					115			
$HfO_2 + 4H = Hf + 2H_2O$			-121					-72					-55		
$HfO_2 + 4F = HfF_4 + O_2$				-279					-226					-185	
$HfO_2 + 2C_2F_2 = HfF_4 + CO_2 + 3C$					-248					-224					-201

TABLE II (cont.)

FREE ENERGY OF REACTION, ΔF, kcal-mole^{-1} AT 70 PSIA

Wall Temperature	3000°F					4000°F					5000°F				
Gas Species Reacting	HF	CO	H	F	C_2F_2	HF	CO	H	F	C_2F_2	HF	CO	H	F	C_2F_2
OXIDES (cont.)															
$SiO_2 + 4HF = SiF_4 + 2H_2O$	11					23					36				
$2SiO_2 + 2CO = 2SiC + 3O_2$		380					360					341			
$SiO_2 + 4H = Si + 2H_2O$			84					-21					-5		
$SiO_2 + 4F = SiF_4 + O_2$				-165					-138					-111	
$SiO_2 + 2C_2F_2 = SiF_4 + CO_2 + 3C$					-138					-128					-118
BORIDES:															
$ZrB_2 + 8HF = ZrF_4 + 2BF_2 + 4H_2$	-31					-25					-17				
$ZrB_2 + 3CO = ZrC + B_2O_3 + 2C$		16					70					120			
$ZrB_2 + 6H = Zr + B_2H_6$			-21					52					107		
$ZrB_2 + 4F = ZrF_4 + 2B$				-255					-210					-172	
$ZrB_2 + 2C_2F_2 = ZrF_4 + 4C + 2B$					-139					-113					-93
$TiB_2 + 8HF = TiF_4 + 2BF_2 + 4H_2$	-11					-5					3				
$TiB_2 + 3CO = TiC + B_2O_3 + 2C$		9					51					123			
$TiB_2 + 6H = Ti + B_2H_6$			-32					40					94		
$TiB_2 + 4F = TiF_4 + 2B$				-235					-190					-152	
$TiB_2 + 2C_2F_2 = TiF_4 + 4C + 2B$					-119					-93					-73
CARBIDES:															
$TiC + 4HF = TiF_4 + CH_4$	8					39					62				
$TiC + 2CO = TiO_2 + 3C$		78					97					111			
$TiC + 4H = Ti + CH_4$			-60					-51					19		
$TiC + 4F = TiF_4 + C$				-258					-209					-168	
$TiC + 2C_2F_2 = TiF_4 + 5C$					-142					-112					-87
$TaC + 5HF = TaF_5 + CH_4 + H$	211					329					425				
$TaC + 2CO = TaO_2 + 3C$		108					128					146			
$TaC + 4H = Ta + CH_4$			-64					-53					20		
$TaC + 5F + 4H = TaF_5 + CH_4$				-244					-47					122	
$TaC + 5F = TaF_5 + C$				-98					4					137	
$2TaC + 5C_2F_2 = 2TaF_5 + 12C$					-2					250					472
$WC + 6HF = WF_6 + CH_4 + H_2$	132					63					WC-decomposes				
$WC + 3CO = WO_3 + 3C$		106					192					WC-d			
$WC + 4H = W + CH_4$			-142					-41					WC-d		
$WC + 6F = WF_6 + C$				-256					-170					WC-d	
$WC + 3C_2F_2 = WF_6 + 7C$					-50					-9					WC-d
$ZrC + 4HF = ZrF_4 + CH_4$	-19					10					32				
$ZrC + 2CO = ZrO_2 + 3C$		82					101					116			
$ZrC + 4H = Zr + CH_4$			-56					-11					22		
$ZrC + 4F = ZrF_4 + C$				-285					-238					-194	
$ZrC + 2C_2F_2 = ZrF_4 + 5C$					-169					-143					-107
$HfC + 4HF = HfF_4 + CH_4$	-46					-21					4				
$HfC + 2CO = HfF_4 + 3C$		93					106					125			
$HfC + 4H = Hf + CH_4$			-68					-21					13		
$HfC + 4F = HfF_4 + C$				-312					-269					-224	
$HfC + 2C_2F_2 = HfF_4 + 5C$					-196					-172					-147
CARBON:															
$C + HF = CF_4 + 2H_2$	128					153					175				
$C + 4H = CH_4$			-98					-51					-15		
$C + 4F = CF_4$				-134					-81					-36	

TABLE III

COMPATIBILITY OF REFRACTORY METALS WITH
FLOX/PROPANE EXHAUST GAS SPECIES

Material	Compatibility at 3000°F and 70 psia that is based on Free Energy Calculations[1]				
	HF	CO	H	F	C_2F_2
W	NR	NR	NR	R	R
Mo	NR	R	NR	R	R
Ir	NR	NR	--	R	NR
Hf	R	R	--	R	R
Ta	NR	R	--	R	R
C	NR	--	R	R	--

(1) NR = Reaction not probable
R = Reaction probable

metals react with F_2. W and Ir are compatible with CO. Carbon is compatible with HF but reacts with both H and F.

The results of thermodynamic analysis on the compatibility of the ceramic materials with the exhaust gas species at 3000°F are summarized in Table IV. The ceramic materials are compatible with CO but are generally not compatible with the fluorine gas species or hydrogen. Only Al_2O_3 and SiO_2 are not expected to react with HF.

In addition to the free energy analysis, calculations were made to establish the extent of reactions that occur when the candidate material is exposed to all of the species in the exhaust gas. This method, originated by Gordon and Boerlin (Reference 19), assumes that the material is in complete thermodynamic equilibrium with the exhaust species at a particular temperature and pressure. Consideration is not given to physical surface regression phenomena, such as thermal shock and liquid runoff. All probable reactions of the candidate material and species are considered and involves simultaneous solution of equilibrium constant equations under adiabatic conditions. The results provide the amount of the candidate material that entered into the reaction with the combustion products. This method is used to calculate theoretical compositions of propellant exhaust gases and is programed on the IBM 7094.

The candidate materials along with the exhaust gas species were programed to estimate the amount of wall material expected to react with the exhaust gas. An excess of the candidate wall material was used so that the reactions would theoretically continue until equilibrium was reached. Since the computer program was set up to establish theoretical chemical compositions of propellant exhaust gases, the data on Ir, Hf, Ta, TiC, ZrC, TiB_2, ZrB_2 were not in the computer program.

TABLE IV

COMPATIBILITY OF CERAMICS WITH
FLOX/PROPANE EXHAUST GAS SPECIES

Material	Compatibility at 3000°F and 70 psia that is based on Free Energy Calculations[1]				
	HF	CO	H	F	C_2F_2
Al_2O_3	NR	NR	R	R	R
ZrO_2	R	NR	R	R	R
HfO_2	R	NR	R	R	R
SiO_2	NR	NR	NR	R	R
ZrB_2	R	NR	R	R	R
TiB_2	R	NR	R	R	R

(1) NR = Reaction not probable
R = Reaction probable

IV, C, Material Selection (cont.)

The materials W, WC, Mo, ZrO_2, SiO_2, and Al_2O_3 were programed with the gas species from the throat exhaust products of mixture ratio 4.5 (55.7% HF; 24.7% CO; 1.2% H_2, 8.3% H; 0.1% C_2F_2; and 10% F). One mole of exhaust gas was programed with a 10.1 moles of wall material.

The results shown in Table V indicate that W, WC, and Mo wall materials would not react with the exhaust species at 3000, 4000, and 5000°F, and the Al_2O_3, SiO_2, and ZrO_2 would react with the fluorine compounds.

On the basis of the properties of the candidate materials, including the thermodynamic calculations of chemical reaction with the exhaust gas species and the literature on compatibility of materials with exhaust gases containing fluorine, several thermal barrier compositions were selected.

Tungsten and molybdenum were selected for the metallic base of the coating, because of their high melting temperature and compatibility with the exhaust gas species. The thermal conductivity of these metals is too high to provide coatings with reasonable thicknesses, so the thermal conductivity must be lowered by the addition of ceramic material. Alumina and zirconia were selected because of their high temperature compatibility and past performance as thermal barrier materials.

Gradated coatings were also selected to improve thermal shock resistance of the coating and to provide relatively thinner coatings. Nichrome-ZrO_2 mixtures and Ni-Al_2O_3 mixtures were selected to provide the thermal resistance in undercoats with topcoats of pure Mo or W to provide compatibility with the exhaust gas stream. The use of the nichrome and nickel mixtures were selected to operate at a maximum temperature of 2000°F.

TABLE V

REACTION PRODUCTS FROM COMPUTER PROGRAM MADE WITH THE ASSUMPTION THAT COMBUSTION GASES (MR 4.5) AND CANDIDATE MATERIALS REACH EQUILIBRIUM

Material	Reaction Temperature, °F	Wall Material Reaction Product, Moles
W	3000	None
W	4000	None
W	5000	None
WC	3000	None
WC	4000	None
WC	5000	None
Mo	3000	None
Mo	4000	None
Mo	5000	None
Al_2O_3	3000	AlF_3 - 0.283
Al_2O_3	4000	AlF_2 0.0001, AlF_3 0.0385, AlOF 0.0078
Al_2O3	5000	AlF 0.0011, AlF_2 0.0024, AlF_3 0.0262, AlOF 0.1037
ZrO_2	3000	ZrF_4 0.0406
ZrO_2	4000	ZrF_3 0.0023, ZrF_4 0.0388
ZrO_2	5000	ZrF_3 0.0100, ZrF_4 0.0351
SiO_2	3000	SiF_3 0.0052, SiF_4 0.0773
SiO_2	4000	SiF_2 0.0008, SiF_3 0.0326, SiF_4 0.0374, SiO 0.0028
SiO_2	5000	SiF_2 0.0038, SiF_3 0.0454, SiF_4 0.0141, SiO 0.0900, SiO_2 0.0076

IV, C, Material Selection (cont.)

In addition to the thermal barrier materials, nichrome was used as a primer because of the success in using it in past programs, and because of the compatibility of nickel and nickel alloys with fluorine gas species. (Reference 20)

D. METAL-CERAMIC MIXTURES

The refractory metal and ceramic oxides must be compatible at the 3000°F surface temperature both chemically and mechanically (expansion), and the thermal resistance of the mixtures must be known to select the coating thickness.

1. Compatibility of Refractory Metals and Ceramics

Available data on the reactivity of the refractory metals with ceramics indicate that W is compatible with ZrO_2 and Al_2O_3 above the melting point of the ceramic (Reference 21). Krier (Reference 22) revealed that Al_2O_3 and ZrO_2 did not react with molybdenum at a temperature of 3272°F. Compatibility above this temperature was not disclosed, but it is estimated to be above 4000°F on the basis of the similarity of W and Mo.

2. Thermal Expansion

The thermal expansion of dense tungsten, molybdenum, and ZrO_2 and Al_2O_3 are shown schematically in Figure 9. The expansion of W and Mo are low compared to the ceramics and nichrome. Mixtures of the ceramics in the metal enhance compatibility with the stainless-steel substrate. In the previous program, the W-Mo and ceramic mixtures were not adversely affected by the difference in expansion as long as sufficient cooling was used to maintain a tube wall interface temperature of 1600°F.

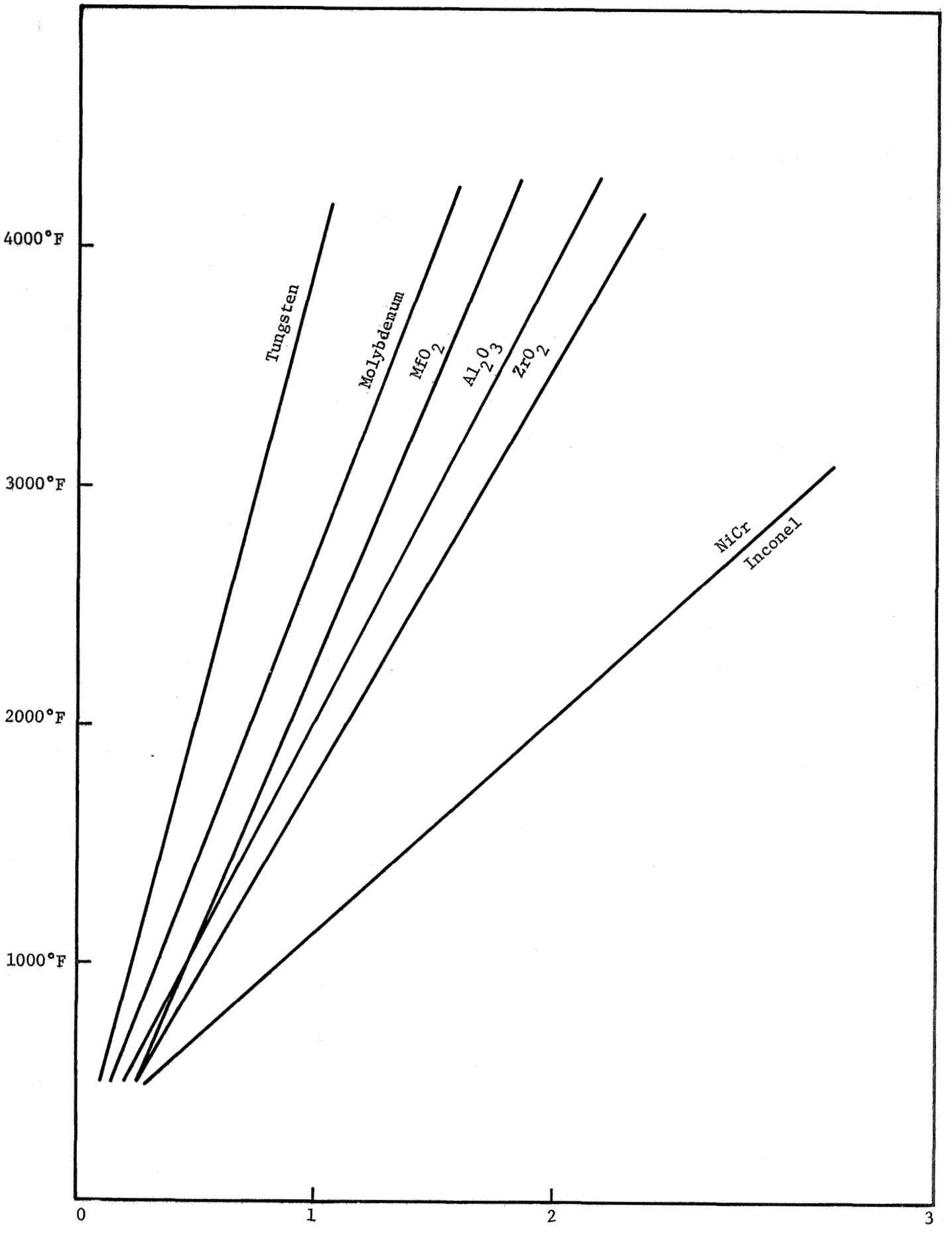

Figure 9. Thermal Expansion of Candidate Materials

3. Thermal Resistance

The thermal resistance of the coating is the thickness/thermal conductivity. The thermal conductivity of sprayed materials is considerably lower than wrought material because of the difference in density shown in Figure 1. The thermal resistance of sprayed mixtures of either W or Mo with ZrO_2 and W or Mo with Al_2O_3 are shown in Figures 10 and 11 as a function of thickness and composition. The thermal conductivity of these coating mixtures were obtained in previous programs in the laboratory using a procedure which will be described in the evaluation section of the report. The thermal conductivity of the deposited material is generally less than 40% (see Figure 1) of handbook values and is a function of the density of the coating.

E. PROCESS SELECTION

Plasma-arc deposition was selected at the start of the program because of its successful use in applying thermal barriers on previous programs.

Plasma-arc deposition has been used to apply a variety of composites, including mixtures of refractory metals and ceramics. The technique is fast, versatile, and can be directly applied to the inside diameter of a chamber in close tolerances. A material that will melt without decomposition can be sprayed by the arc plasma. In addition, oxygen sensitive material can be sprayed since the carrier gas in the plasma can be adjusted to neutral or reducing. Coatings produced by spraying are less dense than pressed and sintered structure. Because of the reduced density, sprayed coatings have lower thermal conductivity and result in thinner coatings than wrought material for a given thermal resistance. The disadvantage of plasma spraying is that it is restricted to substrates of simple, regular shapes because coverage can only be achieved along the line of sight to the spray gun.

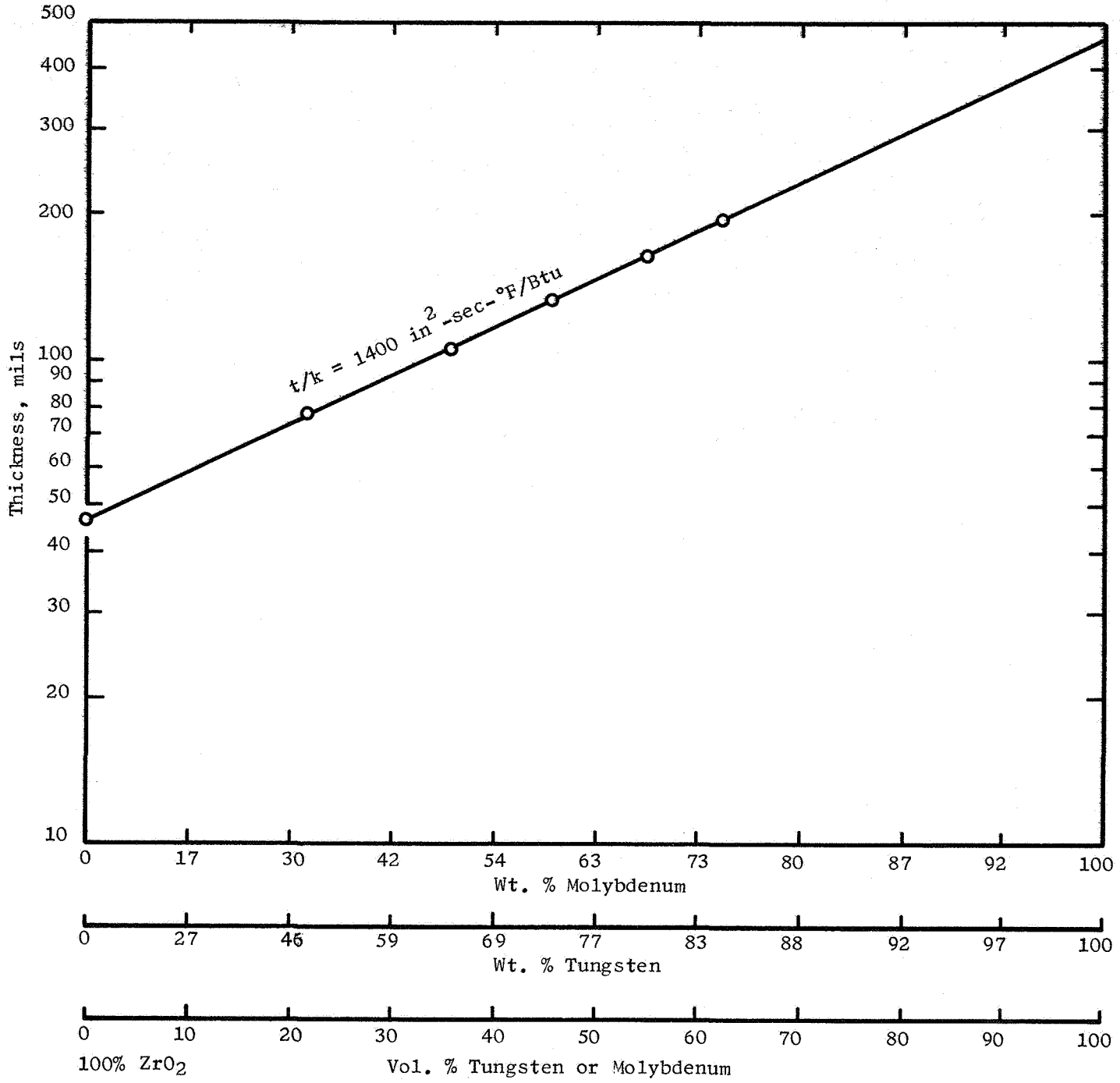

Figure 10. Thermal Resistance as a Function of Coating Thickness and Coating Composition.

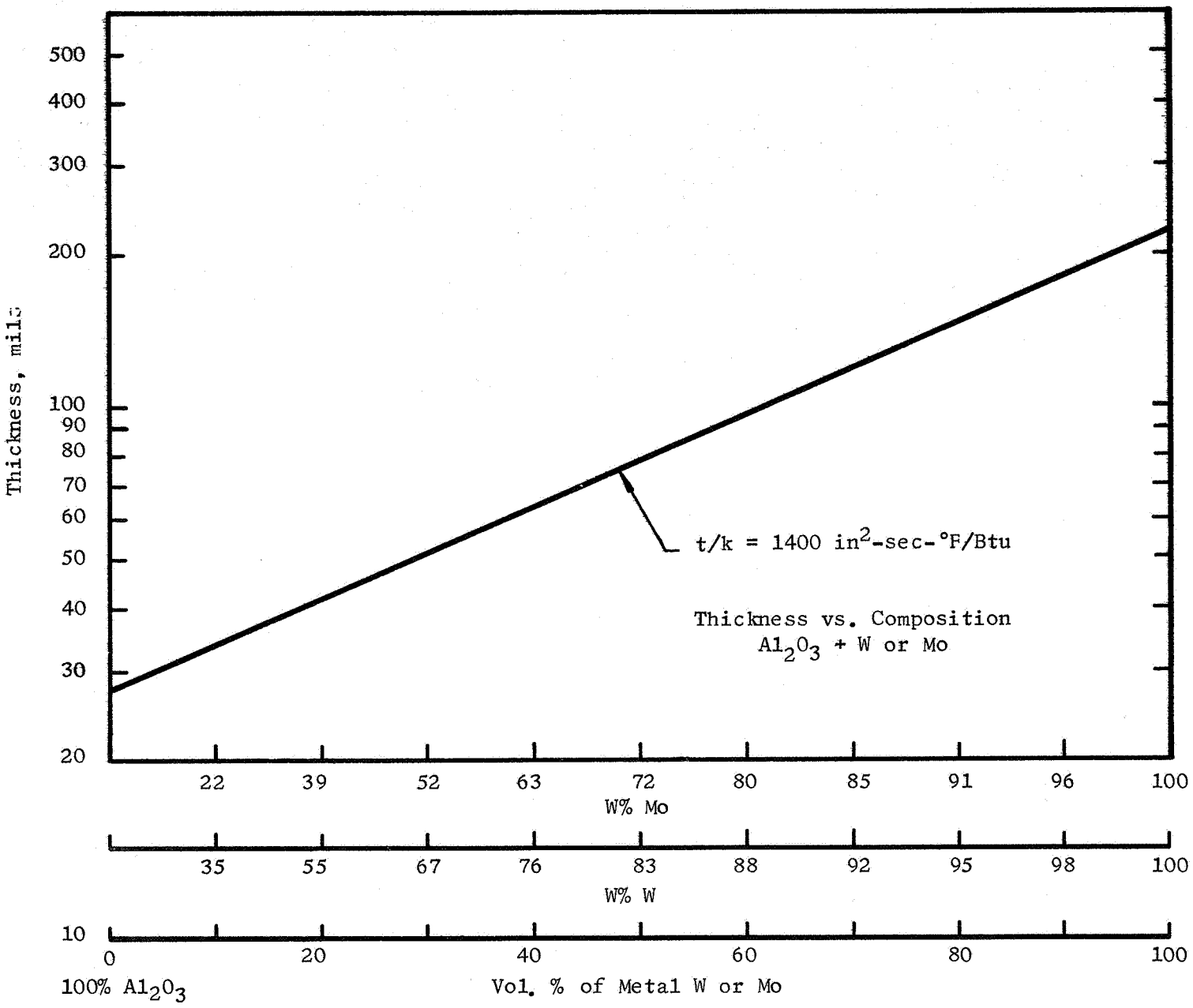

Figure 11. Thermal Resistance as a Function of Thickness and Composition.

V. EXPERIMENTAL PROCEDURES

A. SPECIMEN PREPARATION

Two types of specimens were used in the testing of the thermal barrier -- a disk coupon, and a five-tube internally cooled specimen shown in Figure 12. Both the disk specimens and the 5-tube specimens were evaluated in the laboratory and the 5-tube specimen was evaluated in the exhaust stream of flox/propane combustors.

The disk specimen was used for inexpensive screening of candidate coatings to narrow the field of promising coating specimens for final evaluation with the more expensive 5-tube specimen. The disk specimens were prepared by plasma torch spraying a candidate coating on a stainless-steel disk (0.025-in. thick x 3.25-in. dia). The disks were first grit-blasted on one surface using 24-mesh silicon carbide grit to produce a 250 to 300 RMS micro-inch surface roughness. A 0.25-in.-wide ring at the perimeter of the disk was shielded from the grit blast to provide a sealing surface for O-rings when the disk is installed in a water-cooled holding fixture.

After grit-blasting the disks were plasma-spray coated using a 35 kw plasma torch (Model 57, TAFA Division, Humphreys Corp.), a powder feeder (Sylvester Corp. Mark IX), and specimen-positioning fixture.

The plasma torch was mounted horizontally on a screw-driven traversing head to permit lateral traverse across the specimen face at a programed speed of 12 in./min. The powder was fed through the Mark IX powder feeder. The feed rate varies with the type of powder or mixture being sprayed, and the thickness of deposit required. The feed rate was regulated by the feed screw on the powder feeder. A shield of argon gas was also maintained around the spray cone and spray impingement area to exclude air from the test specimen hot surface.

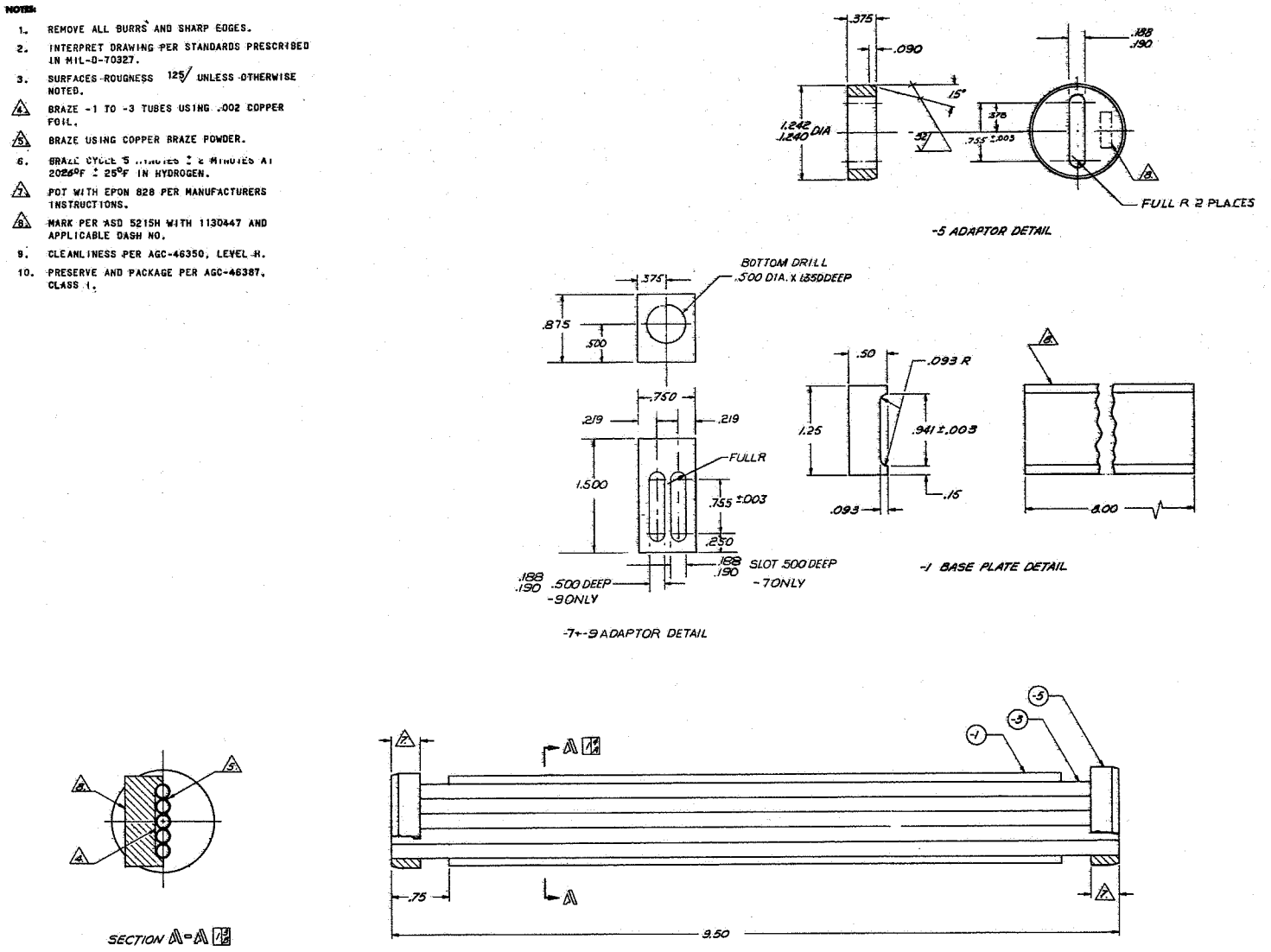

Figure 12. 5-Tube Specimen

V, A, Specimen Preparation (cont.)

The disk test specimen and 5-tube specimen were held in a frame that was mechanically oscillated vertically in front of the torch at a predetermined oscillation rate and amplitude (specimen surface speed -- 300 in./min). During deposition, cooling water was pumped through the specimen holder (disk specimen) or specimen tubes. The deposition rate of the plasma sprayed coatings was about 2 mils/pass.

B. LABORATORY DISK AND 5-TUBE PLASMA TESTS

The equipment for thermal shock testing of thermal barrier coatings on disk specimens and on 5-tube specimens was similar to that used for spraying. One difference was the addition of a specially designed test bench for cycling specimens in the plasma torch flame under controlled heat flux conditions. The torch generated heat flux was measured with a water-cooled calorimeter and the specimen flame surface temperature was continuously measured with a recording pyrometer. Plasma gases were supplied to the torch through flowmeters. Specimen holders, calorimeter and torch were cooled by a high-pressure water system. The disk and 5-tube specimens were tested with heat fluxes of approximately 2.4 Btu/in.^{2}-sec-°F, the values established in heat transfer analysis.

Distance of the gun nozzle from the specimens or calorimeter was adjusted to obtain the heat flux required at the specimen surface. The plasma flame carrier gas was nitrogen with argon gas introduced just downstream of the nozzle to provide an inert gas shield over the flame impingement area.

The heat flux at the specimen surface was measured with a water-cooled circular foil calorimeter. The desired heat flux (2.4 Btu/in.^{2}-sec-°F) for a particular test series was established by adjusting the nozzle to calorimeter distance and regulating the power input.

V, B, Laboratory Disk and 5-Tube Plasma Tests (cont.)

Test specimens were mounted on either side of the calorimeter on a rotating head with hot surfaces at the same distance from the nozzle. Manual rotation of the holding fixture presents either test specimen or the calorimeter in turn to the plasma torch flame. This ensured that the specimens were exposed to the same heat flux as measured by the calorimeter. The calorimeter and specimens were cooled by high-pressure (150 psig), high-velocity water flow.

Coating surface temperature was continuously recorded during flame exposure with a Pyro-650 recording pyrometer (Instrument Development Laboratories, Inc.). The pyrometer was aligned to view the center of the plasma flame impingement area on the specimen before each test.

The condition of the coatings during flame exposure was observed by direct vision to detect melting, cracking, or spalling. Following thermal shock testing, a further visual examination under 40X magnification was made of the coatings.

The thermal resistance of the coatings was calculated by using the gas-side surface temperature from a Pyro-650 optical pyrometer and heat flux measurement from the water-cooled copper calorimeter. A water side temperature of 350°F was used which was the saturation temperature for 150 psi pressure water. The calculations were based on the equation:

$$Q/A \text{ (heat flux)} = \frac{T_g \text{ (gas-side temperature)} - T_2 \text{ (water-side temperature)}}{t/_K \text{ (stainless steel)} + t/_K \text{ (coating)}}$$

where t = thickness and K = thermal conductivity

The accuracy of this method was ascertained by comparing the thermal conductivity of similar coatings made by the above method and by the

flash method of determining thermal conductivity (Reference 23). The data obtained from both methods from similar coatings was comparable as shown in Figure 13.

C. FLOX/PROPANE -- 5-TUBE TESTS

The flox/propane test was designed to establish the compatibility of the thermal barrier coatings with the thermal and chemical environment of the exhaust stream of a flox/propane engine.

The flox tank was insulated and jacketed with LN_2 and the oxidizer lines to the injector were contained in insulated troughs flooded with LN_2 before and during the tests. The oxidizer tank was pressurized with helium which was also used for the oxidizer purge. The flox composition was obtained by filling the correct proportions of fluorine and oxygen from the pressurized gas bottles prior to the tests.

The propane tank was insulated and jacketed with LN_2 and the temperature maintained by adjusting the pressure of the LN_2. The fuel pressurization and purge gas was nitrogen.

1. Combustor Components

The combustor consists of the valves, injector, and combustion chamber. Two injectors and two combustor chamber combinations were used in the evaluation program.

a. A six-element water-cooled injector (PN 1131125) was used for the first six test firings. The orifice pattern of the injector consists of six triplets (F-O-F) elements with the fuel orifices 0.020 in. dia

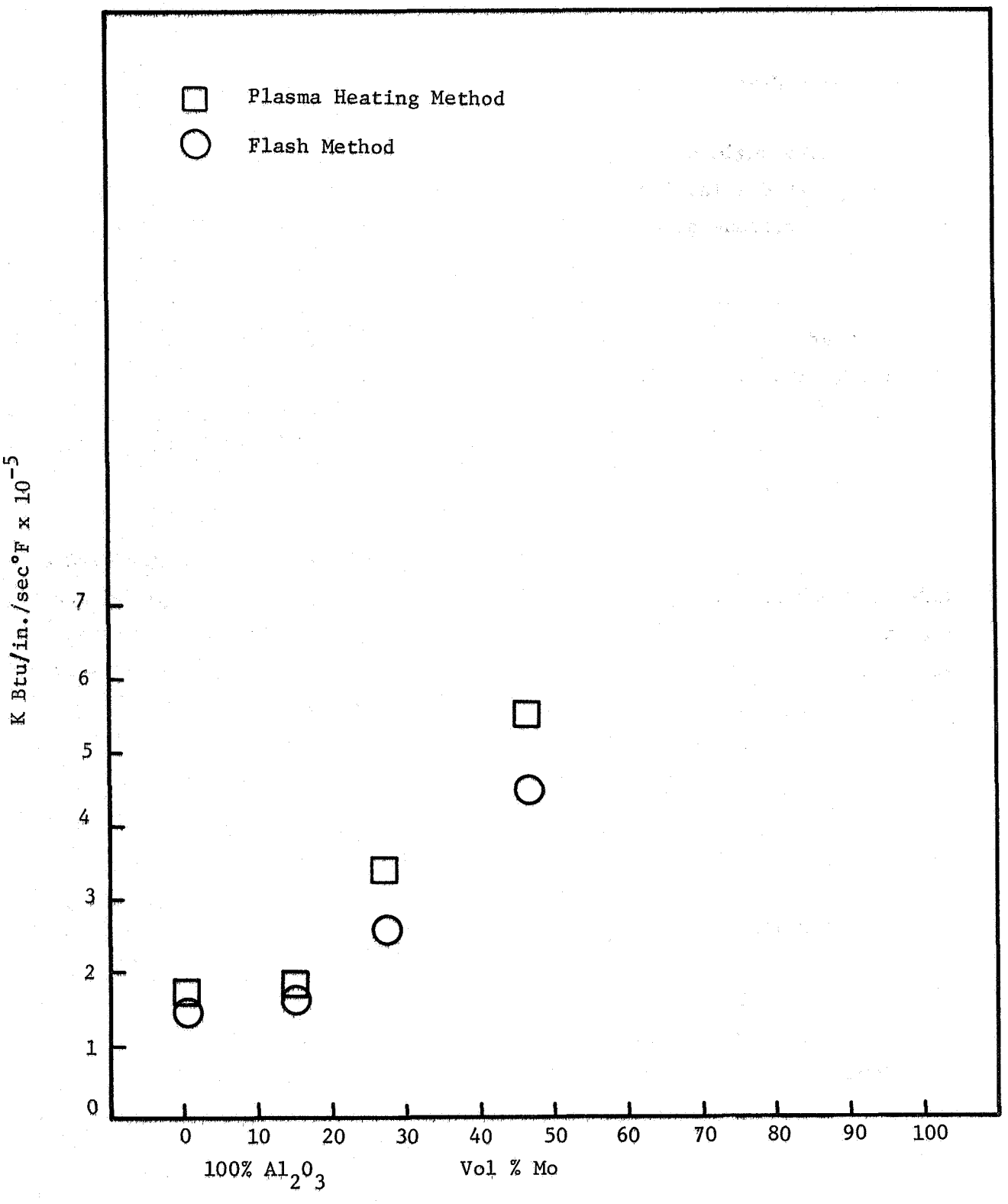

Figure 13. Comparison of Thermal Conductivity of Mo-Al_2O_3 Mixtures as Determined by the Plasma Heating Method and Flash Method.

at an included angle of 60 degrees. The oxidizer orifices are 0.051 in. dia and impinge at 0.2 in. from the injector face. The use of this injector was discontinued because of the low performance, 79 to 83% c*.

b. A 17-element injector, PN 709151-21, was used for the remainder of the program. The performance with the injector ranged from 86 to 94% of c*. The orifice pattern is shown in Figure 14 and consists of nine triplets (F-O-F) and eight doublets (O-F). The fuel orifices are 0.0177 in. dia and the oxidizer orifices are 0.0295 in. dia. The face of the injector was fabricated from nickel.

c. The original chamber consisted of a steel case with a 1/2-in.-thick graphite liner, 2-1/4-in. ID and 15 in. long. In the 50-sec tests, the steel shell melted at the steel-graphite liner interface. To prevent melting, the steel shell was wrapped with copper tubing to provide a water coolant jacket. The graphite liner was wedged into the chamber, and had to be replaced after each test because of cracking.

The second chamber and the one used with 17-element injector was water-cooled with water-cooled adapters to hold the injector and the nozzle (Figure 15). The graphite extended the full length of the chamber. This graphite chamber was used for eight test firings without cracking.

The water-cooled nozzle used for all of the tests is shown in Figure 15. The nozzle insert was fabricated from Nickel 200 with the coolant flow directed axially with water inlets at the forward end and the outlets rotated 90 degrees at the aft end. The throat diameter of the chamber is 1.135 in.

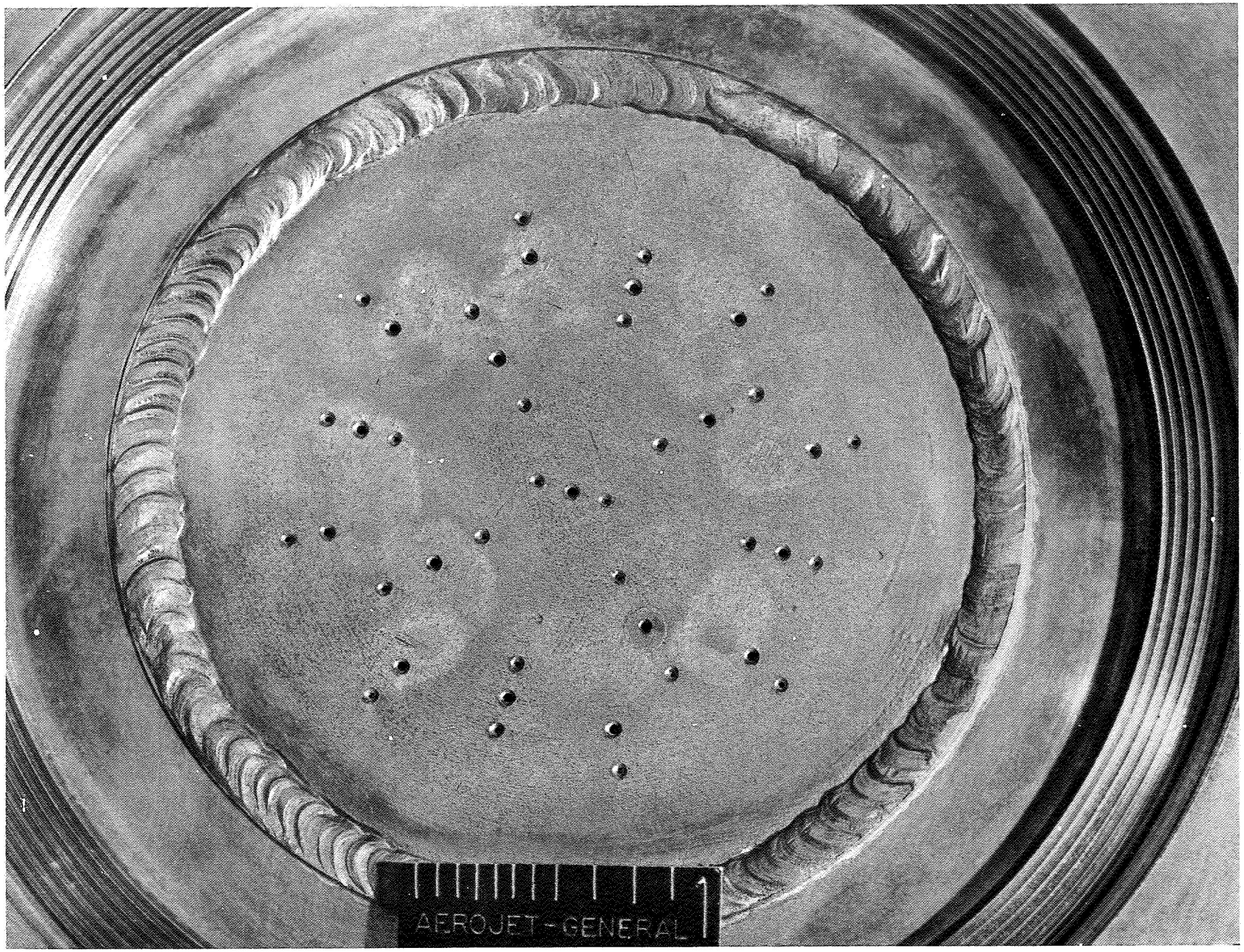

Figure 14. Orifice Pattern for 17 Element Injector.

VKC Neg. 168209

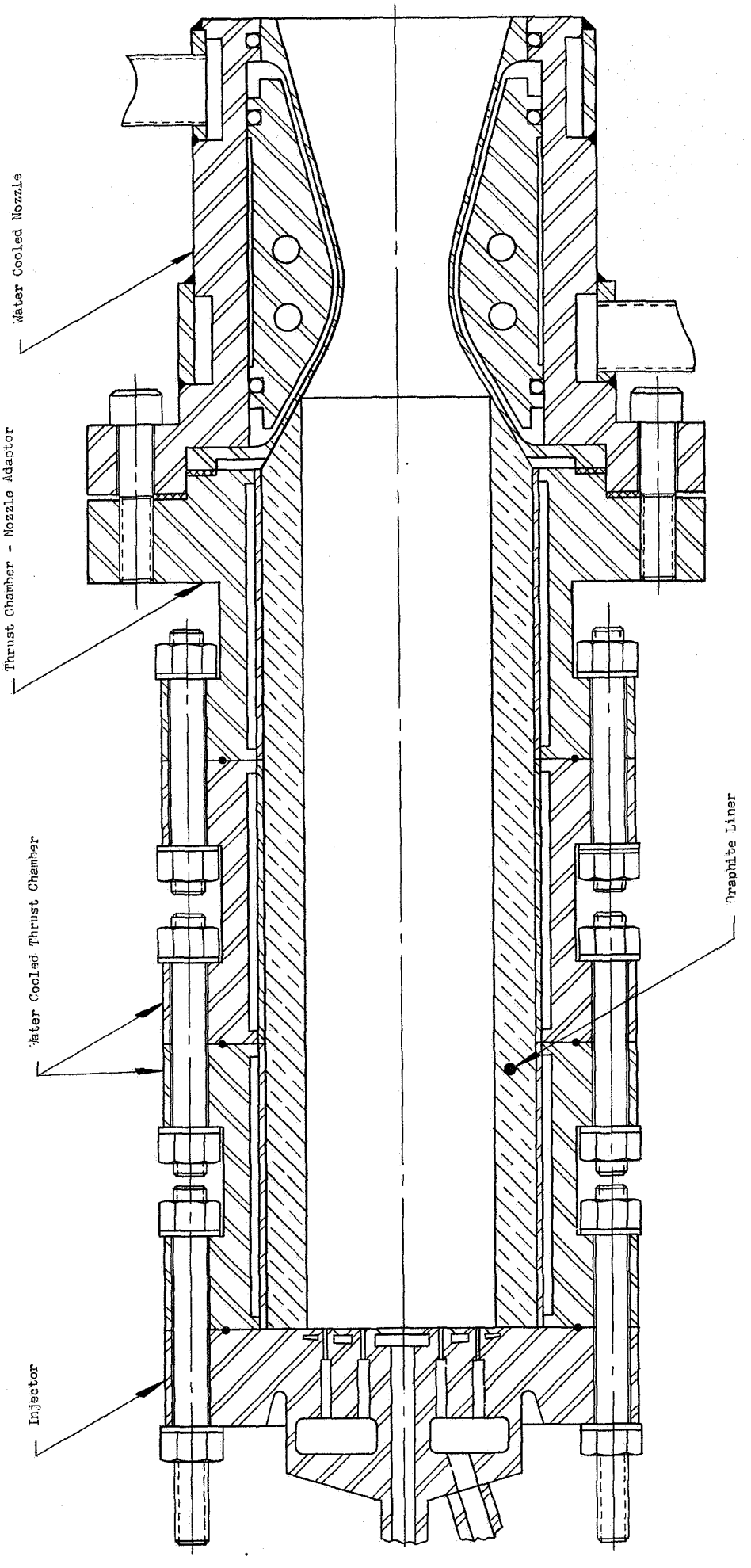

Figure 15. Flox/Propane Engine Assembly

V, C, Flox/Propane -- 5-Tube Tests (cont.)

Prior to using the flox/propane combustor, flow and heat-transfer analyses were made to establish the distance and angle of the coated specimen in relation to the combustor. The objective of this analysis was to establish a specimen position which would provide thermal and chemical environments on the coating surface similar to that at the throat of the combustor.

2. Exhaust Stream Flow Studies

An analysis was conducted to define the angle at which the specimen must be placed in the gas stream. The purpose of the angular location is to produce exhaust species at the specimen surface similar to that at the throat. The theoretical exhaust gas species are primarily a function of temperature and the temperature at the specimen surface can be controlled by the gas velocity at the specimen surface. The specimen must be placed at an angle to produce oblique shock in the supersonic stream of sufficient strength to reduce the Mach number of the gases to unity the same as that at the throat. In establishing the angle, consideration was given to the flow separation because of the possibility of air entrainment.

Under the test conditions of the combustor, the flow separation occurs when the ratios of the nozzle wall pressure/ambient pressure reduces to about 0.4. Since this is well within the test conditions, flow would separate well upstream of the nozzle exit resulting in the air entrainment and the contamination of the exhaust in contact with the specimen.

Air entrainment was minimized by placing the specimen in the position as depicted in Figure 16. The deceleration of the gases impinging on the specimen should raise the pressure to a value considerably higher than the ambient. Due to this pressure barrier, air entrainment into the separation wedge would be minimized.

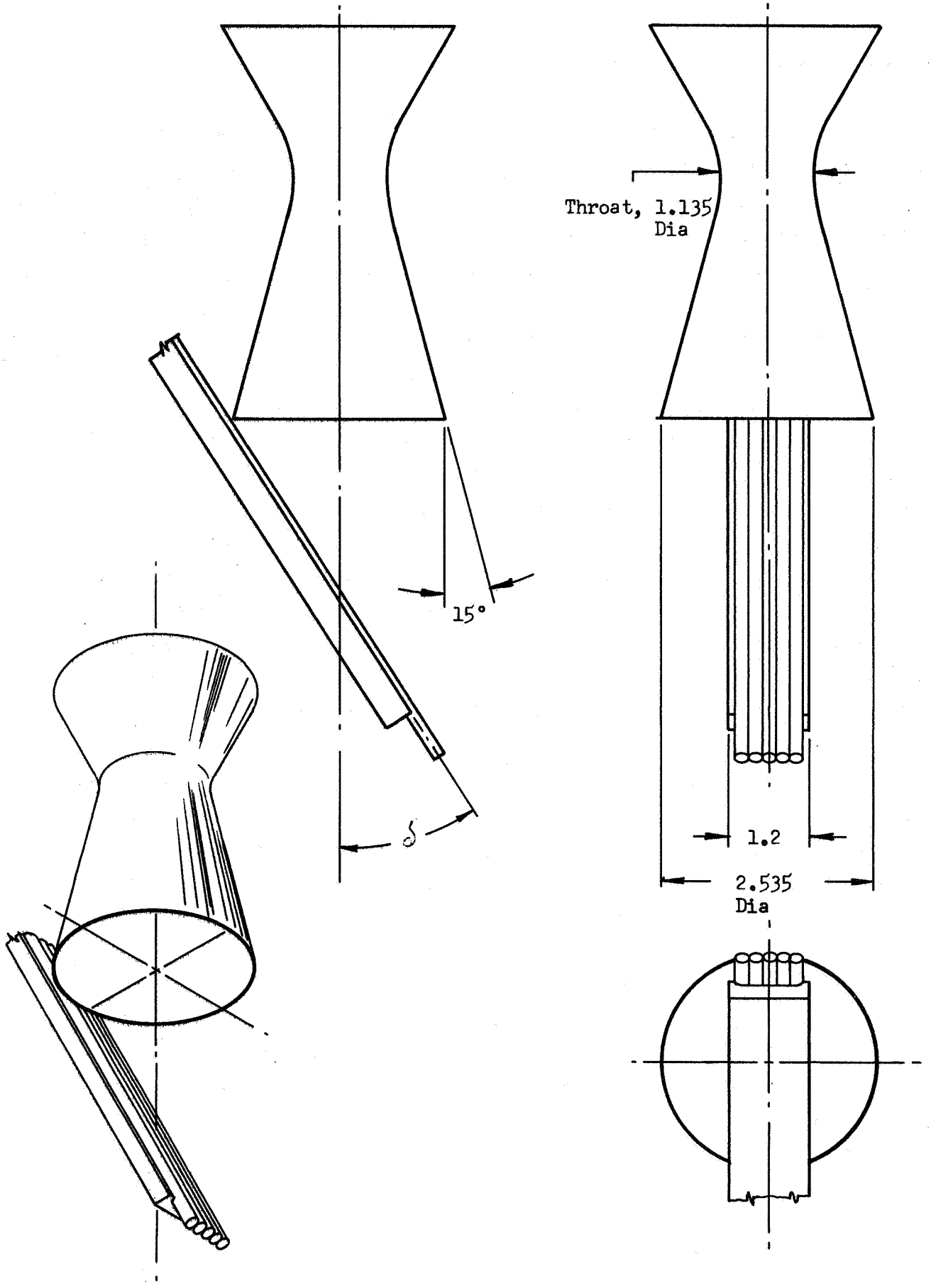

Figure 16. Gas Dynamic Test Configuration of Coated Tube Bundle.

V, C, Flox/Propane -- 5-Tube Tests (cont.)

The method of predicting the angle that the specimen should be placed is depicted in Figure 17. The position of separation was established at an area ratio of approximately 2.5 with the flow turning from the wall at an angle of 15 degrees. With these initial conditions, the angle δ, the specimens must make with the nozzle neutral axis was calculated (Reference 24) to be 22 degrees, using the oblique shock equations as follows:

$$\cos \delta = \tan \theta \left[(\gamma + 1)\, M_1^2/2(M_1^2 \sin -1)\right]$$

$$P_2 - P_1 = 4\, q_1\, (M_1^2 \sin^2 \theta - 1)/(\gamma + 1)\, M_1^2$$

$$M_2 = \left[(\gamma - 1)\, M_1^2 \sin^2 \theta + 2\right]^{1/2} / \left[\sin (\theta - \delta)\right]^{1/2} \left[2\, \gamma\, M_1^2 \sin^2 \theta - (\gamma - 1)\right]^{1/2}$$

where:
- δ = angle of flow deflection across an oblique shock
- θ = shock-wave angle measured from upstream flow direction
- γ = ratio of specific heats
- M = Mach number
- P = static pressure
- q = dynamic head

Subscripts:
- 1 = represents conditions prior to the shock
- 2 = represents conditions after the shock

The combustion products making contact with the test specimen were assumed to be similar to that at the throat because the gas species present are a function of the temperature, but are relatively invariant to changes in pressure. Since there is no loss of stagnation temperature across the shocks, the temperature of the gases adjacent to the specimen where the Mach number is 1.0 are the same as at the throat. Thus, the species should be similar as those at the throat.

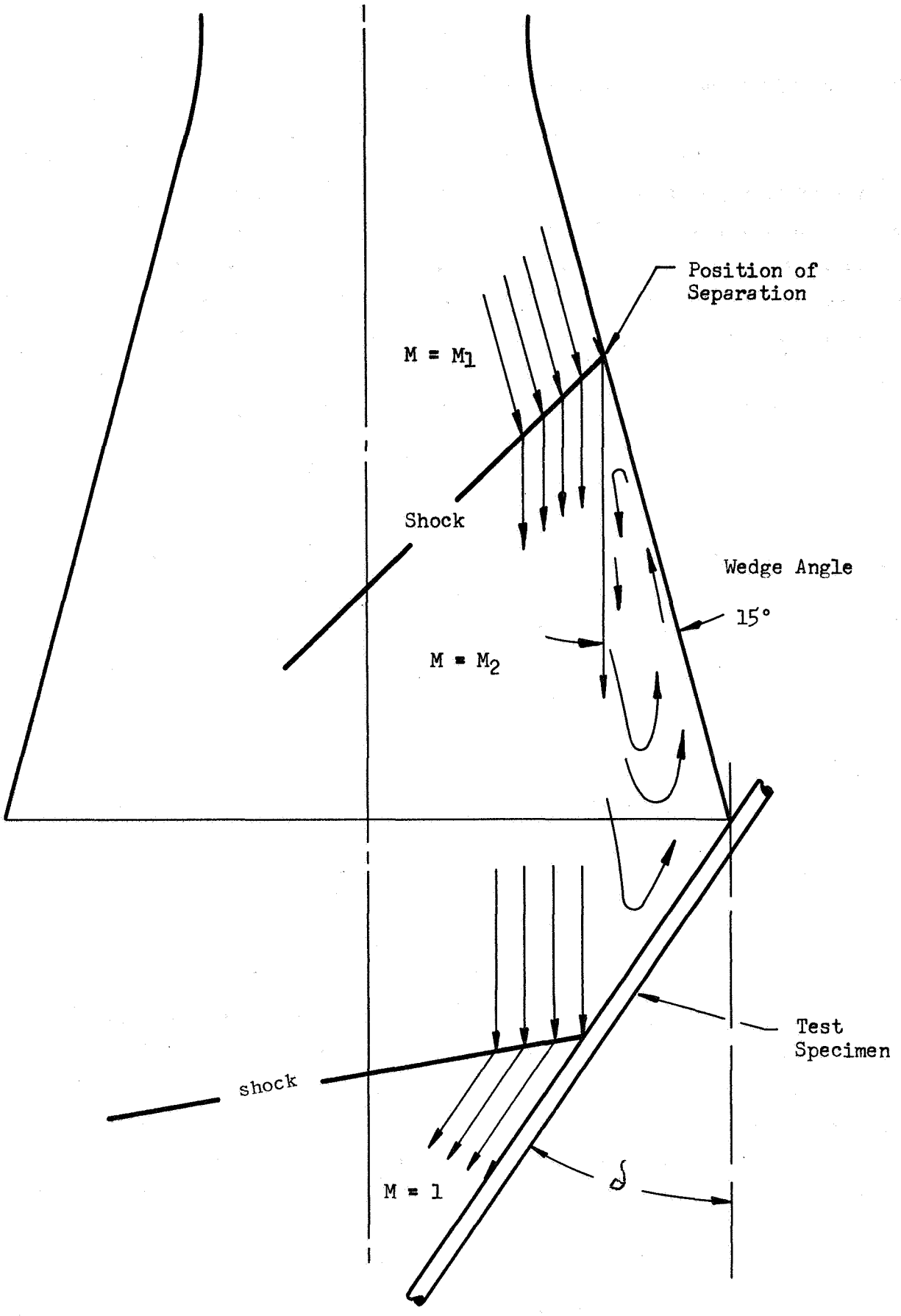

Figure 17. Model Used to Predict Gas Conditions.

Due to the uncertainty of predicting the point of separation, the analysis was carried further to determine the inaccuracies that would result from changes of the location of separation. While separation was predicted to occur at an area ratio of 2.5, the extreme boundaries at which separation could take place are at area ratios of 2 and 3.5. By continuing the shock analysis for these boundaries and β = 22 degrees, it was found that separating at an area ratio of 2 would result in a Mach number of approximately 0.7 over the test specimen, while separating at an area ratio of 3.5 would result in a Mach number of 1.25. These Mach number changes are not large enough to cause any appreciable change in the gas species.

It was, therefore, concluded from these flow analyses, that the specimen should be placed in the exhaust stream in the manner depicted in Figure 17 with δ equal to 22 degrees. This should result in a sonic gas velocity (M=1) over the tubes and a gas composition identical to that at the throat. The supersonic gas will separate from the nozzle wall; however, air will not contaminate the gases in the region of the test specimen due to a high-pressure barrier in this region. The inability to accurately predict the location of separation will have very little effect on the gas conditions over the tube bundle.

3. Heat-Transfer Analysis and Calibration Tests

Heat-transfer analysis was made to correlate surface temperatures of an uncoated specimen to film coefficients to ensure that the required heat flux would be obtained. Heat flux of 3.2 Btu/in.^{2}-sec and film coefficient of 6×10^{-4} Btu/in.^{2}-sec-°F were established for the uncoated specimens in the flox/propane environment. A plot of film coefficient versus heat flux for a specimen placed at the 22 degrees angle position established in the flow analysis, is shown in Figure 18. As shown, a surface temperature of 1150°F is required in an uncoated water-cooled specimen to obtain the required heat flux of 3.2 Btu/in.^{2}-sec.

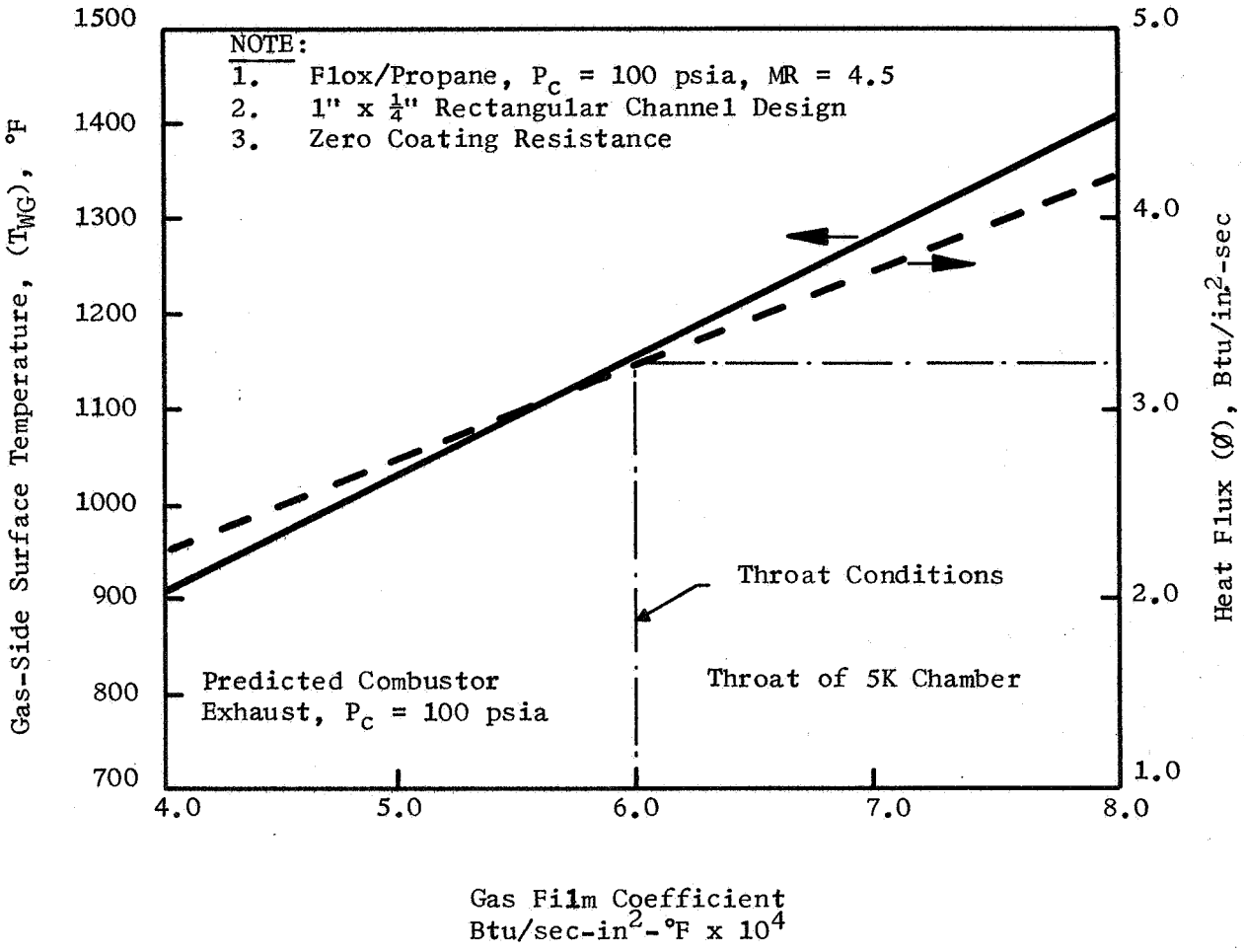

Figure 18. Gas Side Surface Temperature of an Uncoated Specimen and Heat Flux as a Function of Combustor Gas Film Coefficient.

V, C, Flox/Propane -- 5-Tube Tests (cont.)

Calibration tests were conducted to establish the specimen distance from the combustor and to measure the heat flux. To obtain this information, a special flat calibration specimen was designed and fabricated (Figure 19) consisting of a rectangular coolant channel 1/8 in. deep by 1 in. wide. The gas-side face plate was 1/16 in. thick in which fifteen 0.010-in.-dia chromel-alumel-sheathed thermocouples were brazed into slots. A carbon phenolic shield with a window 0.875 in. by 1-5/8 in. was used to provide a known exposure area for measuring overall heat flux. The water coolant temperature rise was measured with thermistors placed in the water inlet and outlet parts of the specimen. The temperature differences along with the water flow rate were used to establish heat flux and specimen placement. The calibration specimen was placed at an angle of 22 degrees with the centerline of the combustor, as shown in Figure 20.

Three 5-sec calibration test firings were made with the instrumented calibration specimen. The first two firings were made at a nominal chamber pressure of 100 psia and the third was made at a nominal pressure of 120 psia. A mixture ratio of 4.5 was used for all three firings. Surface temperatures of the exposed area of the calibration specimen increased for the first 2 sec and then remained relatively constant, indicating steady state had been reached. The surface temperatures ranged from 1100 to 1390°F in all three firings which indicated a heat flux range of 3 Btu/in.^{2}-sec-°F to about 4.2 Btu/in.^{2}-sec-°F (Figure 18). This range compared with the predicted heat flux of 3.2 Btu/in.^{2}-sec-°F. Surface temperature did not vary significantly with chamber pressure. The data obtained from these tests showed that the desired heat flux and exhaust gas species were obtained by positioning the specimen at a 22-degrees angle with the flox/propane combustor.

The carbon phenolic shield eroded in the test firing and a section of about 1-1/8 in. by 1/2 in. was ejected. The poor performance of carbon phenolic for the short duration indicated that another shield material such as graphite was required for the flox/propane coating evaluation.

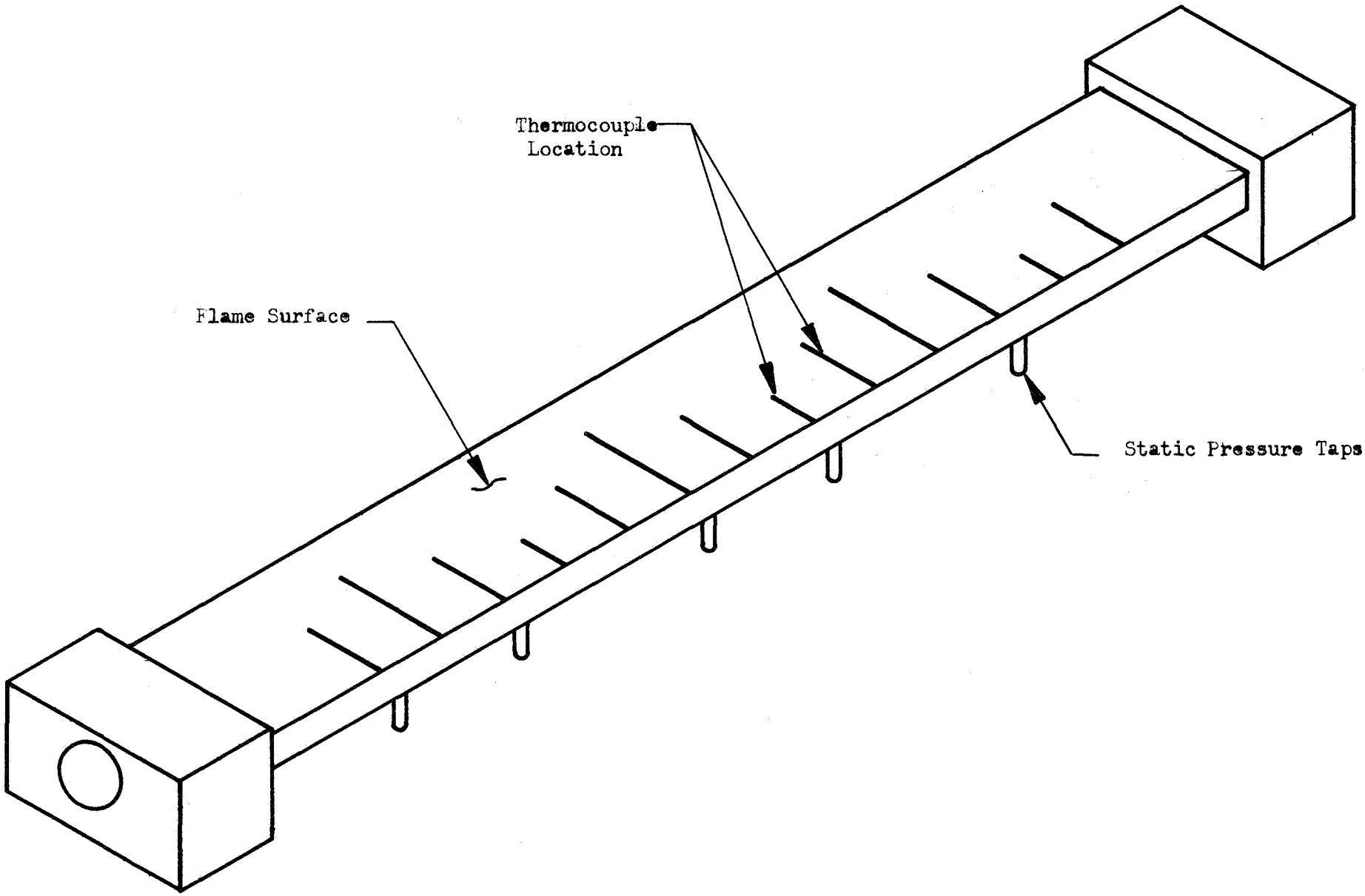

Figure 19. Calibration Specimen

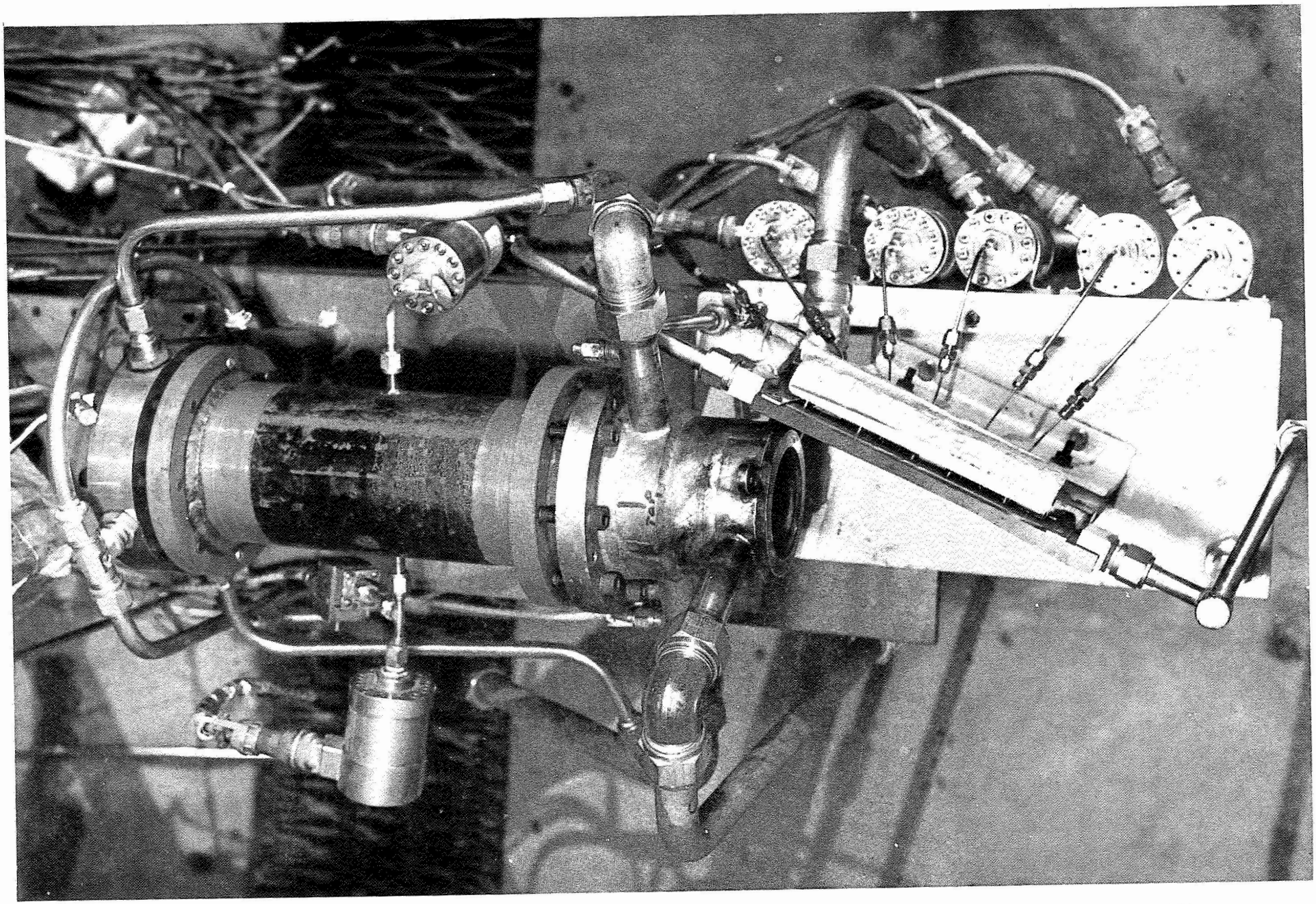

VKC Neg. 867-687

Figure 20. Top View of Calibration Specimen Positioned in the Exhaust Stream of Flox/Propane Combustor.

VI. THERMAL BARRIER EVALUATION

The thermal barrier evaluation consisted of testing coated disc and 5-tube specimens in the laboratory with final testing of coated 5-tube specimens in the exhaust of the flox/propane combustor.

A. LABORATORY EVALUATION

1. Disk Coupons

The composition and coating thicknesses selected for the coupon tests are shown in Table VI. The coupon tests were conducted to establish thermal shock resistance and thermal resistance of the coating. These tests were made on the stainless steel coated specimens by heating the specimen with a hydrogen plasma at a heat flux of 2.4 Btu/in.^{2}-sec-°F. An argon shield was used around the flame but was not effective at these low heat fluxes because the torch-to-specimen distance was long (2-3/4 in.) and good argon coverage was not obtained.

The thermal resistance values for the selected coatings in the disk coupon tests are shown in Table VI. The thermal resistances were low in specimens 5, 7, 9, 11, and 14, and reflect the high material losses of 30 mils or greater in these specimens. The high material loss was due to the test environment which was primarily air and does not reflect the compatibility of the coatings in the flox/propane environments. Material losses, however, were associated with the coating composition. Coatings with 50% or less tungsten (specimens 2 and 12) had low material losses, whereas coatings containing 65% W or greater (specimens 5, 7, 9, 11, and 14) had material losses of 30 mils or greater.

All of the coatings were subjected to thermal shock tests consisting of ten thermal cycles of 10-sec heating and 5-sec cooling. Cracking was not observed on any of the specimens. One of the coatings separated away

TABLE VI

DISK COATING EVALUATION

No.	Composition, wt %	Thickness, mils	Coating Surface Temperature, °F	Thermal Resistance, $in.^2$-sec°F/Btu	Material Loss, mils
1	ZrO_2	44	3850	1320	2
2	68% ZrO_2 - 32% Mo	86	4340	1445	6
3*	52% ZrO_2 - 48% W	78	3950	1310	3
4	51% ZrO_2 - 49% Mo	106	4250	1500	4
5**	35% ZrO_2 - 65% W	120	3350	1155	30
6	40% ZrO_2 - 60% Mo	140	4080	1430	5
7*	26% ZrO_2 - 74% W	135	3560	1135	39
8	32% ZrO_2 - 68% Mo	166	4140	1365	6
9	20% ZrO_2 - 80% W	165	(a)		40
10**	25% ZrO_2 - 75% Mo	196	4340	1535	6
11**	16% ZrO_2 - 84% W	194	3700	1230	34
12**	1st layer - 50% ZrO_2 - 50% Nichrome	45	3900	1350	5
	2nd layer - 52% ZrO_2 - 48% W	30			
13**	1st layer - 50% ZrO_2 - 50% Nichrome	45	4340	1580	4
	2nd layer - 68% ZrO_2 - 32% Mo	25			
14	1st layer - 50% ZrO_2 - 50% Nichrome	45	2900	900	35
	2nd layer - 25% ZrO_2 - 75% W	50			
15	1st layer - 50% ZrO_2 - 50% Nichrome	45	4400	1515	5
	2nd layer - 40% ZrO_2 - 60% Mo	46			

(a) Coating separated from disc and reliable temperature could not be obtained.
* Compositions selected for 5-tube specimen in the laboratory.
** Compositions selected for 5-tube specimen in flox/propane combustor.

from the stainless-steel substrate (specimen 9). In this test, the coating was cracked around the circumference of the specimen, prior to the shock tests. During the shock tests, the backside of the coating in the area of the crack was not cooled, resulting in overheating and subsequent melting at the coating-disc interface and separation. All of the other specimens withstood the tests without separation.

Photographs of the disk specimens, after plasma testing, are shown in Figure 21. Coatings from specimens 2, 3, 5, 7, 10, 11, 12, and 13 were selected for evaluation in the plasma screening tests of the 5-tube specimens. These compositions were selected to provide ZrO_2-Mo compositions ranging from 32% Mo to 75% Mo, and ZrO_2-W compositions ranging from 48% W to 84% W. Gradated coatings (specimens 12 and 13) were also selected to evaluate the effect of the nichrome in the thermal barrier substrate.

2. Plasma-Screening Tests - 5-Tube Specimens

Coatings selected from the coupon tests were evaluated on the 5-tube specimen in the plasma flame in the laboratory, using the same plasma torch settings as for the coupon tests. A heat flux of 2.4 Btu/in.^{2} sec °F was used. The plasma screening tests consisted of thermal shock cycles of 10-sec heating and approximately 5-sec cooling in an area of the specimens and a 50-sec test in an area at the other end of the specimens. The tube specimens were water-cooled during the tests.

The coatings (Table VII) on all specimens adhered throughout the tests without evidence of failure. A 5-tube specimen, after the plasma tests, is shown in Figure 22. All of the coatings contained cracks. The cracks initiated in the areas exposed to the flame and propagated into the unexposed areas. The cracks were predominately parallel to the length of the tubes and were located in the valleys. Cracks transverse to the direction of

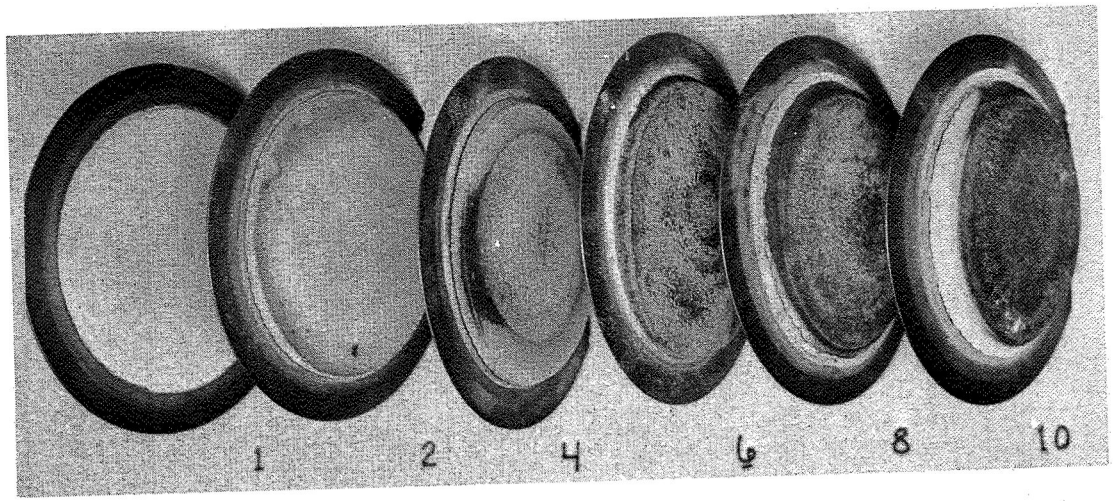

Coating Thickness, Mils	44	86	106	140	166	196
Coating Composition, %	100 ZrO_2	62 ZrO_2 32 Mo	51 ZrO_2 49 Mo	40 ZrO_2 60 Mo	32 ZrO_2 68 Mo	25 ZrO_2 75 Mo

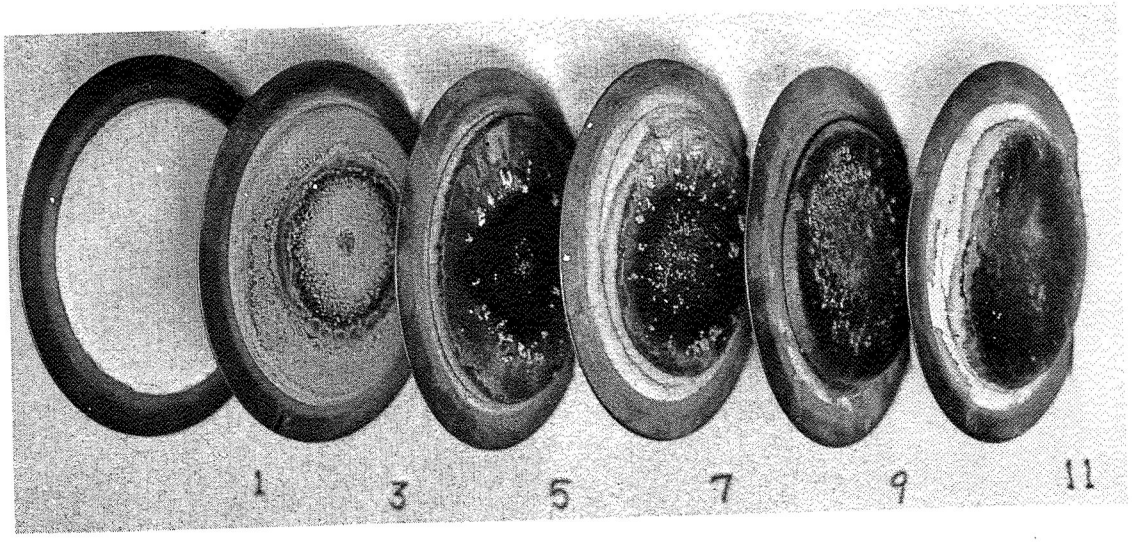

Coating Thickness, Mils	44	78	120	135	165	194
Coating Composition, %	100 ZrO_2	52 ZrO_2 48 W	35 ZrO_2 65 W	26 ZrO_2 74 W	20 ZrO_2 80 W	16 ZrO_2 84 W

Figure 21. Coated Disc Specimens

TABLE VII

THERMAL BARRIER COMPOSITIONS SELECTED FOR THE 5-TUBE PLASMA SCREENING TESTS

Specimen No.	Composition, wt %	No. of Passes	Measured Thickness, mils
1T	68% ZrO_2 - 32% Mo	41	76
2T	52% ZrO_2 - 48% W	30	78
3T	35% ZrO_2 - 65% W	35	106
4T	26% ZrO_2 - 74% W	38	137
5T	25% ZrO_2 - 75% Mo	100	193
6T	16% ZrO_2 - 84% W	47	198
7T	1st layer 50% ZrO_2 - 50% Nichrome	13	47
	2nd layer 52% ZrO_2 - 48% W	10	33
8T	1st layer 50% ZrO_2 - 50% Nichrome	13	46
	2nd layer 68% ZrO_2 - 32% Mo	16	25

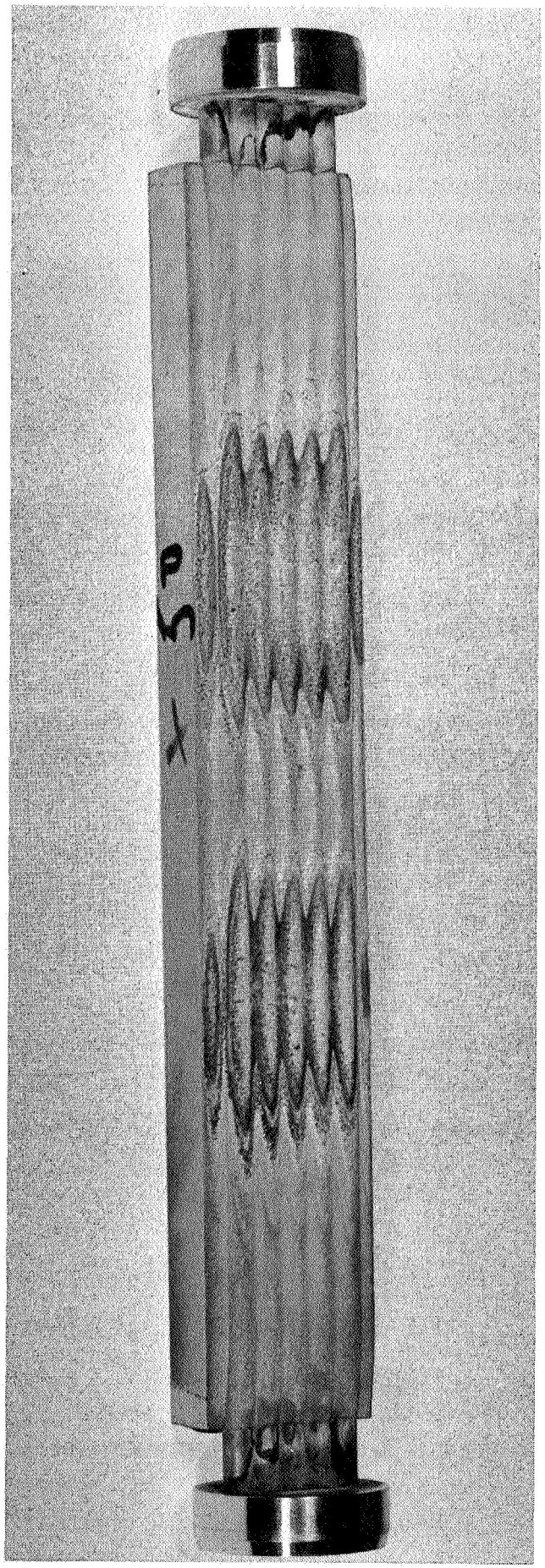

Figure 22. 5-Tube Specimen Coated with 0.078-in. of 52% ZrO_2-48% W after Thermal Shock Test.

the tubes were observed in specimens T-4, T-5, and T-6. The cracks propagated from the outside surface and extended about halfway through the coating.

Metallographic examinations revealed that all of the coatings were bonded to the substrate at the tube crown, but were not bonded in the valleys, as shown in Figure 23. The unbonded areas appeared to be associated with bridging of the valleys because of the mechanics of the coating process. Optimum bonded coatings are obtained with the plasma torch positioned normal to the substrate surface. This position is maintained in spraying the crown of the tube but not in the valley between the tubes. When the torch is not normal to the surface (over the valleys), particles rebound off the sides of the tubes creating a turbulent action which affects the coating adherence. This lack of adherence has been observed in the Titan program but has not affected the reliability of the coating.

All of the coatings withstood the 5-tube thermal shock screening tests. Because of this, the coating compositions for the flox/propane tests were selected to provide information on the effect of coating thickness, layered coatings, W and Mo contents, and to provide a comparison of compatibility of Mo and W coatings. The coating compositions selected for evaluation in the first flox/propane tests were: (a) 25% ZrO_2-75% Mo, and (b) 16% ZrO_2-84% W, and two gradated coatings consisting of 50% ZrO_2-50% Nichrome top-coated with 52% ZrO_2-48% W and 68% ZrO_2-32% Mo.

B. FLOX/PROPANE TESTS

1. Combustor Performance

A total of 18 flox/propane coating tests were made in the program. The first six tests were made with a six-element injector, graphite-lined chamber, and a water-cooled nozzle. The c* for these tests ranged from

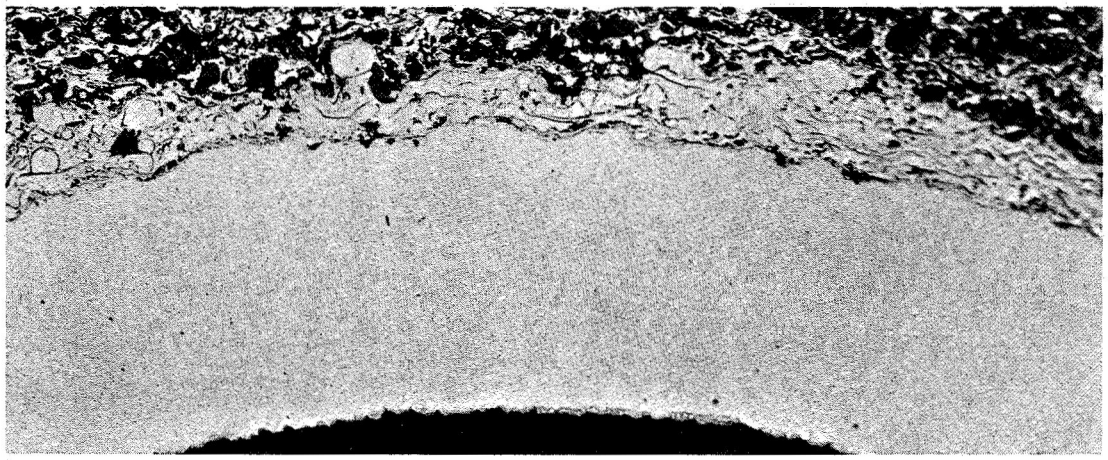

CROWN OF TUBES

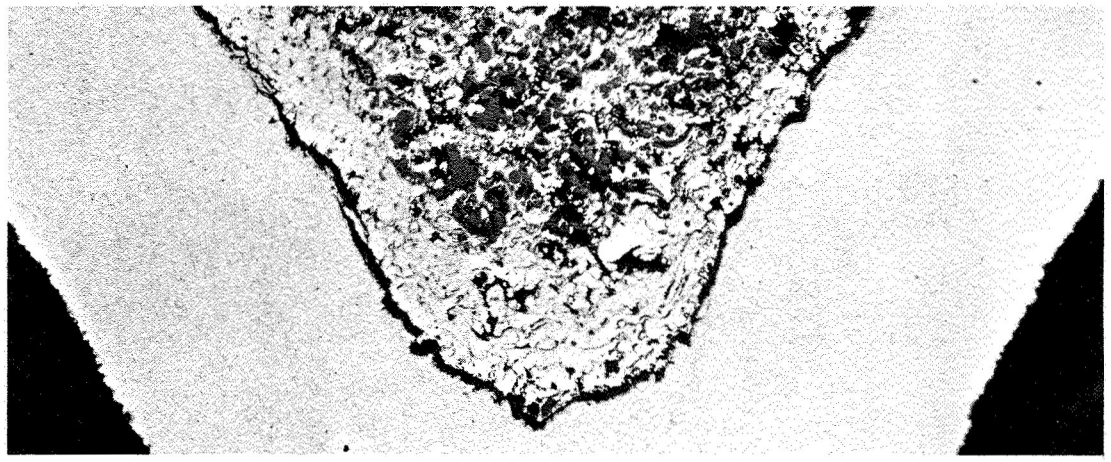

VALLEY BETWEEN TUBES

Figure 23. Comparison of Bondline at the Crown and in the Valley (Specimen No. 8).

79 to 83% of theoretical. Use of the six-element injector was discontinued because of the low performance. The 17-element injector, along with a water-cooled chamber were then used. The chamber was lined with ATJ graphite, and the same liner was used for all the tests with only slight erosion. The c* performance ranged from 86 to 94% of theoretical for these tests using the 17-element injector.

Some carbon buildup was observed on all tests both on the chamber and nozzle wall and injector face. In the tests with the six-element injector, large, flaky, uneven carbon deposits occurred in the chamber compared to thin, uniform deposits when using the 17-element injector. The carbon deposit, in either case, was soft and flaked off easily.

2. Shield Performance

A shield was used in the flox/propane tests to prevent gas flow along the sides of the coated tube specimens, to protect the water inlets, and to provide a known exposed area so that the bulk temperature rise could be measured. The shield was positioned in front of the specimen with a window to provide the impingement area. In the first tests (specimen T-13), a carbon phenolic shield was used. The window size increased from 7/8 in. by 1-5/8 in. to 1 in. by 4 in. in only 10 sec of firing time. Because of the extreme regression, the remainder of the tests were made using a graphite shield as shown in Figure 24. The graphite also regressed due to the severity of the exhaust from about 1/2 in. by 2-1/4 in. to about 1-1/8 in. by 3-1/8 in. in a 50-sec firing as shown in Figure 25. The continuous enlargement of the window due to regression during the firing resulted in a continuous increase in bulk temperature rise throughout the firing. The regression of the graphite also resulted in exposure of the specimen sides and back to the flame. To prevent this, the firing durations were reduced from 50 to 30 sec and finally to 15 sec at which time the window size remained relatively constant throughout the firing.

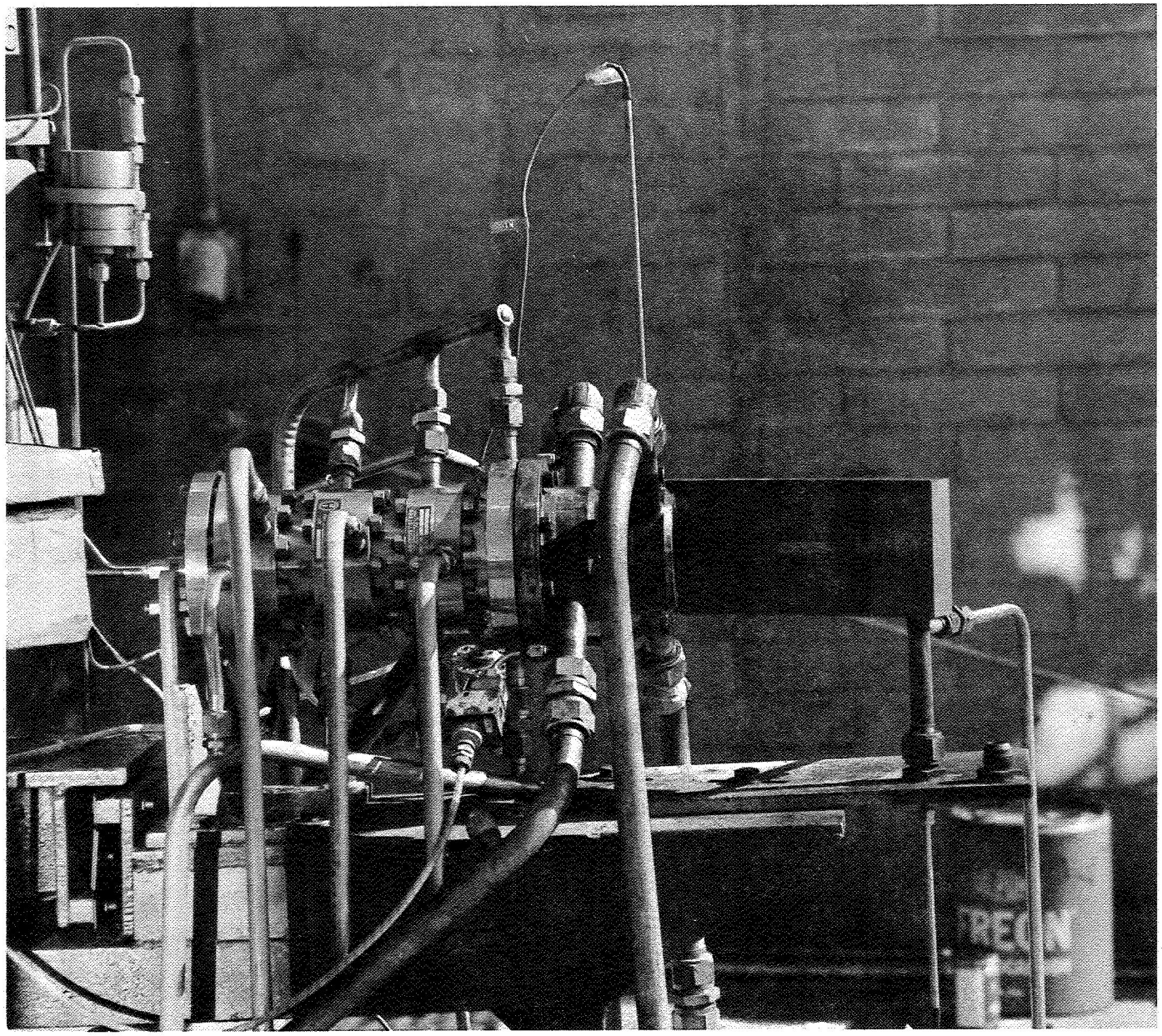

VKC Neg. 168-678

Figure 24. Flox/Propane Combustor with Specimen and Graphite Shield Aligned Ready for Test Firing.

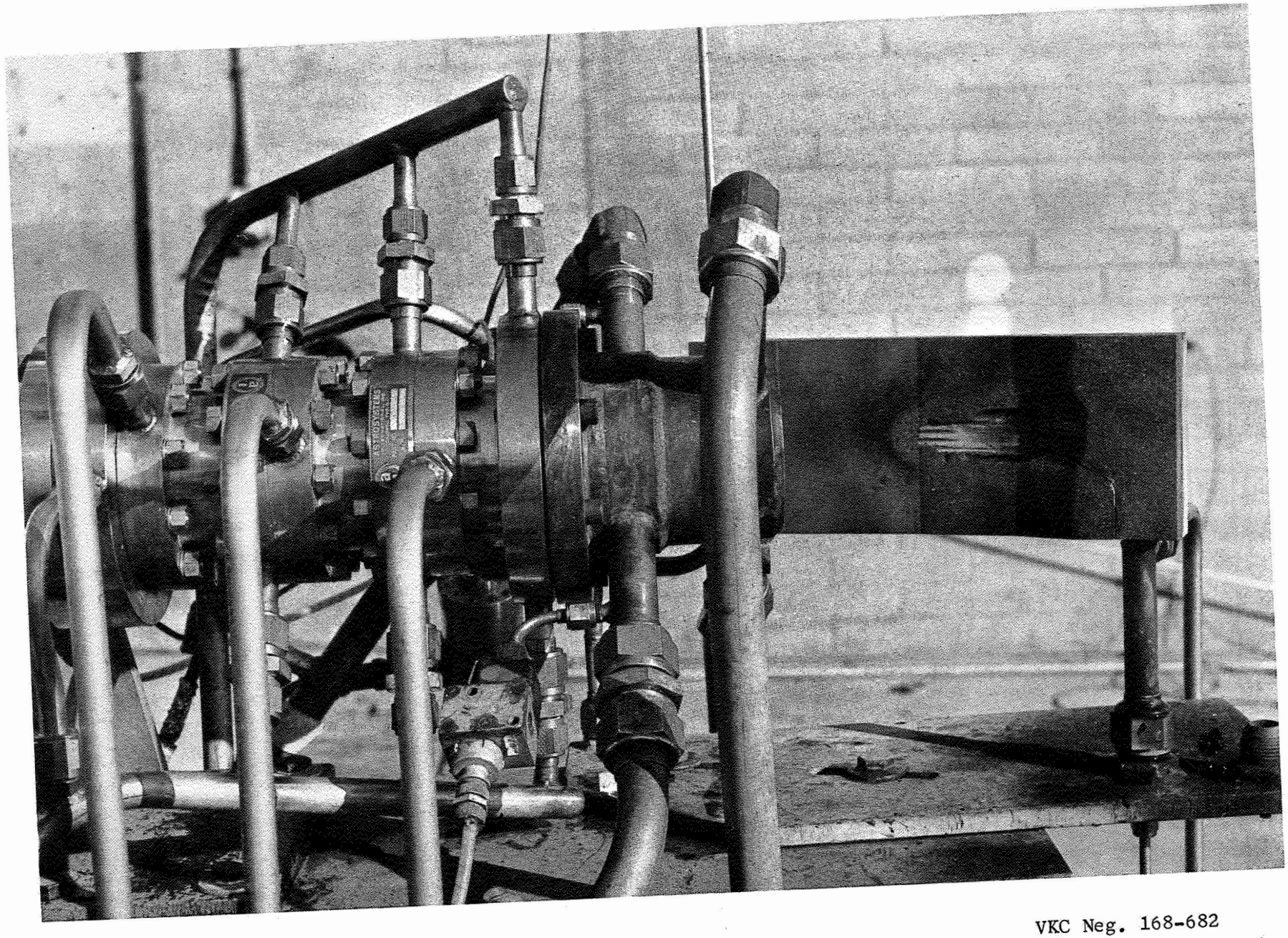

VKC Neg. 168-682

Figure 25. Flox/Propane Combustor and Shield after 50 Second Test Firing.

VI, B, Flox/Propane Tests (cont.)

In all of the tests a reaction occurred between the coating and graphite at the aft end of the window in the shield. In this area, a high heat-transfer condition occurred from turbulence due to the step in the window. As a result of the high heat-transfer condition, melting occurred in this area after only 5 sec in specimen T-19 (molybdenum). The melting occurred at the window edge and coating regression measurements were only affected 1/2 in. up and downstream of this area.

Specimen T-20B was evaluated with a modified shield to eliminate the high heat-transfer conditions. The shield modification consisted of eliminating the aft end of the window which would expose the aft adapter to the exhaust stream and probable burnthrough. The only function of the adapter was to provide an outlet for the water from the tubes; therefore, it was eliminated and the water allowed to exit in the exhaust stream. The regression rates of specimen T-20B were comparable to specimen T-20A which was tested with the original shield. However, the reaction between the shield and coating was avoided in using the modified shield. Specimens T-23 and T-25 were also tested with the modified shield without the indication of the reaction zone.

3. Coating Performance

The regression rate performance of the coatings is shown in Table VIII and schematically in Figure 26. In the combustor tests, the coated specimen (Figure 27) surface temperature ranges from 3000 to 3500°F with the atmosphere theoretically consisting of 57% HF, 25% CO, 10% F, and 8% H. The regression rate of the coatings in this environment decreased with an increase in tungsten or molybdenum content. The lowest regression rate was obtained with the pure metals. The regression rate of ZrC/C was 0.46 mils/sec (not included in Figure 26) and was similar to that of the tungsten and molybdenum. The regression rate for pure metals was approximately 0.4 mils/sec which is relatively high for liquid rocket engine applications. The high regression

TABLE VIII

RESULTS OF FLOX/PROPANE 5-TUBE SPECIMEN EVALUATION

Specimen	Firing Duration, sec	Injector, No. of Elements	Oxidizer/Fuel Mixture Ratio	Chamber Pressure, psia	Efficiency, % c*	Coating Composition, wt %	Coating Thickness mils	Material Loss, mils	Regression Rate, mils/sec	Remarks
T-13	5	6	4.4	100	81	35% ZrO_2 - 65% W	106			
T-13	5	6	4.5	97	79			18	1.8	Specimen contained surface cracks.
T-9	50	6	4.3	101	81 - 83	25% ZrO_2 - 75% Mo	199	80	1.6	FeC particles impinged on specimen surface. Thrust chamber water cooled to prevent FeC formation in future tests.
T-10	50	6	Recorder Malfunction			16% ZrO_2 - 84% W	197	41	0.8	
T-11	50	6	Oscillograph recorder malfunction. No data.			1st Layer 50% ZrO_2 - 50% Nichrome	47	Top Layer eroded	-	
						2nd Layer 52% ZrO_2 - 48% W	30			
T-12	50	6	4.3	100 - 106	83	1st Layer 50% ZrO_2 - 50% Nichrome	46	Top Layer eroded		
						2nd Layer to 68% ZrO_2 - 32% Mo	27			
T-18	30	17	3.8 - 4	98 - 100	89 - 93	16% ZrO_2 - 84% W	199	18	0.6	
T-14	30	17	4.3 - 4.5	98 - 101	88 - 91	1st Layer - 100% ZrO_2	47	12	0.4	Surface cracks in exposed area
						2nd Layer - 100% W	20	13		
T-17	30	17	4.5 - 4.6	98 - 102	87 - 89	37% Al_2O_3 - 63% Mo	125	54	1.8	
T-16	30	17	4.7 - 4.9	101 - 104	88 - 89	25% Al_2O_3 - 75% W	125	55	1.8	
T-15	30	17	4.5 - 4.7	101 - 102	89 - 90	1st Layer 50% ZrO_2 - 50% W	75	27 W completely eroded.		Shield failed after 23 sec, resulting in burnthrough in adaptor and H_2O impingement on specimen surface.
						2nd Layer 100% W	20			
T-19A	5	17	4.9 - 5.3	96 - 98	86 - 88	1st Layer 80% Al_2O_3 - 20% Mo	10			Melting occurred at the aft end of window due to turbulence and high heat-transfer condition.
						2nd Layer 70% Al_2O_3 - 30% Mo	14	-	-	
						3rd Layer 100% Mo	20			
T-19B	15	17	4.3 - 4.5	96 - 99	86 - 90	Opposite end of 19A.		6	0.4	Surface contained small cracks and shiny melted appearance caused by oxidation of Mo.
T-20A	15	17	4.7 - 4.9	99 - 106	88 - 94	1st Layer 80% Al_2O_3 - 20% Ni	10			No apparent surface cracks.
						2nd Layer - 70% Al_2O_3 - 30% Mo	14			
						3rd Layer 100% W	20	9	0.6	
T-20B	0.8	17	-	-	-	Opposite end of T-20A				Aft end of shield removed and water allowed to exit from specimen into the exhaust stream. No visible cracks after three tests.
T-20B	0.8	17	-	-	-	Opposite end of T-20A				
T-20B	15	17	4.6 - 4.8	98 - 100	86 - 88	Opposite end of T-20A		9	0.54	

TABLE VIII (cont.)

Specimen	Firing Duration, sec	Injector, No. of Elements	Oxidizer/Fuel Mixture Ratio	Chamber Pressure, psia	Efficiency, % c*	Coating Composition, wt %	Coating Thickness mils	Material Loss, mils	Regression Rate, mils/sec	Remarks
T-21	15	17	4.5	97 - 100	86 - 88	1st Layer 80% Al_2O_3 - 20 % Ni	10			
						2nd Layer 70% Al_2O_3 - 30% Mo	7	23	1.6	Longitudinal and transverse surface cracks.
						3rd Layer 20% Al_2O_3 - 80% Mo	25			
T-23	15	17	4.5 - 5	98 - 102	89	1st Layer 80% Al_2O_3 - 20% Ni	10			
						2nd Layer 70% Al_2O_3 - 30% Mo	14	7	0.46	Coating contained several transverse cracks. Aft area surface coated with glossy ZrO_2.
						3rd Layer 100% Mo	3			
						4th Layer 100% Zr C/C	15			
T-25	15	17	4.5 - 4.7	99 - 102	87 - 90	1st Layer 80% Al_2O_3 - 20% Ni	10			
						2nd Layer 70% Al_2O_3 - 30% Mo	14			
						3rd Layer 100% W	15	6	0.40	

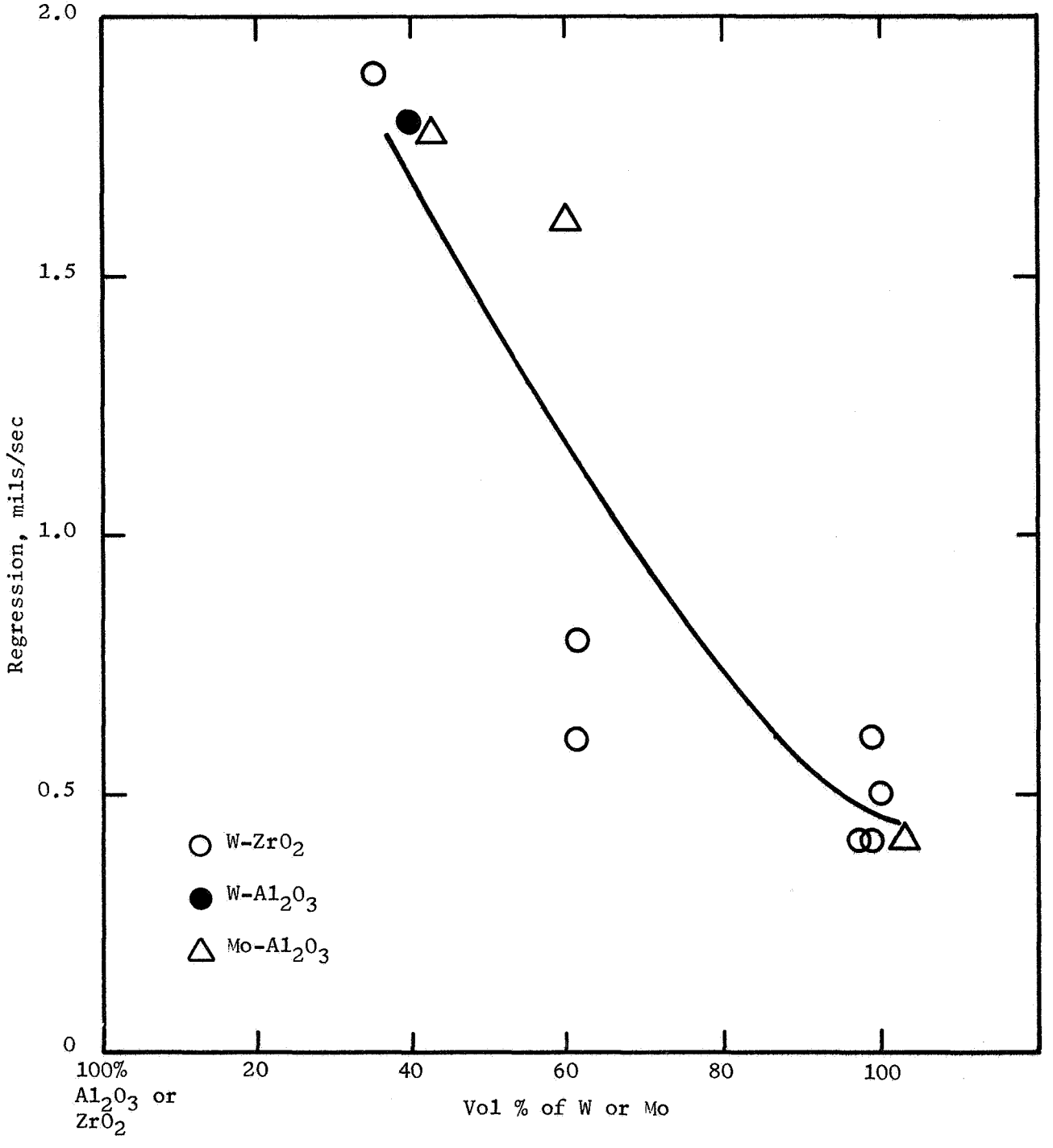

Figure 26. Regression Rate of Thermal Barrier Coatings.

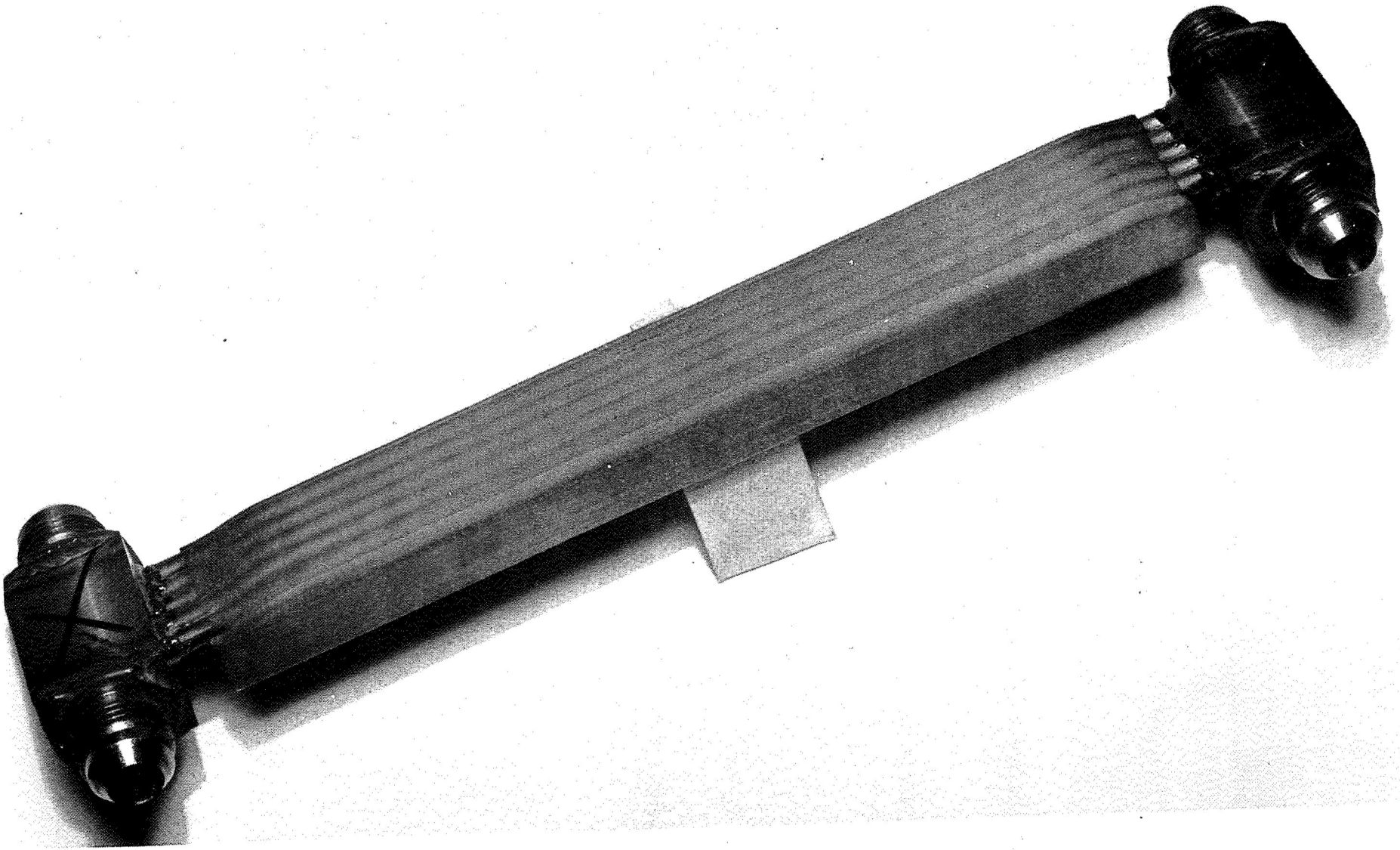

Neg. 167-SP 661

Figure 27. Flox/Propane Specimen Prior to Testing.

rate is partially attributed to oxidation from air entrainment. This is reasoned because of the severe regression observed on the graphite shield which would not be predicted because of the good compatibility of graphite with HF environments. In oxidation environments, however, graphite regression would be expected to be severe.

The mechanism of regression for the coatings is a combination of both chemical corrosion and erosion because of the porosity in the coatings. The plasma-sprayed coatings are estimated to be 75 to 90% dense, resulting in considerable porosity between the sprayed particles. In operation, the coatings are attacked at the particle boundaries and the particle is lifted in the exhaust stream. The regression resistance of the pure metal coatings could be improved by increasing the density of the coating to 95% of theoretical density. Results obtained from solid rocket motor firing, made with the same highly oxidizing propellant with the same size insert revealed that the regression of molybdenum inserts decreased from 5.4 mils/sec for 65% dense, to 4.0 mils/sec for 75%, to 0 regression at 100% dense (Reference 25).

Cracking was observed in the coatings; generally longitudinal cracks were along the valleys between the tubes and transverse cracks were observed at the edge of the heating near the step in the window. The number and size of the cracks increased with coating thickness. The cracks in the thin multilayer coatings only propagated through the top layers whereas in the thick coatings of one composition the propagation of the cracks approached the substrate. However, none of the coatings failed due to cracking or spalling even on the specimens that were subject to several firings in the same area. Based on these observations, the cracking observed in the coating in these tests was not expected to be detrimental to multiple firings. Specific information on each coated specimen is detailed in the following paragraphs:

VI, B, Flox/Propane Tests (cont.)

a. Specimen T-13

The coating on the first 5-tube specimen (T-13), subjected to the flox/propane environment, consisted of 106 mils of 35% ZrO_2 and 65% W. Maximum coating loss on this specimen was 1.8 mils/sec for the 10-sec duration. The coating on specimen T-13 was cracked in both the transverse and longitudinal directions. The transverse cracks extended completely across the specimen, and the longitudinal cracks were located in the valleys of the coating.

b. Specimen T-9

The coating on the second specimen tested (T-9) consisted of 199 mils of 25% ZrO_2 and 75% Mo. Regression of the coating was 1.6 mils/sec for a 50-sec firing. The high erosion rate was attributed to iron and iron carbide in the exhaust stream, which impinged on the coated surface. Iron carbide confirmed by X-ray diffraction analysis, was found on the graphite liner of the chamber, the graphite shield, and on the coating surface. The iron carbide formed at the interface of the graphite liner and steel holder of the chamber. During the firing, a eutectic of the carbon and iron formed at the interface and flowed through cracks in the graphite liner into the exhaust stream. The molten interface was prevented in further firings by increasing the thickness of the graphite liner and by water-cooling the outside diameter of the steel holder.

c. Specimens T-11 and T-12

Specimens T-11 and T-12 were gradated coatings consisting of one layer of 47 mils of 50% ZrO_2 and 50% Nichrome (Figure 28). The second layer of T-11 consisted of 30 mils of 52% ZrO_2 and 48% W, and in T-12 it consisted of 27 mils of 68% ZrO_2 and 37% Mo. The top layers in both coatings

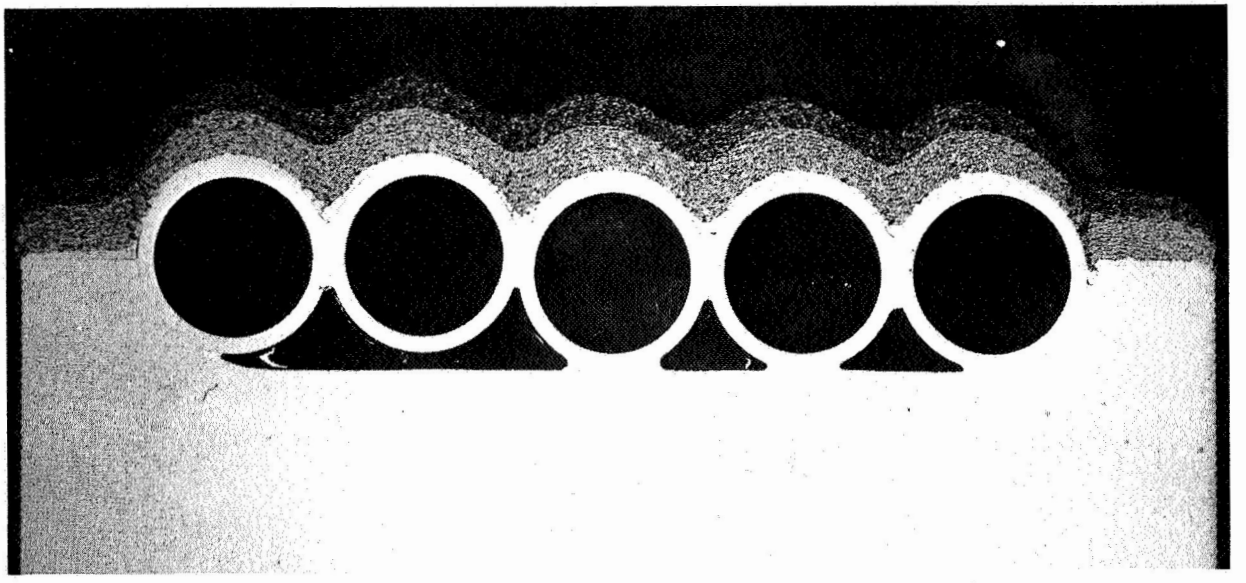

Magnification: 5X Neg. 14617

Figure 28. As Deposited Gradated Coating Consisting of an Underlayer of 50% ZrO_2 and 50% NiCr, and Top Layer of 52% W and 48% ZrO_2 (Specimen T-11).

were completely eroded in 50 sec firings, preventing regression measurements. Based on the performance of other coatings containing ZrO_2, the regression rates are estimated at greater than 1 mil/sec.

d. Specimens T-10 and T-18

This coating (84% W-16% ZrO_2) was tested to determine if coating performance was affected by the change in injectors. Previously, specimen T-10, which contained the same coating composition, was tested with the six-element injector and T-18 was tested with the 17-element injector. As shown in Table VIII, the regression rate of specimen T-10 was 0.8 mils/sec for a 50-sec tests compared to T-18 which was 0.6 mils/sec for a 30-sec test. Transverse cracking obtained in this coating is shown in Figure 29 as typical of that found in the thick coatings. The graphite shield in the test firings showed considerable regression even though the firing time was decreased to 30 sec. The window regressed from the original dimensions of 1/2 in. by 2-1/4 in. to 1-1/8 in. by 2-3/4 in.

e. Specimen T-14

This coating was designed with a tungsten flame liner to be compatible with exhaust gas and underlayers to provide the thermal resistance. The regression rate on this coating was 0.4 mils/sec for a 30-sec test. The tungsten topcoat cracked in the exposed area and the corners of the tungsten curled, indicating the coating would not withstand refiring. The cracking and curling was due to the relatively different thermal expansion of the ZrO_2 and tungsten. At 3000°F, the thermal expansion of dense ZrO_2 is 1.7% and for dense tungsten is 0.75%. This same relationship is believed to exist for the plasma-sprayed coatings which are estimated to be 75 to 90% of theoretical density.

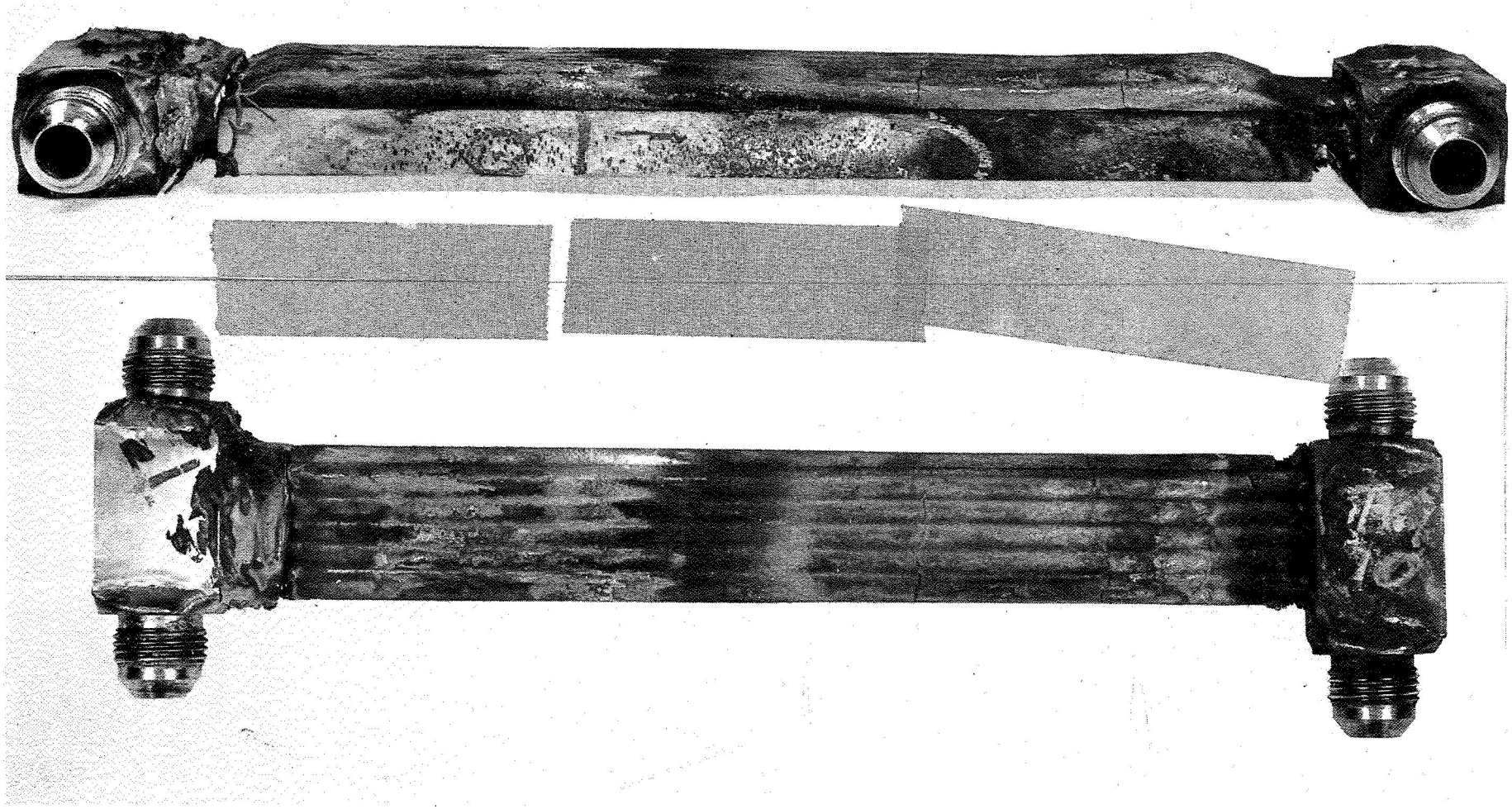

Neg. 458

Figure 29. Transverse Cracks in a Fired Coating Consisting of 84% W-16% ZrO_2 (Specimen T-10).

VI, B, Flox/Propane Tests (cont.)

f. Specimen T-15

This specimen also had a tungsten flame liner similar to T-14, but the first layer consisted of 50% W-50% ZrO_2 to provide better thermal shock resistance and a better thermal expansion transition than the 100% ZrO_2 first layer used in T-14. Less cracking was observed in T-15 than in T-14; however, the results were not clear-cut because more regression occurred in T-15. The higher regression was due to water impingement on the specimen surface. The water impingement occurred at 23 sec after fire switch when the aft end of the graphite shield ejected and burnthrough occurred in the adapter.

g. Specimens T-16, T-17, and T-21

These specimens were designed to show the chemical compatibility of Al_2O_3 compared to ZrO_2 and to compare the chemical compatibility of W and Mo with the exhaust gas species. The regression of all three coatings was severe when compared to the ZrO_2-metal mixtures. Even with the high Mo contents (80%) in specimen T-21, the regression rate was 1.6 mils/sec revealing that oxide mixtures are not suitable for the flox/propane exhaust gases.

h. Specimen T-19

This coating consisted of a flame liner of molybdenum to provide compatibility with the exhaust stream. Undercoats of Ni-Al_2O_3 and Mo-Al_2O_3 provided thermal resistance of 1200 to 1300 in.-sec^2/Btu. A cross-section of the coated specimen is shown in Figure 30. The first firing in this specimen was terminated after 5.3 sec because of a fire at the oxidizer connector behind the injector. No damage occurred on the test stand.

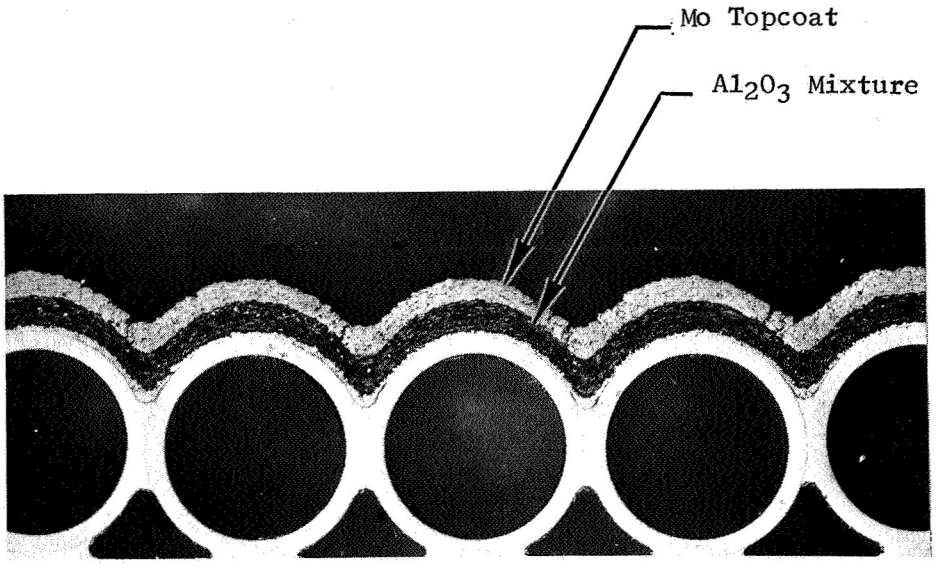

Magnification: 6X Neg. 15828

Figure 30. Prefired Coating Specimen Consisting of Ni-Al_2O_3 Undercoats, and Molybdenum Topcoat (Specimen T-19).

VI, B, Flox/Propane Tests (cont.)

Examination of the coating after the 5.3 sec revealed melting at the aft end of the window in the shield (Figure 31). This melting was due to a high heat-transfer condition in this area caused by the step in the aft window edge. The coating regression was not affected 1/2 in. up and downstream from the window edge, and regression measurements will be avoided in this area.

The other end of the specimen T-19 was fired for 15 sec. A regression rate of 0.4 mils/sec was observed for a 15-sec firing which was the same as that obtained with a pure tungsten liner. The molybdenum coating had a shiny melted surface probably due to the formation MoO_3, which melts at 1460°F. The coating also contained many small cracks.

Metallographic examination of the specimen T-19 revealed that densification occurred in the Mo layer during the test firing (Figure 32). Recrystallization, however, was not observed in the molybdenum coating. The layered structure is due to deformation of the molten molybdenum particle at impact on the substrate. The unmelted particles were too large to melt with the plasma conditions used.

i. Specimen T-20

This specimen was similar to T-19 except that the flame liner was plasma-sprayed tungsten instead of molybdenum. The regression rate on this specimen, using the conventional shield, was 0.67 mils/sec for a 15-sec test with no visible cracks in the coating. Metallographic examination (Figure 33) revealed that the coating was porous compared to the molybdenum coating. The porous structure was less regression resistant than a dense structure as shown in rocket motor firings with nozzle inserts (Reference 25).

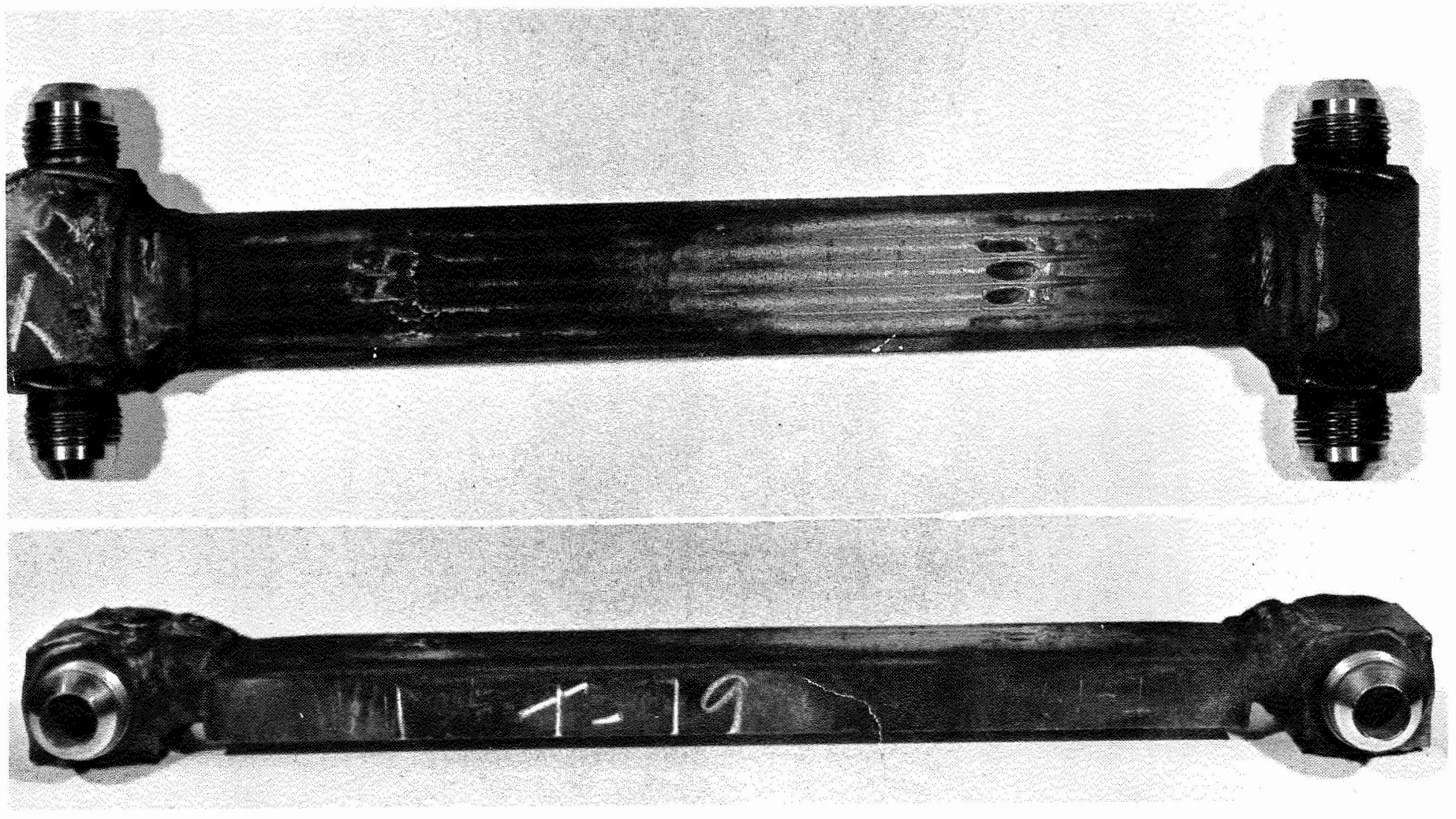

Figure 31. Molybdenum Topcoated Specimen after Flox/Propane Test Firing. Melting Occurred in Mo Topcoat at Edge of Aft Window due to High Heat Transfer Condition.

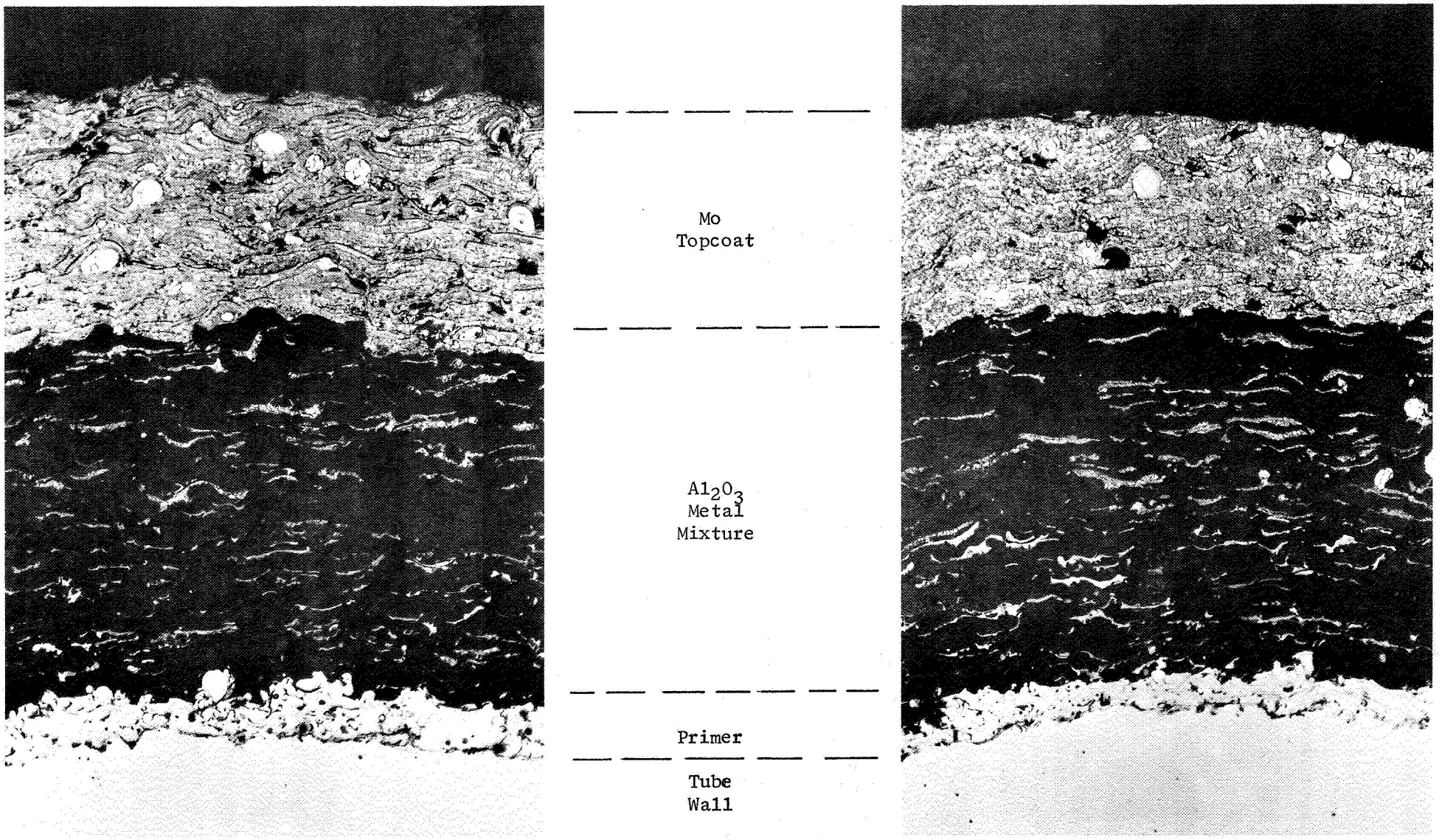

100X Neg. 15842

Prefired

100X Neg. 15843

Postfired

Figure 32. Comparison of Prefired and Postfired Coatings Consisting of Mo Topcoat with Ni-Al_2O_3 and Mo-Al_2O_3 Undercoats (Specimen T-19).

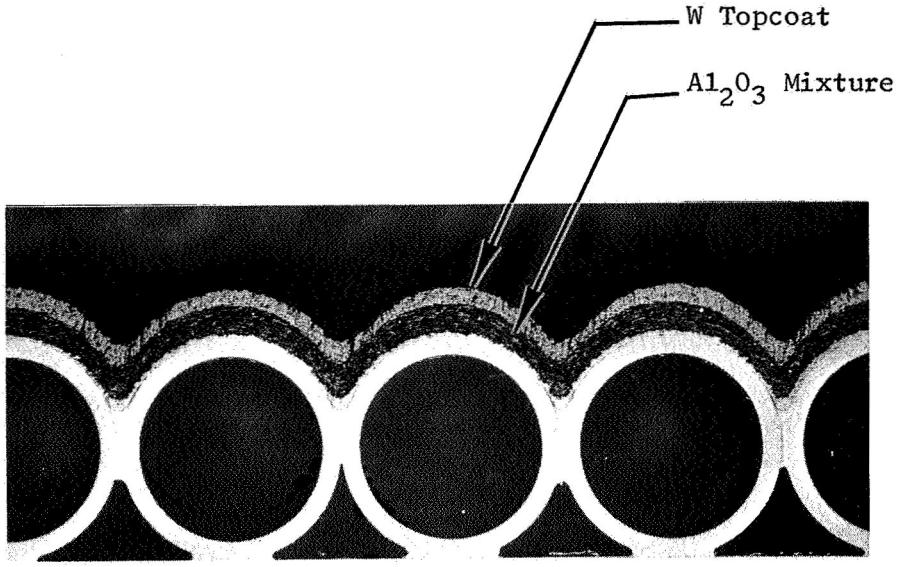

6X Neg. 15831

Figure 33. Prefired Coated Specimen Consisting of Ni-Al_2O_3, Mo-Al_2O_3 Undercoats, and Tungsten Topcoat (Specimen T-20).

Specimen T-20 was refired three times using the other end of the specimen and the modified shield. The three firings consisted of two 0.8-sec and one 15-sec duration tests. The 0.8-sec tests occurred when the system was shut down automatically because insufficient chamber pressure was recorded. Carbon buildup in the tube from the chamber to the transducer caused erroneous pressure pickup and the automatic shutdown. The fired specimen is shown in Figure 34. Examination of the coatings after the 0.8-sec firing and the 15-sec firings revealed no evidence of cracks. The regression rate was 0.6 mils/sec for the 16.6-sec test.

j. Specimen T-23

This specimen consisted of a flame liner of plasma-sprayed hypereutectic ZrC/C. The hypereutectic powder contained approximately 30 vol% excess carbon in the form of graphite flakes. The hypereutectic was used because of its excellent resistance to thermal shock (Reference 26). The material was pressed and cast at Aerojet, and ground to -200 mesh for plasma spraying. The ZrC/C was sprayed with a 2-1/2-in. torch-to-work distance instead of the 4-in. torch-to-work distance to minimize oxidation of the deposition. Even with this added precaution, small amounts of ZrO_2 were obtained in the coating as evidenced by X-ray diffraction tests and metallographic examination. The microstructure of the ZrC layer consisted of ZrC with small amounts of C and ZrO_2. ZrC/C powder with added carbon would be required to obtain carbon-rich coatings and coatings free of ZrO_2. The undercoating was the same as that used for specimens T-19 and T-20 except that a 3-mil Mo layer was used as a diffusion barrier between the oxide and ZrC. The cross-section of the as-sprayed specimen is shown in Figure 35.

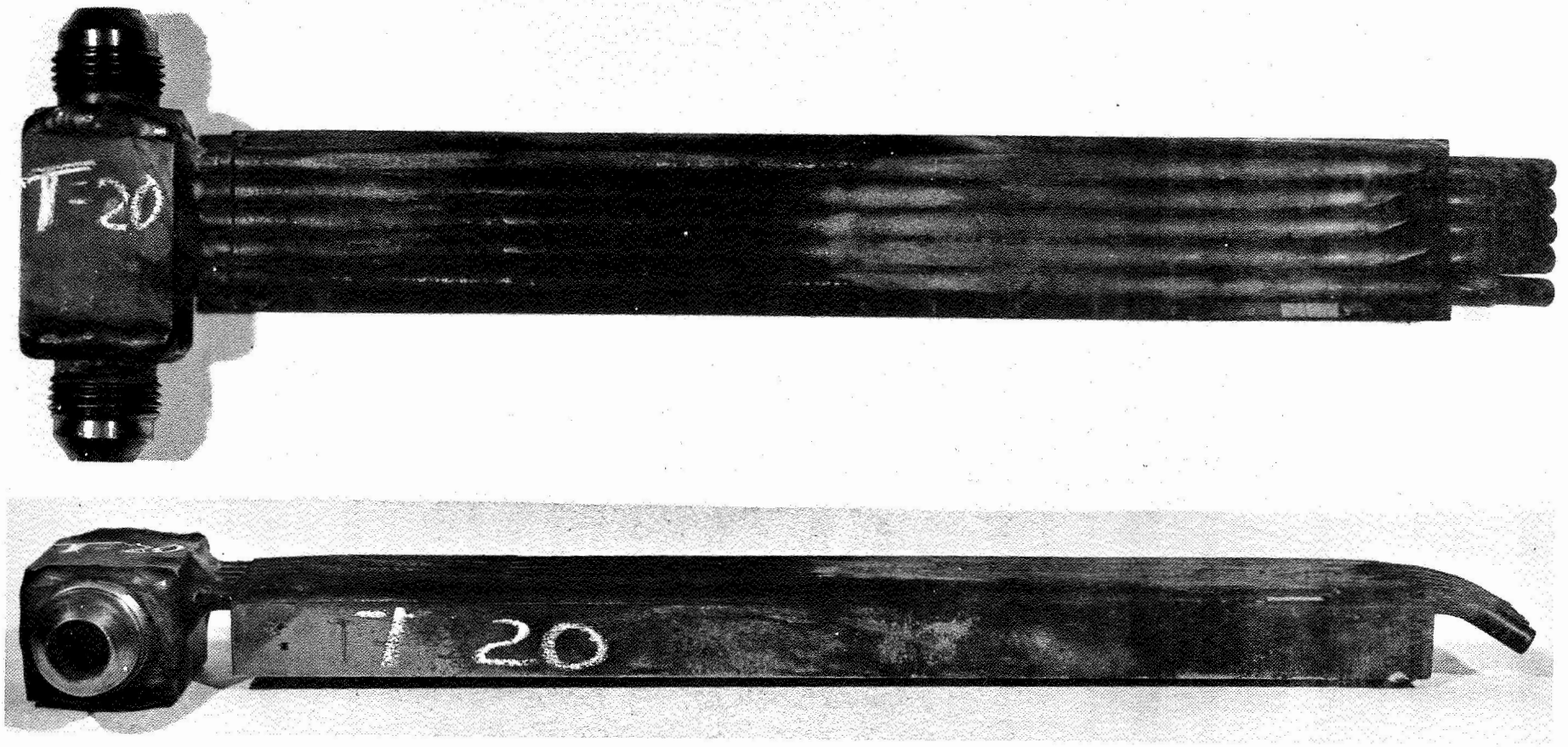

Figure 34. Tungsten Topcoated Specimen after Flox/Propane Test Firing.

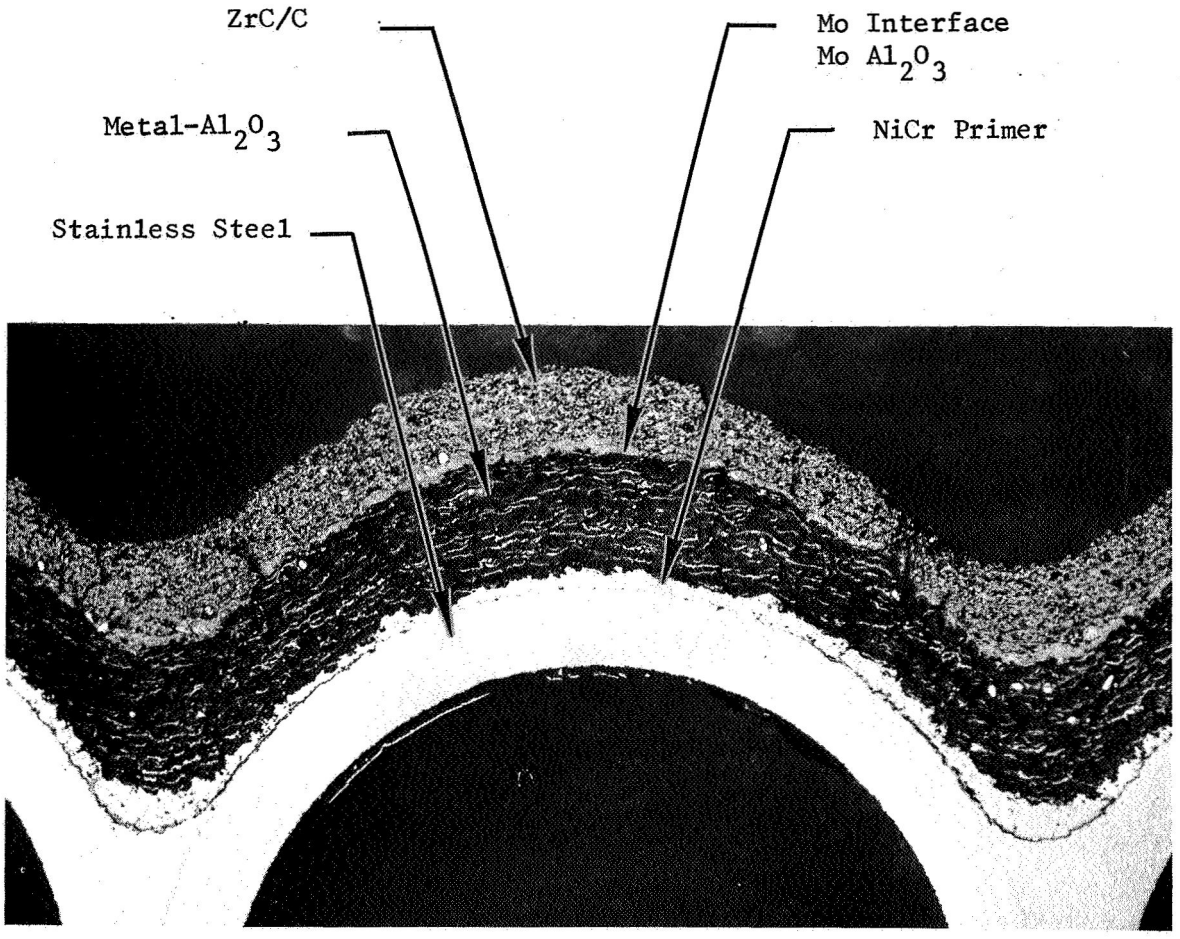

Magnification: 24X Neg. 15839

Figure 35. Prefired Gradated Coating Consisting of Underlayers of Ni-Al_2O_3, Mo-Al_2O_3, Mo Interface and Layer of ZrC/C (Specimen T-23).

The specimen was test fired for 15 sec using the modified shield. The regression rate was 0.46 mils/sec which was comparable to the regression on the Mo and W flame liners. Evidence of thin layers of ZrO_2 occurred 1-1/2 in. from the forward edge of window indicating oxygen species in the exhaust. Several longitudinal cracks were observed in the ZrO_2 layer and a few transverse cracks in the ZrC/C layer.

k. Specimen T-25

This specimen consisted of tungsten flame liner with the same underlayers as specimen T-20. The tungsten liner in specimen T-25 was sprayed by the Material System Division of Union Carbide. The details of the Union Carbide spraying process are proprietary. Their tungsten coatings are estimated at 85 to 90% dense compared to an estimated 75 to 85% for standard plasma spraying processes. A cross-section of prefired specimen T-25 is shown in Figure 36 both at 6X and 24X magnification. The regression on the specimen was about 0.4 mils/sec for a 15-sec firing which was in the same range as for the previous tungsten-coated specimens. To show significant improvement, densities in the range of 95 to 100% may be required. Cracking was observed along the valleys in the tube specimen as shown in Figure 37. Cracks propagated through the tungsten topcoat and terminated at the undercoat. Other coatings were not adversely affected by cracking of this type in sustained firing or under restart conditions.

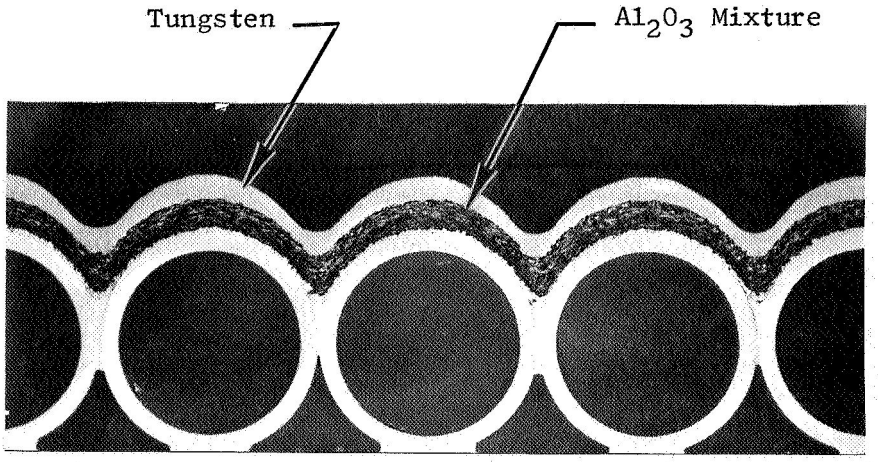

Magnification: 6X Neg. 15834

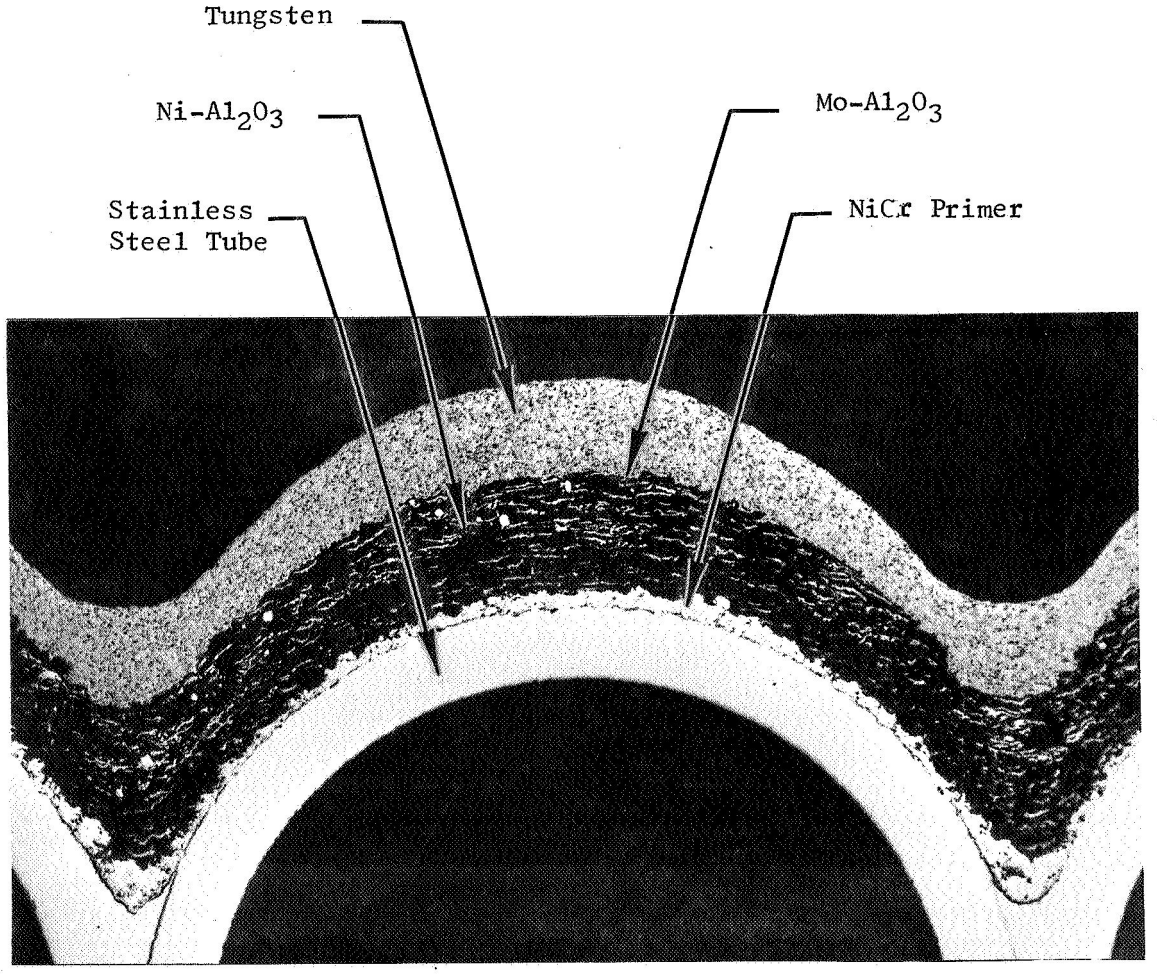

Magnification: 24X Neg. 15840

Figure 36. Prefired Coated Specimen Consisting of Ni-Al_2O_3 and Mo-Al_2O_3 Undercoats and a Union Carbide W-Deposited Topcoat (Specimen T-25).

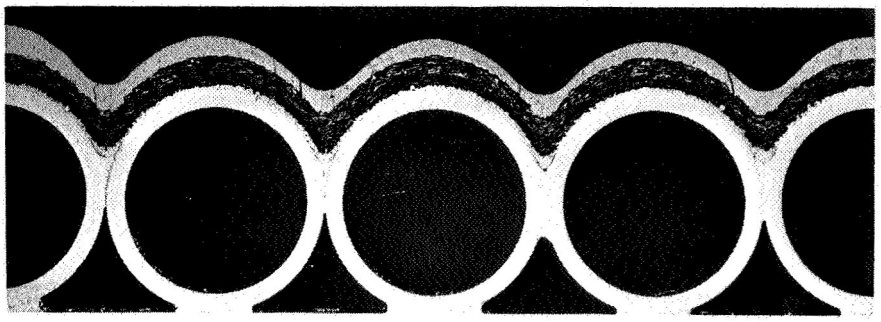

6X Neg. 15835

Figure 37. Postfired Section of Tungsten Topcoated Specimen (Specimen T-25).

VII. CONCLUSIONS AND RECOMMENDATIONS

W, Mo, Al_2O_3, ZrO_2, and ZrC were selected for thermal barriers on the basis of analytical studies in which the thermal and chemical environments were established. Plasma-sprayed thermal barrier coatings, consisting of the selected materials and applied with thermal resistances of 1200 to 1400-in.^{2}-sec-°F/Btu, were evaluated in the exhaust stream of a flox/propane combustor. Coating surface temperatures of 3000 to 3500°F were attained. The exhaust environment was apparently more severe than at the throat of a chamber because of air entrainment, as evidenced by the severe regression in the graphite shield. Because of the air entrainment, the regression data are not directly related to actual service; however, the data were adequate for comparison purposes. Even with the severe exhaust environment, regression rates of 0.4 mil/sec were obtained with flame liners consisting of pure W, Mo, and ZrC/C. Regression rates increased with additions of the ceramics Al_2O_3 and ZrO_2 to the flame liners. The best coatings consisted of a 3-mil-thick Nichrome primer, with a 10-mil layer of 20% Ni-80% Al_2O_3; and a 14-mil layer of 30% Mo-70% Al_2O_3 to provide the thermal resistance. The flame liner for these coatings consisted of pure Mo, W, or ZrC.

Based on these studies, further research is recommended to improve coating performance by refining the coating system and by evaluating the coating in an environment representative of actual service. Coating refinement should be conducted to increase the density of the flame barrier from the present 88% to greater than 95% of theoretical density. Increased density resulted in decreased regression rate in solid rocket motor firings made under controlled conditions. In these latter firings, regression rates of 5 mils/sec were obtained with densities of 65% dense tungsten compared to 4 mils/sec for 75% dense tungsten and zero regression for 100% dense tungsten. In addition to the increase in density, improvements in regression resistance of the tungsten coating are anticipated with the oxidation resistance additives such as silicon. It is recommended that the improved coatings be screened in

the present flox/propane combustor. This combustor was valuable as a screening device to evaluate thermal shock resistance and to provide qualitative data on regression resistance. Final evaluations are recommended in an environment similar to the conditions that exist in an actual rocket engine. For these tests, it is recommended that a rectangular chamber be used capable of exposing test panels to the combustion gas at the throat, chamber, and exit cone areas.

REFERENCES

1. Evaluation of High Temperature Materials Systems with an Arc-Plasma-Jet, TD Report No. ASD-TDR-62-655, July, 1962, Contract AF 33(616)-7838, Project 7381, Task No. 738103.

2. Development of Thermal Barrier Coatings for Regeneratively Cooled Rocket Engine Thrust Chambers, BSD-TDR-119, Contract AF 04(647)-652, SA4, 28 June 1963, (C).

3. Thermal Barrier Liners for Regeneratively Cooled Combustion Chambers (U), BSD-TDR-139, Contract AF 04(694)-212, SA3, 30 November 1964 (C).

4. S. J. Grisaffe, "Analysis of Shear Bond Strength of Plasma Sprayed Alumina Coatings on Stainless Steel", NASA TND 3113, November, 1965.

5. The Evaluation of Material Systems for High Temperature Aerospace Applications, Technical Report AFML-TR65-339, Contract AF 33(615)-1312, July, 1965.

6. Protective Coatings for Refractory Metals in Rocket Engines, Final Report No. IITRI-B237-45, Contract NAS 7-113, 19 December 1965.

7. Thrust Chamber Materials and Design Concepts Evaluation, Phase I Report AFRPL-TR-66-97, May, 1966, TRW, Inc.

8. D. L. Peters, "Chemical Corrosion of Rocket Liner Materials and Propellant Performance Studies" Publication No. U-2384, Ford-Aeroneutronics Division, 15 December 1963.

9. M. Ebner, "Stability of Refractories in Hydrogen Fluorine Flames", J. Am. Ceramic Soc., Vol. 44, No. 1, 1961, p. 7.

10. Principles Governing the Behavior of Solid Materials in Severe High Temperature Environments, Union Carbide Research Institute, Final Report No. UCRI-388, Contract DA-01-021-AMC-11926 (Z), 31 May 1966.

11. Gas Metal Reaction in Rocket Nozzles, ASD-TR-62-327, Pt. 1, June, 1962.

12. T. J. Rausch and V. L. Hill, "Protective Coatings for Refractory Metals in Rocket Engines", IITRI-B6058-13, Contract NAS 7-431, 15 June 1967.

13. Investigation of Light Hydrocarbon Fuels with Flox Mixtures as Liquid Rocket Propellants, Pratt and Whitney Aircraft, NASA Report No. CR 54445, Contract No. NAS 3-4195, 1 September 1965.

REFERENCES (cont.)

14. N. E. Van Huff, and D. C. Rousar, "Ultimate Heat Flux Limits of Storable Propellants", Eighth Liquid Propulsion Symposium, Vol. II, CPIA Publication No. 121, 7-9 November 1966, p. 227.

15. W. S. Hines, "Experimental Evaluation of the Limitations of the Commonly Used Convection Correlation for Prediction of Heat Transfer to Liquids at Very High Heat Flux and Flow Rates", Rocketdyne, Contract No. AF 04(647)-318 and -672.

16. JANAF Thermochemical Tables, The Thermal Research Laboratory, Dow Chemical Company.

17. Bichonski and Rossini, Thermochemistry of Chemical Substances, 1936.

18. Working Group on Thermochemistry, proceeding of the first meeting, Vol. 1, November 1963.

19. L. J. Gordon and H. Boerlin, "Proceedings of the First Conference on Kinetics, Equilibria, and Performance of High Temperature Systems", Western States Section, The Combustion Institute, Los Angeles, California, 2-5 November 1959, Butterworth's, Washington D.C., 1960.

20. H. W. Schmidt and J. T. Harper, "Handling and Use of Fluorine and Fluorine-Oxygen Mixture in Rocket Systems", NASA SP-3037, 1967.

21. R. Resnick, and R. Steinitz, "High Temperature Reaction between Tungsten and Several Refractory Components", Fifth Meeting of the Refractory Composite Working Group, Dallas (8-10 August 1961).

22. C. A. Krier, "Coatings for Protection of Refractory Metals from Oxidation", DMIC Report No. 162, 24 November 1964.

23. W. J. Parker, R. J. Jenkins, C. P. Burke, and G. L. Abbott, "Flash Method of Determining Thermal Diffusivity, Heat Capacity, and Thermal Conductivity", J. Appl. Phys. 32, 1679 (1961).

24. Flow Separation in Overexpanded Supersonic Nozzles, Aerojet-General Corporation Report TCER, Contract AF 04(695)-941, 18 July 1966.

25. J. R. Johnson, et al., "Performance of Rocket Nozzle Materials with Several Solid Propellants", NASA Technical Note TND 34228 C.1., May, 1966.

26. Advanced Composite Carbide Nozzles, Interim Report AFRPL-TR-68-61, dated April, 1968, AF 04(611)-11608.